Quantum indistinguishability by path identity and with undetected photons

Armin Hochrainer[*]

Vienna Center for Quantum Science and Technology (VCQ), Faculty of Physics, University of Vienna, 1090 Vienna, Austria and Institute for Quantum Optics and Quantum Information (IQOQI) Vienna, Austrian Academy of Sciences, 1090 Vienna, Austria

Mayukh Lahiri[†]

Department of Physics, Oklahoma State University, Stillwater, Oklahoma 74078, USA

Manuel Erhard[‡]

Vienna Center for Quantum Science and Technology (VCQ), Faculty of Physics, University of Vienna, 1090 Vienna, Austria and Institute for Quantum Optics and Quantum Information (IQOQI) Vienna, Austrian Academy of Sciences, 1090 Vienna, Austria

Mario Krenn[§]

Vienna Center for Quantum Science and Technology (VCQ), Faculty of Physics, University of Vienna, 1090 Vienna, Austria, Institute for Quantum Optics and Quantum Information (IQOQI) Vienna, Austrian Academy of Sciences, 1090 Vienna, Austria, Departments of Chemistry and Computer Science, University of Toronto, Toronto, Ontario M5S 3H6, Canada, Vector Institute for Artificial Intelligence, Toronto, Ontario M5G 1M1, Canada, and Max Planck Institute for the Science of Light, 91058 Erlangen, Germany

Anton Zeilinger[¶]

Vienna Center for Quantum Science and Technology (VCQ), Faculty of Physics, University of Vienna, 1090 Vienna, Austria and Institute for Quantum Optics and Quantum Information (IQOQI) Vienna, Austrian Academy of Sciences, 1090 Vienna, Austria

(published 21 June 2022)

Two processes of photon-pair creation can be arranged such that the paths of the emitted photons are identical. The path information is thereby not erased but rather never born in the first place due to this path identity. In addition to its implications for fundamental physics, this concept has recently led to a series of impactful discoveries in the fields of imaging, spectroscopy, and quantum information science. Here the idea of path identity is presented and a comprehensive review of recent developments is provided. Specifically, the concept of path identity is introduced based on three defining experimental ideas from the early 1990s. The three experiments have in common that they contain two photon-pair sources. The paths of one or both photons from the different sources overlap such that no measurement can recognize from which source they originate. A wide range of noteworthy quantum interference effects (at the single- or two-photon level), such as induced coherence, destructive interference of photon pairs, and entanglement generation, are subsequently described. Progress in the exploration of these ideas has stagnated and has gained momentum again only in the last few years. The focus of the review is the new development in the last few years that modified and generalized the ideas from the early 1990s. These developments are overviewed and explained under the same conceptual umbrella, which will help the community develop new applications and realize the foundational implications of this sleeping beauty.

DOI: 10.1103/RevModPhys.94.025007

[*]armin.hochrainer@univie.ac.at
[†]mlahiri@okstate.edu
[‡]manuel.erhard@univie.ac.at
[§]mario.krenn@mpl.mpg.de
[¶]anton.zeilinger@univie.ac.at

CONTENTS

I. INTRODUCTION

One of the fundamental principles of quantum mechanics is the following: If an event can occur in more than one alternative way, and there is no way to distinguish between the alternatives, interference occurs. Discussing double-slit experiments, Richard Feynman said that this phenomenon "has in it the heart of quantum mechanics. In reality, it contains the only mystery" (Feynman, Leighton, and Sands, 1965). This simple but profound principle can be used to explain many of the other basic quantum mechanics experiments.

In the early 1990s, the group of Leonard Mandel pushed the concept of indistinguishability to a new level. Instead of superpositions of single (or multiple) photons, they created superpositions of the origin of a photon pair itself. By overlapping (or making identical) one of the photon's paths (an idea suggested by Jeff Ou), there is no information anywhere in the Universe about the origin of the second photon. Thus, to apply Feynman's principle, the second photon is in a superposition of being created in either of the crystals. Zou, Wang, and Mandel (1991) (ZWM) exploited this idea in a noteworthy way: They were able to measure phase shifts introduced in photons that they never detected.

Historically, it is interesting that, after some activities over a period of roughly ten years, investigating this phenomenon nearly stopped from around the year 2000 until the field was finally revived in 2014. At that time it was realized that one can extend the scope even further by imaging an object without ever detecting photons that interacted with the object itself; see Fig. 1. An important addition is that the detected light can have an entirely different wavelength than the light interacting with the object. A multitude of critical applications has been discovered since then in quantum imaging, quantum spectroscopy, quantum information science, and other fields, which are interesting for basic research as well as for practical tasks with potential impact on industrial technologies. These new developments have reignited research interest in quantum indistinguishability by making paths identical (path identity), a fact illustrated by the number of related publications, which is shown in Fig. 2. This behavior is denoted as "sleeping beauty" in the scientometrics (Ke *et al.*, 2015; Fortunato *et al.*, 2018).

As a testament to the fundamental importance of the concept, path identity was recently identified as one of the core concepts that should be used in high school education for quantum physics to better understand the idea of a photon (Malgieri, Onorato, and De Ambrosis, 2017).

In this review, we focus on the developments during the last few years, which have enormously widened the scope of ZWM's experiment and Ou's idea. In Sec. II, we demonstrate the concept of *path identity* with three defining examples from the early 1990s, followed by a detailed technical account of the ZWM experiment and its importance in the historical context (Sec. III). After laying the foundations, we explain how to reconstruct properties of objects without detecting the interacting photons (Sec. IV). We then show how information about a correlated photon pair can be obtained without

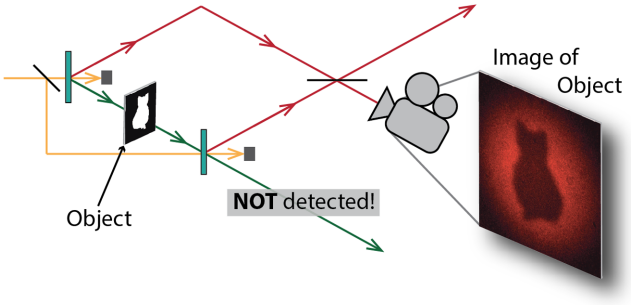

FIG. 1. Quantum imaging by path identity, without detecting the photons that interact with the object (Lemos *et al.*, 2014). The yellow beam coherently pumps two nonlinear crystals such that one of them creates a photon pair. The photon pair is in a superposition of being created in the first or second crystal. When the green photon path is made identity, the red photon is in a superposition of being in the upper or lower path, which leads to interference at a beam splitter. By introducing an object (a picture of a cat) into the overlapped green path, the origins become partially distinguishable, which can be observed in the resulting interference pattern. The image of the cat is constructed without detecting any of the green photons. This concept is entirely different than conventional *ghost imaging*, where both photons need to be detected, and which can be performed classically (Bennink *et al.*, 2004).

detecting one of the photons (Sec. V). The applications to modern quantum information science are discussed based on single-photon and multiphoton entanglement generation (Sec. VI) with a connection to the mathematical field of graph theory (Sec. VII). A novel type of multiphoton quantum interference is subsequently discussed (Sec. VIII). Finally, we

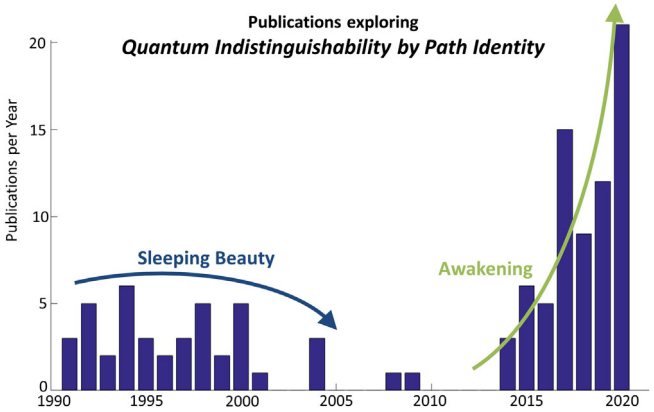

FIG. 2. Papers that explore quantum indistinguishability by path identity. After the Zou-Wang-Mandel experiment and its variations was studied for a decade, research nearly stopped. We can observe an awakening of the research interest in 2014, with exciting new applications including quantum imaging and microscopy, quantum spectroscopy, and quantum information. To create this list, we use all publications that cite the original Zou-Wang-Mandel experiment (Zou, Wang, and Mandel, 1991). From there, we select those papers that actually explore the underlying ideas and concepts rather than just mentioning them. A paper or concept with this behavior is called "sleeping beauty" (Ke *et al.*, 2015).

conclude and raise a number of open questions that would be interesting to be investigate in the future (Sec. IX).

In our review, we focus on true single-photon or entangled photon quantum phenomena. For a detailed account of so-called nonlinear interferometers in the high-gain regime of nonlinear optics, see Chekhova and Ou (2016) and Ou and Li (2020). Furthermore, generalizing the concept of path identity to other degrees of freedom is an interesting question, but beyond the scope of our review.

II. THE PRINCIPLES OF PATH IDENTITY

In this section, we explain the ideas of three experiments from the early 1990s, which define the principles of path identity. All of these experiments employ two photon-pair sources. The paths of one or both photons from the different sources are made identical such that it cannot be distinguished from which source they originate. This path identity leads to several striking quantum interference effects (at a single- or two-photon level) that have seen quantum applications in recent years.

A number of other quantum experiments can be interpreted in this framework. It might help to transfer insights and explanations from these three defining examples to other fields of quantum physics. Helping to find such relations is one of the goals of our review.

A. The Zou-Wang-Mandel experiment: Induced coherence without induced emission

In 1991, ZWM demonstrated an experiment where they induced coherence between two photonic beams without interacting with any of them (Wang, Zou, and Mandel, 1991; Zou, Wang, and Mandel, 1991). They used two nonlinear crystals (NLs) that produce photon pairs. In the experiment, one photon pair is in a superposition of being created in crystal 1 (creating photons in paths a and b) and crystal 2 (creating photons in paths c and d). The notable idea (originally proposed by Zhe-Yu Ou) was to overlap one of the paths from each crystal [Fig. 3(a)], which can be written as the path identity

$$|b\rangle \to |d\rangle. \tag{1}$$

The *which-crystal information* of the final photon in path d is thereby removed. The information of the photon's origin is not erased but was never created in the first place. The resulting state can be written as

$$\begin{aligned}|\psi\rangle &= \frac{1}{\sqrt{2}}(|a,d\rangle + |c,d\rangle)\\ &= \frac{1}{\sqrt{2}}(|a\rangle + |c\rangle)|d\rangle,\end{aligned} \tag{2}$$

which shows that one photon is in a superposition of being in path a or c. If one adds a phase shifter to introduce the phase ϕ in path d between the two crystals, the state becomes

$$\begin{aligned}|\psi\rangle &= \frac{1}{\sqrt{2}}(|a,d\rangle + e^{i\phi}|c,d\rangle)\\ &= \frac{1}{\sqrt{2}}|d\rangle(|a\rangle + e^{i\phi}|c\rangle).\end{aligned} \tag{3}$$

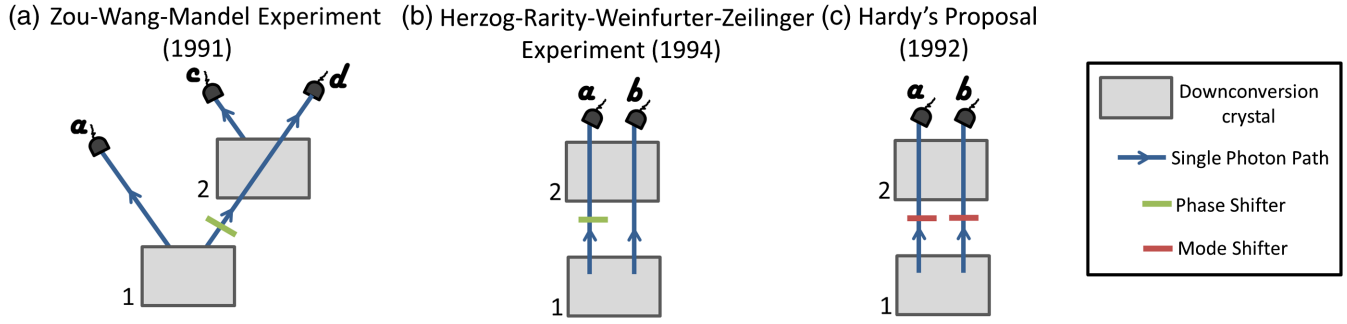

FIG. 3. Three historic experiments initiated the research in path identity. (a) The experiment by Zou, Wang, and Mandel first showed that identifying the path of photons can induce coherence in an unexpected way (Wang, Zou, and Mandel, 1991; Zou, Wang, and Mandel, 1991). (b) Herzog *et al.* (1994) identified that two-photon interference phenomena occur when it is fundamentally indistinguishable in which crystal the photon pair was created. (c) Hardy (1992) proposed the mode shifting and identification of two paths as a method for the generation of quantum entanglement. The source has become a cornerstone of photonic quantum entanglement experiments (Kwiat*S* *al.*, 1999; Pan *et al.*, 2012; Zhong *et al.*, 2018). The review concerns these ideas and their generalizations and applications during the last quarter of a century.

Now the phase is encoded between the photon's path a and c, which never interacted with the phase shifter in the first place. The phase can be extracted if one superposes the paths a and c with a beam splitter and detects one of the outputs. A detailed analysis of this "mind-boggling" experiment (Greenberger, Horne, and Zeilinger, 1993) is shown in Sec. III.B.

It took more than 20 years until it was recognized that this type of interference can be exploited for quantum imaging (Lemos *et al.*, 2014) and spectroscopy (Kalashnikov *et al.*, 2016) in a way that uses the potential to probe at one wavelength and measure at another wavelength. We return to these core insights in Sec. IV.

B. Frustrated down-conversion: Interference in photon pair creation

Shortly after the demonstration of the ZWM interference, an experiment showed quantum interference that occurs when both paths of the photon pairs are identified (Herzog *et al.*, 1994). Similarly, as in the ZWM experiment, the experimental setup [which is depicted in Fig. 3(b)] consists of two crystals that are pumped coherently and in such a way that only one of the crystals creates a photon pair. A photon pair now could be created in the first or second crystal. A phase plate can shift the relative phase between the two processes, which leads to the final state

$$|\psi\rangle = \frac{1}{\sqrt{2}}(|a,b\rangle + e^{i\phi}|a,b\rangle) = \frac{1}{\sqrt{2}}|a,b\rangle(1+e^{i\phi}). \tag{4}$$

One finds that by changing the phase between the two crystals, one can enhance or suppress the production of the photon pairs. This is a notable interference effect because, while a single crystal produces a constant number of photon pairs, adding a second crystal could lead to complete zero output due to destructive interference.

In the other extreme case, constructive interference of two sources can lead to 4 times the intensity of spontaneous parametric down-conversion (SPDC) photons compared to a single crystal, in accordance with the interference law equation (4).

When the distance between the two crystals in Fig. 3(b) is reduced and eventually becomes zero, one essentially obtains a crystal twice the length of the original one that produces 4 times the output. The system can be generalized to constructive interference from more than two crystals, leading to an even greater enhancement of the emission rate.

These facts are analogous to periodic poling, which is used to achieve quasi–phase matching within a single nonlinear crystal in order to enhance the emission rate of down-converted photons. In this process, the nonlinear response of successive slices of the nonlinear crystal are engineered in a way that their outputs lead to constructive interference, and thus enhancement of SPDC over the entire crystal length. Note that the phase ϕ of Eq. (4) is given by $\phi = \phi_p - \phi_s - \phi_i$, where ϕ_i and ϕ_s stand for the phases accumulated in idler and signal beams, and ϕ_p stands for the phase introduced into the pump beam. The phase-matching condition $k_p - k_i - k_s = 0$ can be seen as a condition to maintain this phase relation over the crystal length. Recent generalizations to multiphotonic systems show connections to graph theory and quantum computation, which we explain in Sec. VIII.

C. Entanglement by path identity

In the two previously mentioned experiments, paths of indistinguishable photons are overlapped and phases between photon-pair sources are altered, which led to a new kind of single-photon interference. We now ask what would happen if, instead of the phase, the modes (such as the polarization of the photons) are changed, such that the photons are no longer indistinguishable. A conceptual sketch is shown in Fig. 3(c).

If one pumps only crystal 1, one always gets a vertically polarized photon pair in detectors a and b ($|\psi_1\rangle = |a_V, a_V\rangle$). While pumping crystal 2 only, one always obtains two photons with horizontal polarization ($|\psi_2\rangle = |a_H, a_H\rangle$). If the two crystals are pumped coherently, a pair is generated that is a coherent superposition of the two possibilities, i.e.,

$$|\psi\rangle = \frac{1}{\sqrt{2}}(|a_H, b_H\rangle + |a_V, b_V\rangle). \tag{5}$$

This state describes two photons that are entangled in their polarization.

An entanglement source of this kind was first described by Lucien Hardy in 1992 (Hardy, 1992), only a few months after the ZWM experiment. Hardy described it as a deterministic, collinear emitting source of polarization-entangled photon pairs that can be used for the definitive violation of Bell's inequality. The implementation of this source was achieved by Kwiat *et al.* (1999), and the design of the source is still in use today, especially in the generation of the most complex photonic entanglement states such as a 12-photon entangled system (Zhong *et al.*, 2018), or an 18-qubit entangled photon state of several degrees of freedom (X.-L. Wang *et al.*, 2018).

Despite the frequent use of this source, it took 25 years for the concept of path identity to be generalized to vast classes of entanglement, such as any high-dimensional two-photon system as well as vast types of high-dimensional many-body systems (Krenn *et al.*, 2017). We return to this discussion in Sec. VI.

III. THE ZOU-WANG-MANDEL EXPERIMENT

We now describe the ZWM experiment, first conceptually, then in detail. Afterward, we present several of its fundamental conclusions for quantum physics in general.

A. Description of the experiment

The concept of path identity can be elegantly illustrated with an absorptive element between the two crystals, which influences the which-crystal information, and therefore the interference visibility. The experiment is illustrated in Fig. 4. Two photon-pair sources are denoted by A and B. These two sources are two identical nonlinear crystals pumped by two *mutually coherent* laser beams (not shown in the figure). Two photons belonging to a pair are denoted by S and I (which stand for signal and idler, for historical reasons). Source A emits S and I along paths S_a and I_a, respectively. Likewise, B emits the photons along paths S_b and I_b. The two crystals are pumped weakly such that in most cases only maximally one crystal produces a pair of photons at a time.

The paths S_a and S_b are superposed by a beam splitter (BS) and single-photon counting rate is measured at one or both outputs of the BS. If the concept of path identity is applied, i.e., if I_a is sent through source B and aligned with I_b, interference occurs at the output of the BS. However, in practice, the pump and the down-converted light have finite spectral widths, i.e., finite coherence times. Therefore, further conditions relating to the path lengths of the interferometer are required to be satisfied. If the pump light has a much longer coherence length than the down-converted light, the following condition must be satisfied (Wang, Zou, and Mandel, 1991):

$$|l_{S_a} - l_{S_b} - l_I| \ll L_{\mathrm{dc}}, \tag{6}$$

where l_{S_a} is the optical path length along S_a from A to the BS, l_{S_b} is the optical path length along S_b from B to the BS, l_I is the optical path length along I_a from A to B, and L_{dc} is the coherence length of the down-converted light. If this condition is met, there is no temporal information that would allow one to determine from which crystal a signal photon arrived at the detector. Additionally, all other degrees of freedoms (polarization, frequency, and path of the photon) need to be indistinguishable in order to observe interference. A discussion on conditions required for interference, when ultrashort pump pulses are used, was given by Rojas-Santana *et al.* (2020).

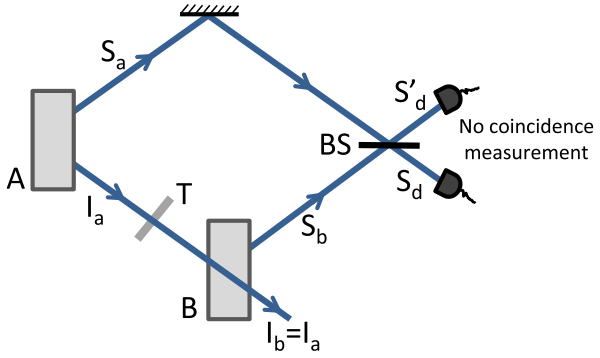

FIG. 4. Zou-Wang-Mandel experiment. A and B are two identical photon-pair sources. A and B emit a photon pair in paths (S_a, I_a) and (S_b, I_b), respectively. Paths I_a and I_b are made identical. An object with the amplitude transmission coefficient T is placed on I_a between A and B. A single-photon interference pattern is observed at both outputs of the beam splitter (BS) if S_a and S_b are superposed. Visibility is proportional to the modulus of the amplitude transmission coefficient.

If beam I_a is blocked between A and B or condition (6) is not met, the interference is lost. In this case, it is possible to determine from which crystal a signal photon arrived by detecting the I photon in coincidence.

We now consider the scenario in which an attenuator with amplitude transmission coefficient T on I_a is placed between sources A and B. The visibility of the interference patterns turns out to be linearly proportional to $|T|$. This can be understood by the quantum mechanical rules of addition of probability. An idler photon passes through the attenuator with a certain probability. The transmission probability is equal to $|T|^2$. When the idler photon passes through the object, we have complete path identity. In this case, there is no information about the origin of a single photon detected after the beam splitter, and thus interference occurs. If the photon does not pass through the object, the path identity is broken, and the signal photon does not contribute to the interference pattern. Therefore, there are three alternative ways through which a signal photon can arrive at the detector: (1) the signal photon has been emitted by crystal B, (2) the signal photon is emitted by crystal A, and the partner idler photon is transmitted through the object, and (3) the signal photon is emitted by crystal A, and the partner idler photon is blocked. Note that alternatives (1) and (2) are indistinguishable, and therefore their probability amplitudes add. Alternative (3) is distinguishable from the rest, and thus its probability adds to the combined probability of the other two. If one determines the total probability in this way, one finds that the visibility is proportional to $|T|$. In Sec. III.B, we provide a more rigorous analysis of the experiment.

B. Theoretical analysis

The original analysis presented by Wang, Zou, and Mandel (1991) and Zou, Wang, and Mandel (1991) was based on quantum field theory. Here we present a conceptually equivalent but simpler treatment. For simplicity, we do not consider the multimode nature of optical fields in this section. Multimode fields are considered later when we discuss imaging and spectroscopy experiments. We also slightly modify the notations used in Sec. II.A.

We denote the photon-pair states produced individually at A and B by $|S_a\rangle|I_a\rangle$ and $|S_b\rangle|I_b\rangle$, respectively. In the experimental condition, these two sources emit coherently, and they rarely produce more than one photon pair jointly. The resulting state, therefore, becomes

$$|\psi_0\rangle = \frac{1}{\sqrt{2}}(|S_a\rangle|I_a\rangle + e^{i\phi}|S_b\rangle|I_b\rangle), \tag{7}$$

where ϕ is an arbitrary phase and we assume that both sources have the same emission probability.

Suppose that the two outputs of the beam splitter are denoted by S_d and S'_d (Fig. 4). The transformation of the states due to the beam splitter is given by

$$|S_a\rangle \to \frac{1}{\sqrt{2}}(|S_d\rangle + i|S'_d\rangle), \tag{8a}$$

$$|S_b\rangle \to \frac{e^{i\phi_S}}{\sqrt{2}}(|S'_d\rangle + i|S_d\rangle), \tag{8b}$$

where ϕ_S is the phase difference due to different propagation distances along paths S_a and S_b.

As previously mentioned, the crucial part of the experiment is to make the paths I_a and I_b identical. This is done by sending I_a through crystal B and then perfectly aligning it with I_b. The quality of this alignment (path identity) can theoretically be modeled by placing an attenuator on beam I_a between the sources A and B. In our case, the attenuator is an object with the complex amplitude transmission coefficient $T = |T|\exp[i\Phi_T]$. An idler photon passes through the object with probability $|T|^2$. Therefore, the object can be treated as a beam splitter and the path-identity condition can be expressed as

$$|I_a\rangle \to \exp[i\theta_I](T|I_b\rangle + R|l\rangle), \tag{9}$$

where $|T|^2 + |R|^2 = 1$ and $|l\rangle$ represents a photon that is lost or absorbed. We note that Eq. (9) essentially reduces to Eq. (1) when $|T| = 1$.

Applying the transformations (8) and (9) to Eq. (7), we find that the state $|\psi_0\rangle$ transforms to

$$\begin{aligned}|\psi_f\rangle = {} & \tfrac{1}{2}(e^{i\theta_I}T|I_b\rangle + ie^{i(\phi+\phi_S)}|I_b\rangle + e^{i\theta_I}R|l\rangle)|S_d\rangle \\ & + \tfrac{1}{2}(ie^{i\theta_I}T|I_b\rangle + e^{i(\phi+\phi_S)}|I_b\rangle + ie^{i\theta_I}R|l\rangle)|S'_d\rangle.\end{aligned} \tag{10}$$

To determine the photon counting rates at outputs S_d and S'_d, we carry out the following steps: (1) we determine the density operator $\hat{\rho}_f = |\psi_f\rangle\langle\psi_f|$, (2) we trace over $|I_b\rangle$ and $|l\rangle$ to obtain the reduced density operator that represents the state of the single photon at the outputs of the BS. The coefficients associated with $|S_d\rangle\langle S_d|$ and $|S'_d\rangle\langle S'_d|$ in the expression of the reduced density operator are proportional to the photon counting rates at S_d and S'_d, respectively. The photon counting rates are found to be given by

$$R_d \propto \tfrac{1}{2}[1 - |T|\sin(\phi_{ab} + \phi_S - \theta_I - \Phi_T)], \tag{11a}$$

$$R_{d'} \propto \tfrac{1}{2}[1 + |T|\sin(\phi_{ab} + \phi_S - \theta_I - \Phi_T)]. \tag{11b}$$

We note that both the amplitude and phase of the object's transmission coefficient appear in the interference pattern. This is a striking phenomenon because the interference pattern is obtained by detecting photons that have never interacted with the object.

In the first decade after the experiment by Zou-Wang-Mandel experiment in 1991, a manifold of theoretical and experimental investigations were reported. Among the notable results during that time were studies of the interference's time delays and coherence times effectively demonstrating the fundamental importance of information in quantum mechanics (Wang, Zou, and Mandel, 1992; Zou, Grayson, and Mandel, 1992; Zou, Wang *et al.*, 1992; Grayson *et al.*, 1993; Zou *et al.*, 1993; Barbosa, 1994; Wang and Rhee, 1999).

A possible relation of the ZWM experiment in terms of a quantum eraser was discussed by Zajonc *et al.* (1991), specifically, whether the overlapping of the idler beams plays the role of an eraser of information. However, in the ZWM experiment, when the idler paths overlap the idler photon never carries any path information. Therefore, there is no information that needs to be erased. As a consequence, interference can be observed without postselection or coincidence detection. An intensity measurement on the signal is sufficient to observe interference. Thus, unlike *quantum erasure experiments*, where information is deleted to observe interference, in the ZWM experiment the which-way information is never created.

This fundamental contrast was analyzed in more detail in several papers (Kwiat, Steinberg, and Chiao, 1994; Ryff, 1995a; Ou, 1997). The ZWM experiment has also inspired new mathematical methods for describing experimental setups where SPDC processes are used and path identity has been employed (Luis and Peřina, 1996; Casado, Marshall, and Santos, 1997; Mista *et al.*, 2000), has been used to experimentally falsify certain variations of de Broglie's deterministic pilot wave interpretation of quantum mechanics (Zou, Grayson *et al.*, 1992), and has inspired proposals to detect effects in quantum cosmology (Yurtsever and Hockney, 2005).

Since it is possible to extract the information about the object from the recorded interference pattern, the concept of path identity has also inspired an entirely new class of imaging, spectroscopy, and tomography experiments. In all these experiments, one does not need to detect the photon that interacts with an object.

C. Nonclassicality of the Zou-Wang-Mandel experiment

The Zou-Wang-Mandel experiment does not have any classical explanation. We now discuss the quantitative evidence that supports this fact. We learn from Eqs. (11) that the

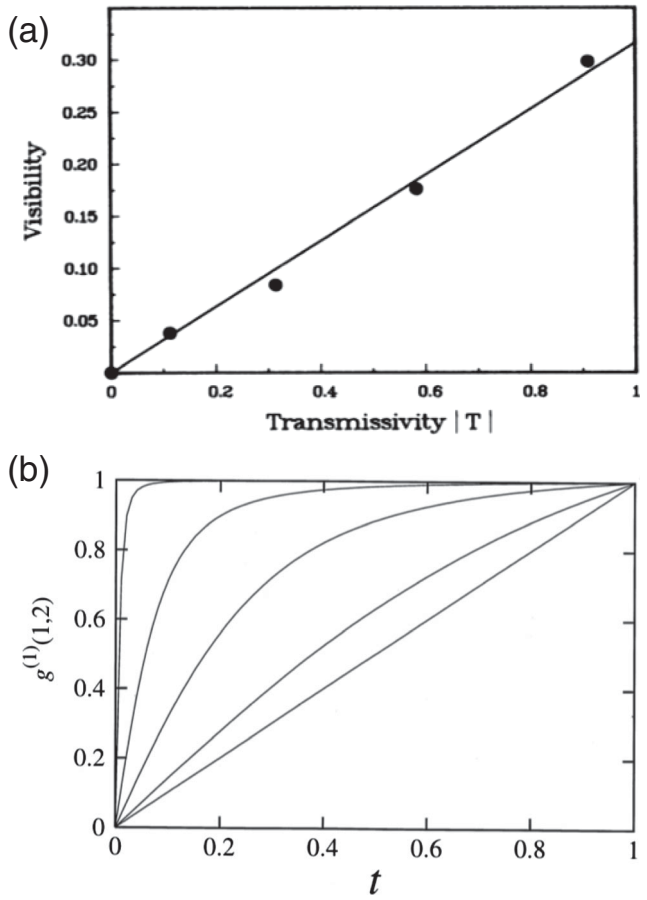

FIG. 5. Nonclassicality of the Zou-Wang-Mandel experiment. (a) Experimental data show that the visibility of the single-photon interference pattern is linearly proportional to $|T|$. Adapted from Zou, Wang, and Mandel, 1991. (b) $g^{(1)}(1,2)$ refers to visibility and t is the same as $|T|$ in the text and in (a). The theoretical curves show that when the effect of stimulated emission is prominent, the linear dependence is no longer observed. Adapted from Wiseman and Mølmer, 2000.

visibility of the interference pattern is linearly proportional to the modulus of the amplitude transmission coefficient of the attenuator. This linear dependence was experimentally verified by Zou, Wang, and Mandel [Fig. 5(a)]. The physical reason for this linear dependence is the fact that the effect of stimulated emission is negligible in that experiment.

When beam I_a is sent through source B and then aligned with beam I_b, it is natural to assume that stimulated emission will take place at B. However, in the experiment A and B are two low-gain nonlinear crystals that are weakly pumped by laser light. In this case, the probability of down-conversion is so low that when emission occurs at B beam I_a is rarely occupied by a photon. Therefore, spontaneous emission dominates over stimulated emission and the quantum state, jointly produced by A and B, becomes a linear superposition of two-photon states. Zou, Wang, and Mandel showed that such a quantum state can explain the linear dependence shown in Fig. 5(a).

Nonclassicality of this experiment was also independently verified by Wiseman and Mølmer (2000). They considered a situation in which the crystal gain can be arbitrarily increased. They showed that for high crystal gain, i.e., when the effect of stimulated emission becomes prominent, the previously mentioned linear dependence is no longer observed [Fig. 5(b)]. For high gain, the problem can be treated using classical nonlinear optics, but in that case the linear dependence is no longer found.

The nonclassicality of the Zou-Wang-Mandel experiment has also recently drawn attention. A good description was presented by Kolobov *et al.* (2017). It has also been shown that if the laser pump is replaced by a single-photon pump, the possibility of stimulated emission becomes strictly forbidden, and even then the interference occurs (Lahiri *et al.*, 2019).

The ZWM experiment's nonclassicality makes it an important milestone in the history of quantum photonic experiments, as we elaborate on in Sec. III.D.

D. Quantum nature of photonic experiments

The classical (nonquantum) theory distinguishes between particles and waves: a classical particle does not display the interference effect, whereas a classical wave does. One of the great successes of quantum mechanics lies in predicting interference phenomena displayed by systems that were previously understood to be classical particles. Well-known examples are neutron (Zeilinger, 1986; Rauch and Werner, 2015) or macromolecule interference (Fein *et al.*, 2019). Quantum theory is also applicable to light, and therefore every optical interference effect can also be understood as a quantum mechanical effect. However, the quantum optics community usually does not perceive such a view as appropriate. An optical phenomenon is called truly quantum mechanical when the classical electromagnetic theory of light is unable to explain it, and the only explanation comes from quantum mechanics. In this review, we use the term *quantum mechanical* in this sense. Therefore, the intensity modulation observed in Young's double-slit experiment or in a Mach-Zehnder interferometer is a classical effect irrespective of the state of light used in the experiment.

Most optical phenomena that involve a measurement of intensity or single-photon counting rate display no quantum mechanical effects. Although the photoelectric effect suggests the quantum nature of light, it has been shown that a successful quantitative theory of photoelectric detection can be developed without considering the quantum nature of light (Mandel, Sudarshan, and Wolf, 1964). The essence of this work lies in the semiclassical theory of light-matter interactions, in which light is treated by classical electromagnetic theory and the atoms by quantum mechanics. It was experimentally demonstrated by Clauser (1974) that the semiclassical theory of photoelectric detection provides incorrect results if one measures *coincidence counts* at two detectors illuminated by light generated by the cascade $9^1P_1 \rightarrow 7^3S_1 \rightarrow 6^3P_1$ in excited ^{202}Hg atoms. Later investigations indicated that most quantum mechanical effects in the optical domain involve coincidence detection of at least two photons (i.e., intensity correlation). Several such phenomena have been studied in the field of quantum optics, for example, photon antibunching (Kimble, Dagenais, and Mandel, 1977) and two-photon interference (Horne and Zeilinger, 1986; Ghosh and

Mandel, 1987; Hong, Ou, and Mandel, 1987; Horne, Shimony, and Zeilinger, 1989).

An experiment by Wang, Zou, and Mandel (1991) and Zou, Wang, and Mandel (1991) turned out to be the first demonstration of the quantum nature of an optical interference effect that relies only on the detection of one intensity, not on correlation measurements. We discussed in Sec. III.C that the Zou-Wang-Mandel experiment cannot be explained using classical wave theory. Here we point out that it is in principle possible to perform this experiment with other quantum entities such as neutrons and electrons. In such cases, the occurrence of interference itself will rule out any classical explanations.

E. Implications for optical coherence theory

1. Path identity and the degree of coherence

Optical coherence theory studies phenomena that are a manifestation of statistical fluctuations present in optical fields (Mandel and Wolf, 1995; Born and Wolf, 1999). For example, when two light beams (or, equivalently, light from two point sources) are superposed, the corresponding fields add linearly. If the field corresponding to one beam is fully not correlated with that of the other beam, no interference occurs. Interference requires correlation between the fields that are superposed. In fact, the visibility of the interference pattern depends on the amount of correlation. Mathematically, a typical interference pattern can be expressed in the general form (Born and Wolf, 1999)

$$R = R_1 + R_2 + 2\sqrt{R_1 R_2}|\gamma_{12}|\cos\phi, \tag{12}$$

where R_1 and R_2 are individual intensity contributions from the interfering fields, ϕ is a phase, and $|\gamma_{12}|$ is the modulus of the degree of coherence, which is a measure of the correlation between the two superposed fields. The visibility is linearly proportional to $|\gamma_{12}|$. The degree of coherence therefore provides a quantitative measure of the ability of light to interfere.

Such an interpretation of interference is not in contradiction with quantum mechanics. This fact can be understood as follows: when two beams are superposed, the absence of "which-way information" implies that the superposed fields are maximally correlated and that intensities of the corresponding beams are equal (Wootters and Zurek, 1979; Greenberger and Yasin, 1988; Mandel, 1991; Jaeger, Horne, and Shimony, 1993; Englert, 1996). In the other extreme case occurring when which-way information is fully available, the superposed fields are completely uncorrelated. This fundamental connection between the two apparently distinct interpretations has been well demonstrated using the ZWM experiment.

According to classical understanding, a change in correlation (the degree of coherence) between the two superposed fields requires a direct interaction with at least one of them. However, according to quantum mechanics one needs to ensure only that the which-way information does not exist, and such an act may not require direct interaction with the fields. The path identity employed in the ZWM experiment allows one to control the correlation between the fields without interacting with any of them. In their experiment, $|\gamma_{12}|$ is equal to the modulus of the amplitude transfer coefficient $|T|$ of the object that never interacts with beams S_a and S_b; see Fig. 4. The ZWM experiment is therefore a landmark experiment that highlights the quantum mechanical aspect of the degree of coherence.

2. Path identity and optical polarization

Polarization properties of a light beam at a point can also be understood as an effect of correlation between the components of electric field vectors at that point (Pancharatnam, 1956; Wolf, 1959). The degree of polarization (P) quantifies how polarized a light beam is at a point. For example, $P = 1$ implies fully polarized light and $P = 0$ implies unpolarized light. In the intermediate case ($0 < P < 1$), the light is partially polarized.

Suppose that we choose two mutually orthogonal transverse directions x and y perpendicular to the direction of beam propagation. If the intensities associated with the individual field components along x and y are equal, the degree of polarization is the modulus of the normalized correlation function of these two field components (Born and Wolf, 1999). Like the degree of coherence, the degree of polarization can also be understood from the principles of quantum mechanics (Lahiri, 2011). The concept of path identity allows us to design an experiment that establishes the quantum mechanical aspect of the degree of polarization.

We consider a modification of the ZWM experiment that is illustrated in Fig. 6. Suppose that the beams S_a and S_b are polarized along directions x and H (horizontal), respectively; both directions are transverse. The direction x encloses an angle γ with the direction H. One can vary the angle γ using a half-wave plate. The correlation between these two superposed field components can be controlled by varying the value of $|T|$. As a result, the polarization properties of light generated by superposition changes. A theoretical analysis shows that the degree of polarization at the output of a BS is given by (Lahiri *et al.*, 2017a)

$$P = \frac{|T| + \cos\gamma}{1 + |T|\cos\gamma}, \tag{13}$$

where the interferometric phase has been set to a multiple of 2π. Figure 6(b) shows the experimental results that support the theoretical prediction. The experiment thus shows that the degree of polarization of a light beam can be changed without interacting with it, an effect that is purely quantum mechanical.

F. Investigation of complementarity

Wave-particle complementarity has been a cornerstone in the development of quantum mechanics since it was introduced by Niels Bohr in 1928 (Bohr, 1928). It defines a relation between the which-way information K (which is related to particlelike behavior) and the interference visibility V (which is related to wavelike behavior). It states that

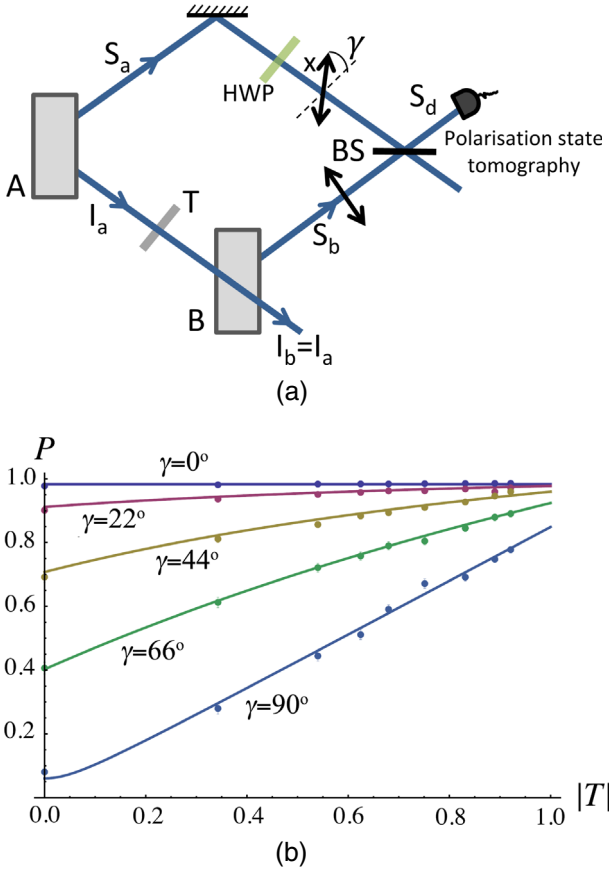

FIG. 6. Degree of polarization and path identity. (a) Schematics of the experiment. (b) Experimentally observed dependence of the degree of polarization on $|T|$ for various values of γ. The solid lines represent theoretical curves considering experimental imperfections. Adapted from Lahiri *et al.*, 2017a.

$$K^2 + V^2 \leq 1. \tag{14}$$

In the ZWM experiment, the visibility V can be optimal only when there is no which-crystal information, K. An extension of the ZWM experiment to three crystals led to more general theoretical (Ryff, 1995b, 2015) and experimental (Heuer, Menzel, and Milonni, 2015b; Heuer, Pieplow, and Menzel, 2015) studies of complementarity.

The quantum state in the experiment performed by Heuer, Menzel, and Milonni (2015b) (depicted in Fig. 7), before the beam splitters, can be written as

$$|\psi\rangle = g_1 e^{i(\phi_s+\phi_i)}|s_3, i_2\rangle + g_2 e^{i\phi_i}|s_2, i_2\rangle + g_3 e^{i\phi_s}|s_3, i_3\rangle. \tag{15}$$

In Eq. (15) ϕ_s and ϕ_i are the phases introduced by the path delay at the top and bottom mirrors. Furthermore, the path identification $|s_1\rangle \to |s_3\rangle$ and $|i_1\rangle \to |i_2\rangle$ is used. The coefficients g_1, g_2, and g_3 correspond to the pump power (and thus the photon-pair rate) of the β-barium borate (BBO) crystals 1, 2, and 3, respectively.

If $g_3 = 0$, $g_1 = g_2 = g_1$, and $\phi_i = 0$, one recovers the original ZWM experiment, and the state in Eq. (15) can be written as

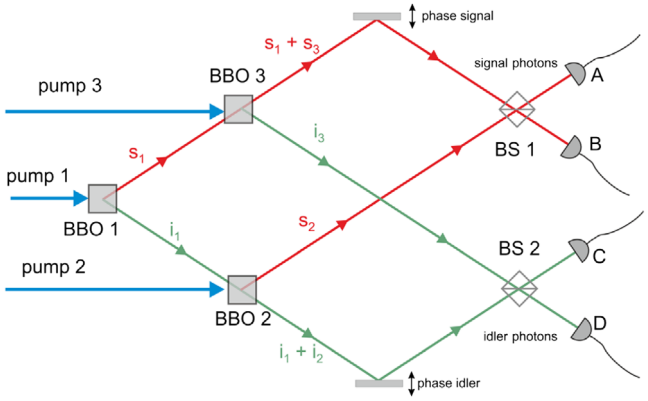

FIG. 7. An extension of the ZWM experiment to three crystals allows for more general tests of the complementarity principle. From Heuer, Menzel, and Milonni, 2015b.

$$|\psi\rangle = e^{i\phi_s}|s_3, i_2\rangle + |s_2, i_2\rangle = (e^{i\phi_s}|s_3\rangle + |s_2\rangle)|i_2\rangle. \tag{16}$$

In the experiment, one has a single photon in perfect, equally weighted superposition between paths s_2 and s_3. Varying the relative phase ϕ_s leads to an ideally perfect modulation of the count rates in detector A, as well as coincidence count rates between detectors A and D. The perfect interference appears because one has no information regarding which crystal the photon pair was created in. Thus, when a photon is observed in detector A one does not know whether the photon arrived at the BS through path s_2 or s_3. This principle indistinguishability of the two events leads to the perfect visibility $V = 1$.

The new situation appears when crystal BBO 3 is pumped as well. There are three possibilities for a photon to arrive at detector A. The first two are through path s_1 or path s_2 (created in BBO 1 or BBO 2). These two possibilities cannot be distinguished, as the idler photons are path identified. However, the photon could also be created in BBO 3. There one has additional information about the idler path because i_2 and i_3 are not identified. This additional path information K decreases the visibility V.

The state for this situation can be written as (with $g_1 = g_2 = g_3 = 1$ and $\phi_i = 0$)

$$\begin{aligned}|\psi\rangle &= (e^{i\phi_s}|s_3, i_2\rangle + |s_2, i_2\rangle + e^{i\phi_s}|s_3, i_3\rangle) \\ &= (e^{i\phi_s}|s_3\rangle + |s_2\rangle)|i_2\rangle + e^{i\phi_s}|s_3, i_3\rangle.\end{aligned} \tag{17}$$

The first two terms in Eq. (17) lead to a modulation of the interference pattern in detector A, whereas the last term contributes to path information, thus leading to an incoherent background in the interference.

One can erase the information of the idler, by detecting the idler photon after the BS2 in detector D. The detection in D makes it impossible to know whether the idler photon arrived through path i_2 or i_3. If one heralds the detector clicks in A on an event in detector D (i.e., measures coincidence counts between A and D), no path information about photon in detector A exists in principle. Thus, one recovers perfect interference fringes.

Heuer, Menzel, and Milonni (2015a) generalized the experiments to stimulated emission configuration by

overlapping i_1 and i_3 with a stimulating HeNe laser and transmission objects in the idler paths. They found general relations between pump powers, transmission magnitude, and visibilities. These experiments demonstrated the connection between fundamental information of the photon pair's origin and visibility well.

G. Transmission measurement with three sources

A variant of the previous experiment analyzing the consequences of the existence of information using cavities was conducted by Lee, Yoon, and Cho (2017). The experimental scheme with three sources [Fig. 8(a)] shows another peculiar feature of the ZWM phenomenon. If two partially reflecting objects are inserted in the idler beam, they act as a cavity for idler photons [Fig. 8(b)].

This gives rise to the observation that the visibility between the signal beams of the last two crystals NL2 and NL3 depends on the properties of the object OS1 placed between the first and second crystals, in particular, on its reflectivity.

In a simplified picture, this effect can be understood as follows. The visibility observed in the original (two-crystal) ZWM experiment depends on the transmission of an object placed in the idler beam between the two crystals. If only a fraction of the idler photons originating from the first crystal are transmitted through the second crystal, an idler photon detected after the setup is more likely to have been emitted by the second source. Thus, partial which-way information can be obtained, resulting in reduced visibility.

Here, however, idler photons that were not transmitted are not absorbed by the object but remain inside the cavity. A fraction of them is transmitted after one or more round trips. Thus, given that the coherence length requirements to observe interference are still satisfied, the quality factor (i.e., the number of round trip times) of the cavity determines the actual probability of transmitting an idler photon after an arbitrary number of round trips. As the number of round trips of an idler photon depends on the reflectivity of both mirrors (objects), so does the observed visibility. In the limiting case of OS1 having perfect reflectivity, an idler photon is never lost unless it passed through OS2, even if it has imperfect transmission. In this case, at least theoretically, unit visibility is observed (regardless of the transmission of OS2).

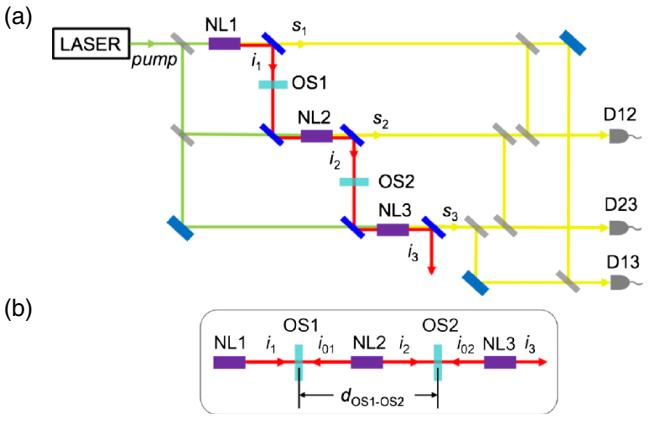

FIG. 8. Three crystal setups. (a) If the coherence lengths are long enough, the reflectivity of optical sample OS1 affects the interference pattern between NL2 and NL3. This is possible because the two samples OS1 and OS2 form an optical cavity. (b) Intuitively, if the reflectivity of OS1 is high, an idler photon from NL2 has many tries to pass through OS2 because idler photons that are not transmitted by OS2 remain inside the cavity and can still be transmitted to NL3 later. This increases the effective transmission and thus the visibility observed at D23. From Lee, Yoon, and Cho, 2017.

IV. RECONSTRUCTION OF OBJECTS WITH UNDETECTED PHOTONS

In this section, we consider experiments that can reconstruct properties of objects without ever detecting the photons that interact with it. The properties can be spatial (for quantum imaging) or in the frequency domain (for spectroscopy). Significant interest in this method comes from the fact that the wavelengths of the detected photon and the probing (idler) photon can be significantly different, thus allowing for novel quantum technologies, as we discuss here.

A. Quantum imaging with undetected photons

The imaging experiment that uses the concept of path identity was demonstrated by Lemos *et al.* (2014). The experiment is illustrated in Fig. 9. The nonlinear crystals NL1 and NL2 are used as photon-pair sources. They are pumped coherently by a laser beam. Each of these crystals can generate a photon pair by the process of SPDC. In the experiment, the signal and idler have different wavelengths: the wavelengths of the signal and idler are 810 and 1550 nm, respectively. A $4f$ lens system is in the path of the idler beam such that the image of NL1 falls on NL2. The object is placed in the idler path between the two nonlinear crystals and at the center of the $4f$ system. Therefore, the object is at the Fourier plane of both crystals. An equivalent $4f$ system is placed in the path of the signal beam (S_1) generated by NL1. After a beam splitter superposes the signal beams, a camera detects the outputs. The camera is placed at the focal plane of a positive lens L_0, which is the Fourier plane of both crystals.

The $4f$ system in the path of the idler consists of two positive lenses [Fig. 9(b)]. The first lens (L_1) focuses the plane wave to a point $\boldsymbol{\rho}_o$ on the object. The spherical wave emerging from this point is converted back to a plane wave by the second lens (L_2). This plane wave then passes through NL2. If an idler photon is emitted in this plane wave mode, its partner signal photon will be in a mode that satisfies the phase-matching condition. The associated plane wave is focused at a point $\boldsymbol{\rho}_c$ on the camera. It follows from the discussion in Sec. III.B that the visibility recorded at $\boldsymbol{\rho}_c$ will be determined by the modulus of the amplitude transmission coefficient at $\boldsymbol{\rho}_o$. Therefore, for an absorptive object the visibility map observed at the camera gives the image. Furthermore, as evident from Eqs. (11), the phase of the object at each point can also be constructed. There are numerous ways of constructing the image. A simple method of subtracting the two outputs of the beam splitter was adopted by Lemos *et al.* (2014).

Figure 10 shows the images of an absorptive object. The object is a piece of cardboard from which the silhouette of a

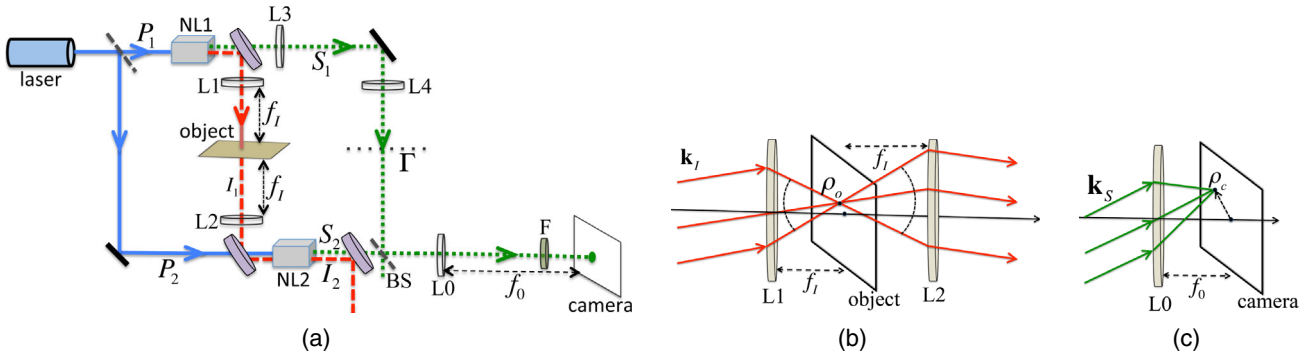

FIG. 9. (a) Imaging setup. NL1 and NL2 are two identical nonlinear crystals pumped coherently by 545 nm laser light. Each crystal can produce a signal (810 nm) and idler (1550 nm) photon by collinear spontaneous parametric down-conversion. Dichroic mirrors separate signal and idler light and are sent to different paths. The alignment of I_1 and I_2 gives the path identity. The object is placed on I_1 between NL1 and NL2. $4f$ lens systems are used in the signal and idler arms. (b) $4f$ lens system on an idler path. An idler wave vector is focussed at a point $\boldsymbol{\rho}_o$ on the object plane. The emerging spherical wave from $\boldsymbol{\rho}_o$ is converted back to a plane wave. (c) Detection system. The corresponding signal wave vector is focused at a point $\boldsymbol{\rho}_c$ on the image plane (camera). Adapted from Lahiri *et al.*, 2015.

cat has been removed [Fig. 10(b)]. Interference patterns that contain the image obtained at the two outputs of the BS are shown in Fig. 10(a). When the two outputs are added, the image disappears [Fig. 10(c)]. This is expected from Eqs. (11). When one of the outputs is subtracted from the other, the image contrast is enhanced because the background becomes nullified [Fig. 10(d)].

The different wavelengths of signal ($\bar{\lambda}_S$) and idler ($\bar{\lambda}_I$) photons also play a role in the image magnification. It can be shown using an explicit calculation that the magnification is given by $M = f_0\bar{\lambda}_S/f_I\bar{\lambda}_I$, where f_0 and f_I are the focal lengths illustrated in Fig. 9(a). A rigorous theory of the imaging experiment was provided by Lahiri *et al.* (2015), and comprehensive analysis of the image quality in terms of pump power was conducted by Kolobov *et al.* (2017).

Since its demonstration in 2014 the technique has been further investigated and developed. Imaging has been performed without using beam splitters employing the effect of frustrated down-conversion [see Sec. II.B, Fig. 3(b)], thereby allowing more stable and fast image acquisition (Kviatkovsky *et al.*, 2020; Paterova *et al.*, 2020; Kviatkovsky, Chrzanowski, and Ramelow, 2022) and even leading to experiments that recorded videos with undetected photons (Gilaberte Basset *et al.*, 2021). The imaging resolution and its dependence on the involved wavelengths has been studied, which led to applications of microscopes to the midinfrared regime, where the image can be detected using standard near-IR cameras (Kviatkovsky *et al.*, 2020; Paterova *et al.*, 2020); see Fig. 11. The resolution limit is determined by the undetected light that passes through the object. Thus, it is in principle possible to obtain resolution characterized by a wavelength much shorter than the detected wavelength (Viswanathan, Lemos, and Lahiri, 2021b; Fuenzalida *et al.*, 2022). Note that the quantum imaging experiment discussed by Lemos *et al.* (2014) is enabled by the momentum correlation between twin photons, whereas the imaging experiments discussed by Viswanathan, Lemos, and Lahiri (2021a, 2021b) and Kviatkovsky, Chrzanowski, and Ramelow (2022) are enabled by the position correlation. These are two complementary domains of quantum imaging with undetected photons.

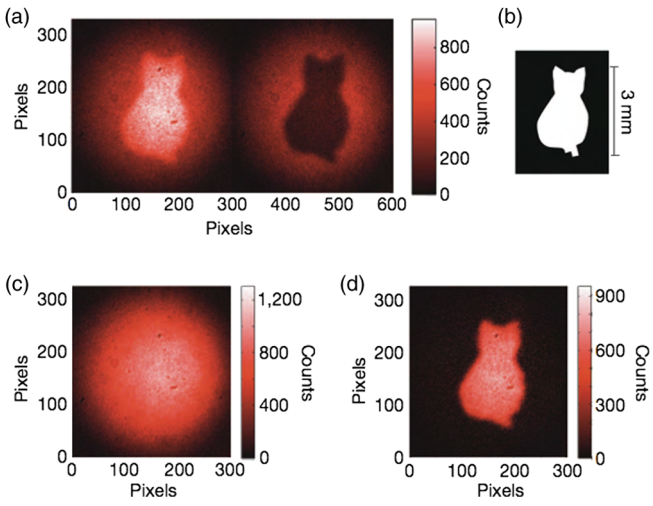

FIG. 10. (a) The two outputs of the beam splitter. The image of the cat shows the area where interference occurs. (b) The absorptive object: the cat. (c) The sum of the outputs of the beam splitter contains no image. (d) Subtraction of the outputs leads to enhancement of the image contrast. Adapted from Lemos *et al.*, 2014.

We stress that imaging by path identity is fundamentally different from ghost imaging (Pittman *et al.*, 1995; Gatti *et al.*, 2004). In ghost imaging, the light that interacts with the object must be detected and coincidence or an equivalent measurement must be performed (Fig. 12). In contrast to ghost imaging, imaging by path identity does not involve the detection of the light that illuminates the object, and it does not involve any coincidence or equivalent measurements. Besides, ghost imaging can be understood purely classically (Bennink *et al.*, 2004), while imaging by path identity is a genuinely quantum mechanical phenomenon, as described in Sec. III.C.

B. Quantum spectroscopy with undetected photons

In Sec. IV.A, we explained how the principle of path identity is used for imaging. This effect, based on the

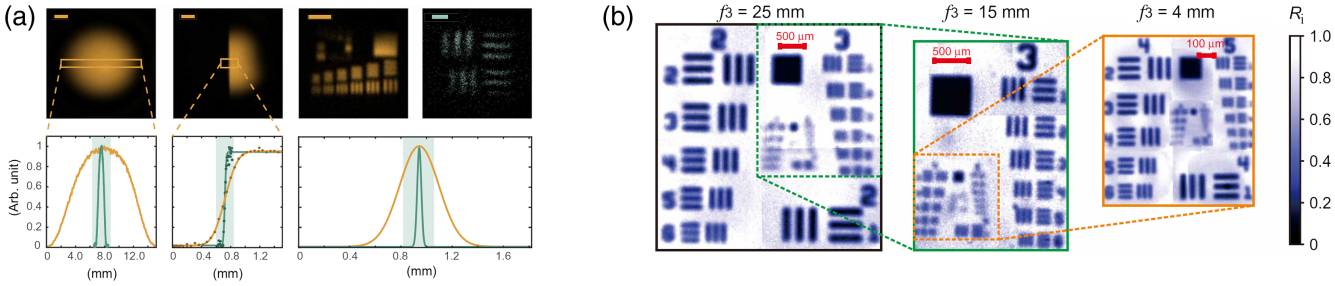

FIG. 11. Midinfrarer microscopy with undetected photons. Two separate experiments demonstrated how a magnification system in the idler photon can lead to a microscope where the magnified image can be observed with standard infrared cameras. (a) Characterization of an imaging arrangement. The yellow curves indicate the unmagnified setup, while the green one shows the magnified one. The system shows a magnification of roughly 10 times. From Kviatkovsky *et al.*, 2020. (b) Resolution test measured with different focusing lenses. From Paterova *et al.*, 2020.

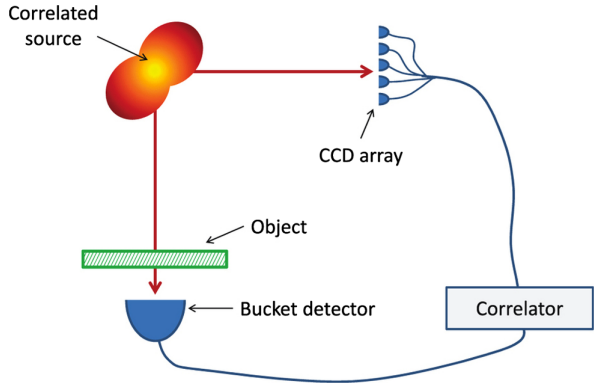

FIG. 12. Ghost imaging is fundamentally different from imaging by path identity. In ghost imaging, the photons interacting with the object must be detected, and coincidence or an equivalent measurement must be performed. Adapted from Ragy and Adesso, 2012.

distinguishability of the photons in the spatial degree of freedom, can be applied to distinguishability in any degree of freedom, such as frequency domain. In Sec. IV.C, we explain how distinguishability in the frequency domain is

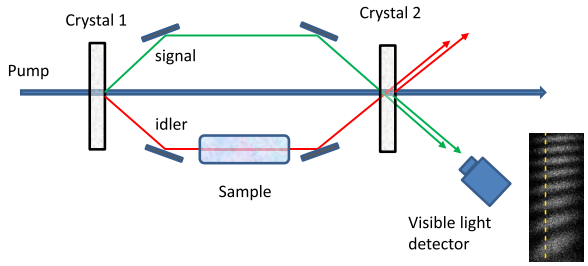

FIG. 13. Principle scheme of spectroscopy with undetected photons. Two nonlinear crystals probabilistically emit identical and frequency correlated photon pairs. Identifying the paths of the respective photon pairs then allows one to observe interference in the signal photon. The acquired phase in the interference pattern depends on all three photons involved, the pump, signal, and idler, which are all at different frequencies. The interference visibility is governed by the transmission of the sample placed in the idler beam. Thus, at an absorption line of the sample under study the visibility in the spectrogram detected at the camera disappears. From Jean-Pierre Wolf.

exploited to accomplish spectroscopy with undetected photons. Today, spectroscopy is one of the most important workhorses in various fields in science and technology. Ranging from biology, chemistry, and climate research to fundamental cosmology, spectroscopy reveals key information about these diverse systems in a broad range of the electromagnetic spectrum (Stewart, 2004). Especially noteworthy are the infrared and far-infrared regions of the electromagnetic spectrum. These spectral ranges are typical for vibrational and rotational modes of different molecules, such as carbon dioxide.

However, special optical equipment and especially detectors with low efficiencies pose significant technological obstacles. Kalashnikov *et al.* (2016) used the principle of path identity to probe the spectrum of carbon dioxide and detected it at a different wavelength. Particularly notable is that the detection wavelength can be chosen such that it lies in the visible range where efficient detectors exist (Wolf and Silberberg, 2016).

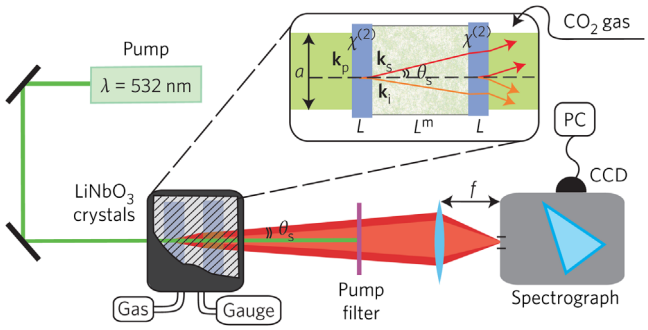

FIG. 14. Experimental details of spectroscopy with undetected photons. Two lithium niobate nonlinear crystals are employed to create the nondegenerate but perfectly frequency correlated photon pairs. A quasicollinear emission scheme is used to identify their respective paths, and the emission angle θ of the down-conversion is small relative to the pump beam waist a. A vacuum chamber is used to host the two nonlinear crystals and the sample of interest, which is CO_2 here. A lens images the down-converted photons onto a slit to select a specific angular emission spectrum. The following spectrograph enables precise determination of the signal wavelength. Finally, a two-dimensional spectrogram in the angular-wavelength dimensions is recorded by a camera. Adapted from Kalashnikov *et al.*, 2016.

In Sec. III we studied the explicit dependencies of the expected intensities upon an object in the idler path; see Fig. 4. The linear relation between the observed visibility and the absorption of the idler beam suggests that this technique could be used for absorption spectroscopy. Wolf and Silberberg (2016) explored this effect to detect infrared absorption lines of carbon dioxide molecules (CO_2) detecting visible light. The principle scheme is depicted in Fig. 13. Two nonlinear crystals made from lithium niobate ($LiNbO_3$) emit nondegenerate photon pairs correlated in their frequencies. The idler photon is centered at around 4161 nm and can be absorbed by the CO_2 molecules between the two nonlinear crystals, as shown in Fig. 13. Overlapping the signal and idler photon paths identically at the second nonlinear crystal allows one to observe interference in the signal photon. The interference visibility is thereby determined on the transmission of the CO_2 gas sample. Figure 14 shows the experimental apparatus. In contrast to the idealized scheme in Fig. 13, all rays in Fig. 14 are guided collinearly through the absorbing medium. The nonlinear crystal is pumped with a 532 nm laser. It produces quasicollinear photon pairs perfectly correlated in their degenerate wavelength at $\lambda_s = 610$ nm and $\lambda_i = 4161$ nm for signal and idler photons, respectively. After the two nonlinear crystals and the medium to be studied, the intensity

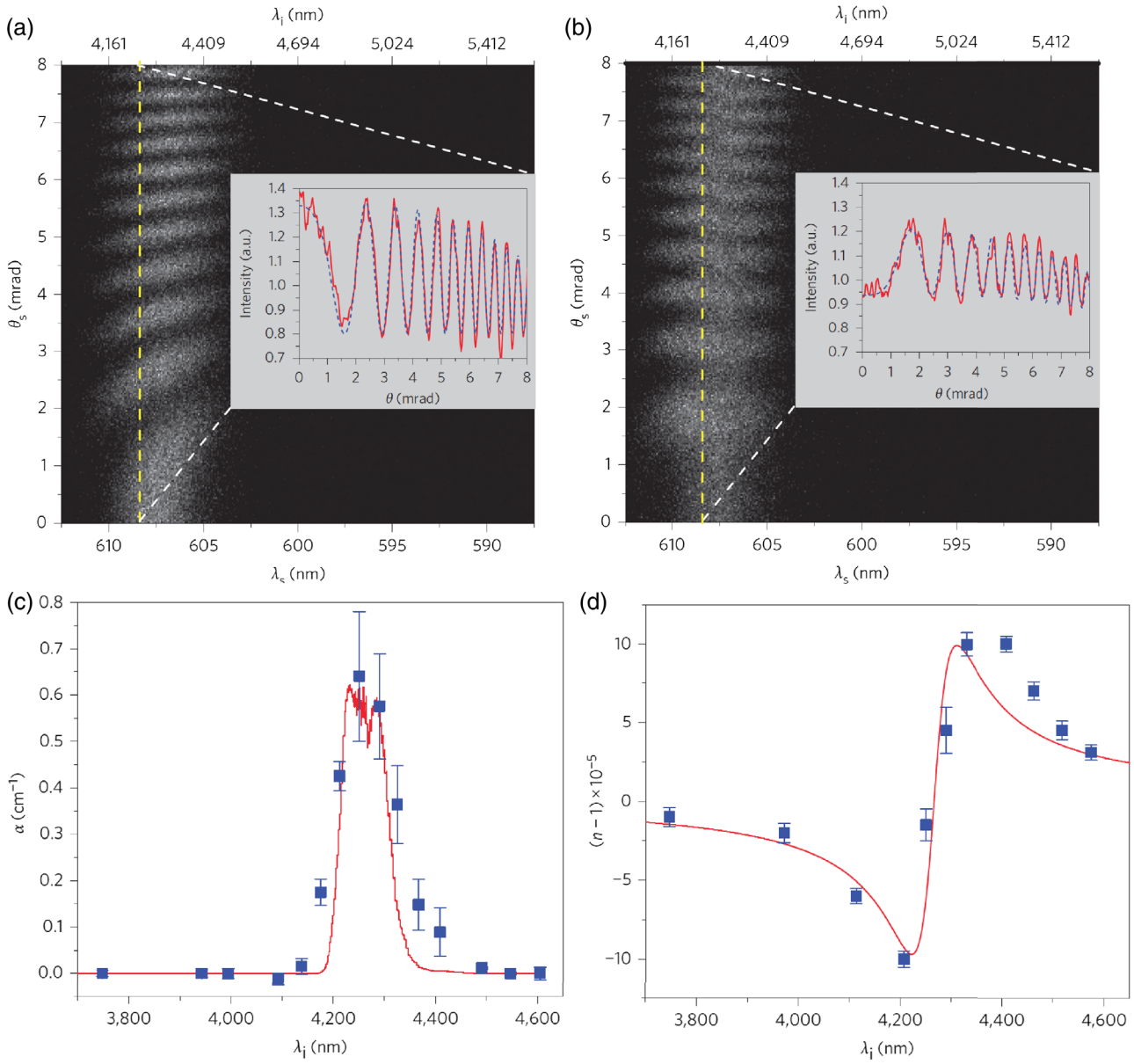

FIG. 15. Experimental results. (a) Calibration measurement in a quasivacuum regime (inset). Selecting a specific wavelength cut and fitting Eq. (18) yield the absorption coefficient for the vacuum and a phase reference. (b) Spectrograph with a filled carbon dioxide chamber. The decrease of visibility and the phase shift is due to the absorption and refractive index change between the vacuum in (a) and the carbon dioxide in (b). The data displayed in (c) and (d) show the wavelength dependence of the absorption and refractive index coefficient in the vicinity of the resonance for carbon dioxide at a pressure of 10.5 torr. The blue squares represent experimental measurements, and the red curve is a theoretical calculation using HITRAN data for (c) and a Kramers-Kronig relation for (d). Data figures from Kalashnikov *et al.* (2016).

of the signal photon is given by the following relationship (Belinsky and Klyshko, 1992; Klyshko, 1993):

$$I(\lambda_s,\theta_s) \propto \frac{1}{2}\mathrm{sinc}^2\left(\frac{\delta}{2}\right)[1+|\tau_{i,m}|\cos(\delta+\delta_m)],$$
$$\delta(\lambda_s,\theta_s) = \frac{L(k_p-k_i-k_s)}{\cos(\theta_s)},$$
$$\delta_m(\lambda_s,\theta_s) = \frac{L_m(k_p-k_i-k_s)}{\cos(\theta_s)}, \tag{18}$$

where θ_s describes the emission angle, the phase shifts depending on the wavelengths and emission angles resulting from the nonlinear crystals δ, and the medium to be studied δ_m. The wave vectors k_j are related to the wavelength and their respective refractive index n_j via $k_j = 2\pi n_j/\lambda_j$. Furthermore, the transmittivity amplitude $\tau_{i,m}$ is connected by $\exp(-\alpha_m L_m)$ to the amplitude absorption coefficient α_m. For vanishing transmittivities $\alpha_m = 0$ the visibility V also vanishes. Here the visibility is defined as $V = (I_{\max} - I_{\min})/(I_{\max} + I_{\min})$. Light scattering, especially in biotissues, can be taken into account; for details see the Supplemental Material of Kalashnikov *et al.* (2016).

Imaging the SPDC radiation onto a slit in front of the spectrograph results in a two-dimensional wavelength-angular spectrogram recorded with an electron multiplying charge-coupled device (or EMCCD) camera. The small angular spread of the SPDC of about 10 mrad introduces the necessary phase shift between a signal and idler to measure the visibility. Using a spectrograph allows one to precisely control the detected visible spectrum at around 610 nm. Energy conservation within the down-conversion process combined with knowledge of the pump and signal wavelengths allows one to infer the idler wavelength interacting with the medium to be studied. Figure 15 shows a typical experimental measurement of a two-dimensional wavelength-angular spectrogram. A calibration measurement under ideal near-vacuum conditions is performed first; see Fig. 15(a). Next the medium of interest, in this case CO_2, is placed between the two nonlinear crystals. Owing to absorption and refractive index differences between CO_2 and the vacuum, the observed visibility drops and the relative phase changes, respectively, as shown in Fig. 15(a) and 15(b). Selecting one specific wavelength cut and fitting Eq. (18) to the experimentally measured data allows one to determine the absorption coefficient α_m as well as the refractive index n_m [depicted in Fig. 15(d)].

The complex refractive index describes both the absorption and the refractive index in a single complex number. The Kramers-Kronig relations connect the real and imaginary parts of the complex refractive index. If one of the two parts of the complex number is known, the other part is uniquely determined. Using these relations, the experimental data can be subjected to a consistency check. Indeed, the experimentally observed absorption spectrum and refractive index changes reproduce the Kramer-Kronig relations well, as depicted in Figs. 15(c) and 15(d). Further developments of these works have shown how one can perform spectroscopy without a spectrometer. Lindner *et al.* (2020, 2021) instead used one displaceable mirror, which introduces additional phase shifts. A Fourier transform of the interferograms of many mirror positions gives a spectrum from which one can then extract properties of the samples.

The suggested method of spectroscopy with undetected photons allows the direct measurement of the complete imaginary refractive index of a medium (Paterova *et al.*, 2018a). The strength of this technique lies in the possibility of probing the medium at far-infrared to even terahertz frequencies (Tonouchi, 2007) and detecting the signal at visible wavelength. And, indeed, in 2020 an experiment demonstrated quantum sensing and quantum spectroscopy in the terahertz regime (Kutas *et al.*, 2020, 2021) using an adaptation of the experiment by Herzog *et al.* (1994) described in Fig. 3(b). Kutas *et al.* (2020, 2021) showed how terahertz photons interact with the sample in free space, and information about the sample thickness was gathered by measuring visible photons; see Fig. 16. In this way, they could use a standard, uncooled CMOS camera for the detection and do not need any expensive pulsed laser. Specifically, they used a pump laser with a wavelength of 660 nm. Photon pairs are generated using SPDC, with a signal wavelength of 661 nm and an idler frequency in the terahertz regime. In these frequency regimes, down- and up-conversion of thermal

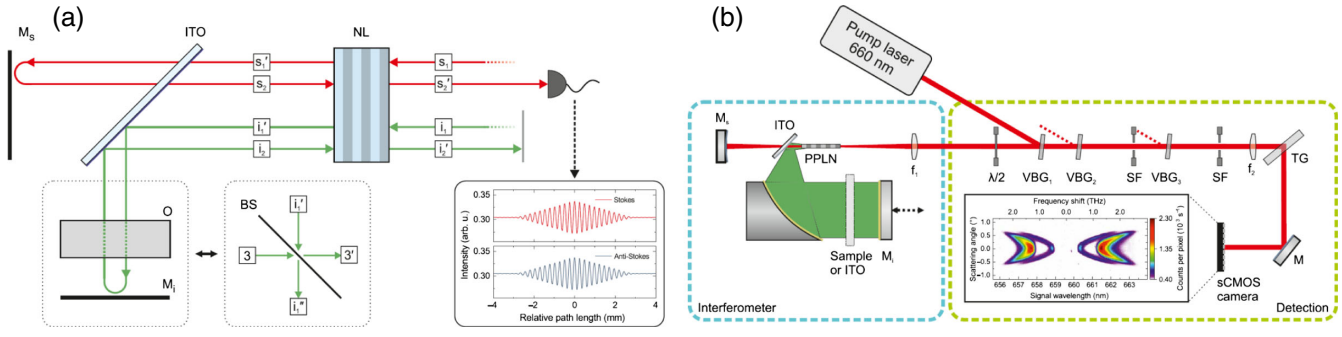

FIG. 16. Terahertz quantum sensing using frustrated photon-pair generation. (a) A conceptual depiction shows that the signal s_i goes through the nonlinear crystal (NL) and is directly reflected back. The idler i_i is reflected at an indium tin oxide (ITO) coated glass and interacts with the object before it is reflected back to the crystal. Two-photon quantum interference there allows one to measure the depth information of the object. (b) Concrete plot of the experimental setup, with pump laser, wave plates ($\lambda/2$), a nonlinear periodically poled lithium niobate crystal (commonly known as PPLN), volume Bragg grating (VBG), transmission grating (TG), and spatial filters (SFs). Adapted from Kutas *et al.*, 2020.

radiation are significant and need to be carefully studied (Haase *et al.*, 2019). The terahertz idler interacts with the object while the signal is untouched. The signal and idler and the laser all arrive at the crystal after a reflection, leading to a potential second pair-creation process. As the creation processes are coherent, the two creation processes interfere. The object's refractive index results in a change of optical length of the idler photon, and thereby a shift of the envelope of the interference pattern. Haase *et al.* (2019) first measured the refractive index by standard interferometric methods and could thereby directly infer the depth of the object by observing the shift of the envelope. In a follow-up work, Kutas *et al.* (2021) showed how to extend their technique to spectroscopy in the terahertz regime. Specifically, they demonstrated the absorption measurements of the molecules.

A combination of the imaging and spectroscopy techniques allows one to perform spectroscopy without using a spectrometer by detecting photons only on a camera (Paterova *et al.*, 2017). The sensitivity of the spectroscopy technique can be enhanced by performing spectroscopy using multiple sources in a series (Paterova and Krivitsky, 2020), thus combining the cavity case (Ou and Lu, 1999) with the spectroscopy using the undetected photon technique.

C. Optical coherence tomography with undetected photons

Optical coherence tomography (OCT) is a method in classical optics to determine optical properties of a sample at specific depths within it (Huang *et al.*, 1991; Fercher *et al.*, 2003). The technique is typically implemented in a Michelson interferometer [Fig. 17(a)]. A thick sample is placed in one path of the interferometer. Light is partially reflected from the sample's front surface and partially penetrates the sample before it is reflected from various inside layers. The reflected light is then recombined with light from the second path of the interferometer and interference is observed. By employing light with a short coherence length, the path-length requirements to observe interference are met only if the reflection occurs at a particular depth of the sample. Thus, properties determined from the interferogram (such as reflectivity) correspond to a particular depth of the sample. An adjustment of the path-length difference by moving the mirror in the second path allows one to tune the depth at which the object is probed. In this way, the method provides a way of imaging different "depth sections." Among other fields, the technique is frequently used in the life sciences and medicine (Fujimoto *et al.*, 1995; Puliafito *et al.*, 1995; Spaide *et al.*, 2018).

The technique can be extended using the concept of path identity. In this case, the interference resulting from indistinguishability of the origin of a photon pair is used to probe sample properties in a laterally resolved way. Instead of employing a classical interferometer, a Zou-Wang-Mandel (Vallés *et al.*, 2018) or a Herzog-Rarity-Weinfurter-Zeilinger (Paterova *et al.*, 2018b) arrangement have been used to probe a sample placed in the undetected beam between the two photon-pair sources.

The schemes based on path identity make use of the coherence length requirements of the nonlinear interferometer; see Jha *et al.* (2008). In particular, they exploit the fact that interference is observed only if the path-length difference between the signal and idler photons is tuned in a way that does not allow one to recover the source of a photon pair by a difference in the detection times of the two photons.

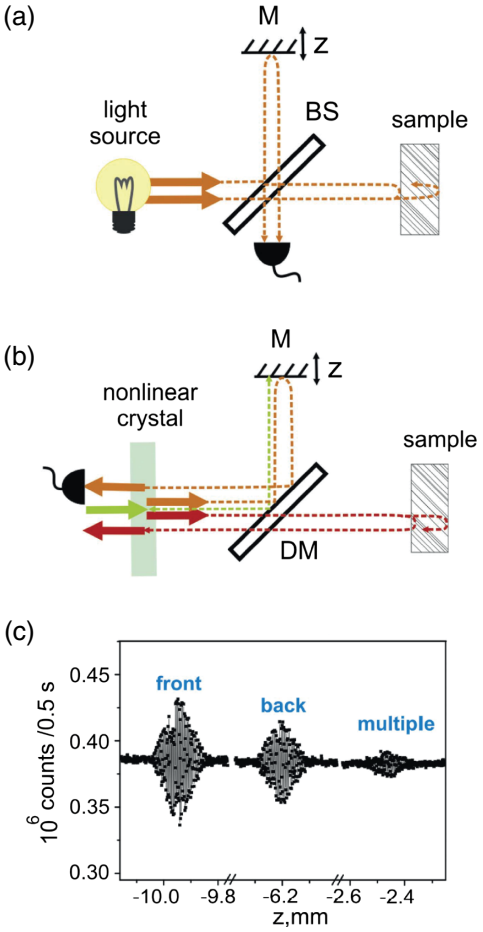

FIG. 17. Classical optical coherence tomography and optical coherence tomography with undetected photons. (a) Classical OCT is typically implemented with light of a short coherence length in a Michelson interferometer. The reflection from different layers within the object produces an interference pattern if recombined with light that has traveled the corresponding distance in the second path. The sample can be laterally resolved by tuning this distance using the mirror M. (b) The specified implementation of OCT with undetected photons uses nondegenerate photon pairs produced by a nonlinear crystal. The signal (idler) beam emitted toward the right is reflected back through the crystal via the mirror M (via the sample). Consequently, interference in the rate of detected photon pairs can be observed. Only the signal beam is detected toward the left of the source. The observed interference is affected by the properties of the sample if the coherence length requirements are met. This is the case if the idler photon is reflected at a particular depth of the object that corresponds to the length of the signal path. It is thus possible to probe different depths of the sample. (c) Example showing the detected rate of signal photons (at 582 nm) as the signal path length is scanned by translating the mirror M in the z direction. The sample in the idler beam (at 3011 nm) in this case is a Si window. Reflections at both the front and back surfaces as well as multiple reflections result in interfering signal photon rates at the corresponding mirror positions. Adapted from Paterova *et al.*, 2018b.

This allows one to perform the following procedure. If the object is thick and partially transparent, multiple possibilities exist for the idler beam to be reflected between the two SPDC processes. Reflections at different depths of the sample correspond to different path lengths of the idler beam between the two possible SPDC processes. Typically, the idler beam can be reflected by layers within the sample that are separated by a lateral distance that exceeds the coherence length. In this case, it is possible to tune the path length of the signal beam to observe interference corresponding to a particular path length of the idler beam [Fig. 17(b)]. Thus, the transmission and phase shift at different depth sections of the sample (for which the path-length requirements are met) affect the observed interference pattern in the signal beam.

As an example, we show a result of the experiment by Paterova *et al.* (2018b). They used the method to determine the positions of reflective layers in different samples, including the reflections off the front and back surfaces of a Si window [Figs. 17(b) and 17(c)]. The object is probed using IR light, while the wavelength of the detected light lies in the visible range.

This allows one to probe sections of different depths of the object that reflects only undetected light, while the detection and the scanning of the depth is performed in another light beam, which typically is at a different wavelength.

Recently, a further adaptation of this scheme was demonstrated that featured the detection in the Fourier domain, i.e., replacing the detector by a spectrometer (Vanselow *et al.*, 2020). This modification allows one to reconstruct the properties of the sample at different depths via a Fourier transform [see (Fercher *et al.* (2003) for the classical technique] of the spectroscopic data. It thus eliminates the requirement to physically move a mirror in order to scan the path length; see Fig. 18. This allows, in the classical regime, for orders of magnitude higher sampling rates and significantly higher mechanical stability. Those advantages are crucial for practical applications and the development of future quantum technologies.

D. Dual-wavelength properties

The previously discussed imaging, spectroscopic, and tomographic schemes have one important common feature: the wavelength of the detected light can be different from the wavelength of the light that probes the sample. This fact opens up new possibilities in these fields because now one can probe samples at a frequency (wavelength) for which efficient and cheap detectors are not available.

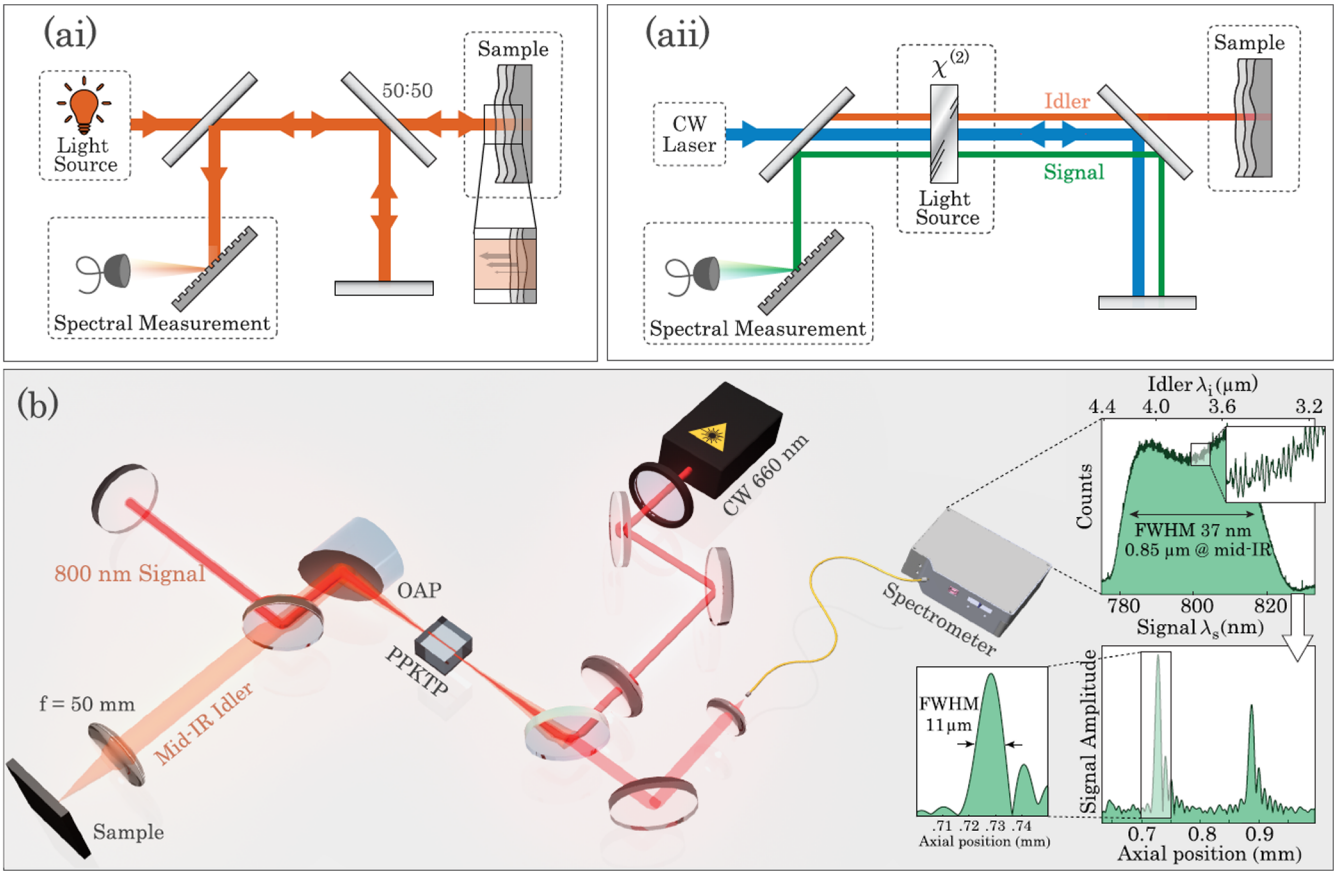

FIG. 18. Fourier-domain optical coherence tomography (FDOCT). (a)(i) Classical FDOCT. (a)(ii) The quantum version with undetected photons. In the experiment of Vanselow *et al.* (2020), they produced a midinfrared photon that interacted with the sample. The information is obtained through a spectrometer that detects the 800 nm signal photon. FDOCT has no moving parts and thus promises significantly higher sampling rates and stability. Adapted from Vanselow *et al.*, 2020.

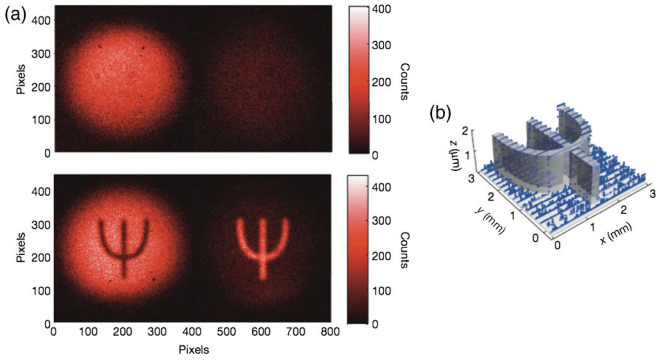

FIG. 19. (a) Top panel: no image is obtained when the object is imaged by 810 nm light. Bottom panel: both outputs of the beam splitter contain the image when the object is placed in the idler beam (1550 nm). (b) The phase object that is invisible to 810 nm light. Adapted from Lemos *et al.*, 2014.

As an example, we consider the imaging experiment. Here the wavelength of the detected light is 810 nm, and the wavelength of the light probing the object is 1550 nm. Figure 19 shows images of a phase object that is invisible to the detected light. This is because the chosen object [Fig. 19(b)] introduces a relative phase shift of approximately 2π for the detected light. However, the same object produces an approximately π phase shift for 1550 nm light and is therefore imaged in this scheme [Fig. 19(a)]. It is therefore impossible to realize transmission imaging by illuminating it with the detected light. However, one can obtain the image of this object in the imaging scheme with undetected photons. These two-wavelength effects not only have potential for commercial applications in terahertz or deep-UV spectroscopy but also lead to interesting questions on whether interference properties scale with λ_S or λ_I. The surprising answer is, with neither, as we now show.

E. Wavelength dependence of interference fringes with undetected photons

It was shown that the setup for quantum imaging with undetected photons (Fig. 10) can be used for interferometry with undetected photons (Hochrainer *et al.*, 2017a). The associated phenomena exhibit several noteworthy features compared to standard classical interferometry.

In a traditional two-path interferometer, spatial fringes appear if the interfering beams are misaligned relative to one another. A tilt of one of the beams results in a striped interference pattern, whereas the additional propagation distance or defocused lens system causes circular fringes to appear.

In a Zou-Wang-Mandel experiment, it is possible to observe analogous interference fringes if the undetected idler beam from one source is slightly misaligned with respect to the other (Hochrainer *et al.*, 2017a). Without directly interacting with the interfering signal beams, spatial interference patterns are formed as depicted in Fig. 20.

While such patterns in classical interferometry are often explained as the wave fronts of the two interfering beams being tilted or curved with respect to one another, it is not possible to attribute a specific phase structure to one photon beam of a down-converted pair. Thus, a classical explanation

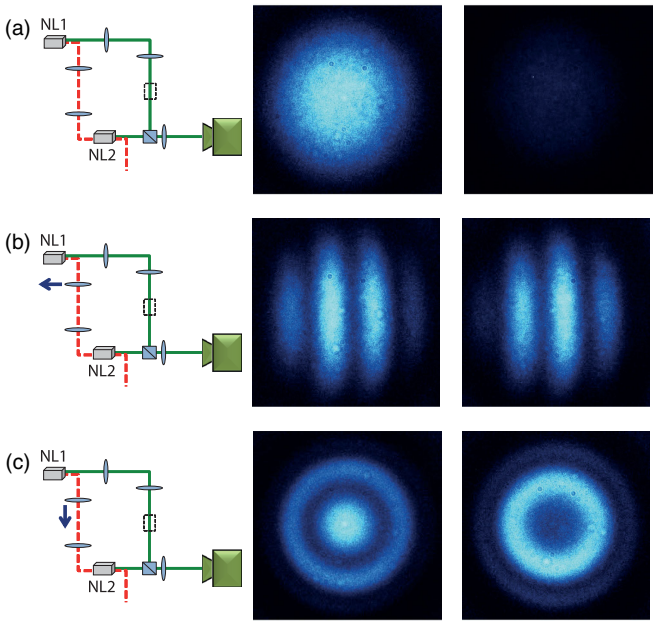

FIG. 20. Interference fringes produced with undetected photons. The spatial interference pattern observed in the superposed beam can be controlled by manipulating a third beam, which is not detected. The appearance of the pattern is analogous to that obtained if the same manipulations were performed on one of the interfering beams in a traditional two-path interferometer. From Hochrainer *et al.*, 2017a.

fails to explain the observed interference phenomenon, which can be understood in a similar way as the phase imaging with undetected photons; see Sec. IV.A. It relies on the fact that a single phase factor is attributed to the photon pair as a whole and not to the individual photons of a pair.

The observation of a spatial structure in ZWM interference can explain earlier results obtained by Grayson and Barbosa (1994), in which a reduced visibility was observed due to a slight misalignment of the undetected beams. If the total intensity over the entire spatially structured interference pattern is determined using a bucket detector, the fringes amount to a lower measured visibility.

In classical interferometry, the scaling of the spatial structure of the interference patterns depends on the wavelength of the interfering light. Because of the different wavelengths of signal and idler beams, the following question arises: which wavelength characterizes the pattern of interference fringes that are controlled with undetected photons? As the fringes are manipulated in the idler beam and observed in the signal beam, two wavelengths are involved in their formation.

This question was analyzed by comparing circular fringes obtained after defocusing the lens system in the idler beam to circular fringes obtained if the same lens manipulation were performed on one of the interfering beams in an analogous classical interferometer (Hochrainer *et al.*, 2017a). In the classical case, the radius ρ_n of the nth minimum and maximum obeys[1] (Born and Wolf, 1999)

[1]The integer $n = 0, 1, 2, \ldots$ corresponds to the maxima, and the half integer $n = 1/2, 3/2, 5/2, \ldots$.

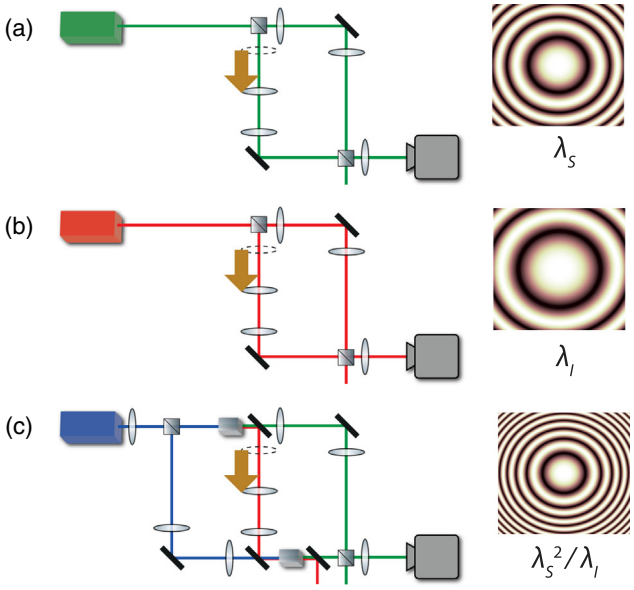

FIG. 21. Wavelength dependence of circular interference fringes. The first two lines depict classical interferometers and circular fringes obtained by shifting the lens by a fixed distance. In (a) the light is at the signal wavelength (810 nm), whereas in (b), it is at the idler wavelength (1550 nm). (c) The interference fringes obtained in the ZWM setup, where the spacing of the fringes corresponds to the equivalent wavelength $\lambda_{\mathrm{eq}} = \lambda_S^2/\lambda_I$. From Hochrainer, 2019.

$$\frac{d}{2f_C^2}\rho_n^2 + \varphi_0 = n\lambda, \tag{19}$$

where d denotes the effective additional propagation distance that is caused by the lens shift, f_C represents the focal length of the lens in front of the camera [see Fig. 20(c)], φ_0 subsumes all spatially independent phase factors, and λ is the wavelength of the interfering light.

If Eq. (19) is applied to the circular fringes produced in the ZWM interferometer, the wavelength characterizing the pattern is determined to be (see Fig. 21)

$$\lambda = \frac{\lambda_S^2}{\lambda_I}. \tag{20}$$

Note that this observed "equivalent wavelength" (420 ± 7 nm) is significantly smaller than any of the involved wavelengths (signal, 810 nm; idler, 1550 nm), even the pump (532 nm).

This peculiar feature is understood as a combined effect of the phase shifts being introduced at the wavelength of the undetected idler photons and the detected photons at the signal wavelength (Hochrainer *et al.*, 2017a). Because of momentum conservation in nondegenerate SPDC, the photon at the longer wavelength is emitted at a larger angle with respect to the optical axis than its partner photon at the shorter wavelength. The difference in emission angles is determined by the wavelength ratio. This results in a wavelength-dependent scaling of the interference pattern, which in our case leads to fringes with a smaller spacing than expected when one considers only the idler wavelength. The same effect gives rise to the wavelength-dependent magnification (or demagnification in this case) in quantum imaging with undetected photons; see Sec. IV.A.

V. RECONSTRUCTION OF THE QUANTUM STATE OF UNDETECTED PHOTONS

The experiments described in Sec. IV make use of induced coherence without induced emission in a multimode setting. The results show that it is possible to determine properties of a sample placed in one of the beams by performing measurements only on the other beam. Instead of employing photon pairs in a known quantum state in order to determine unknown properties of an object, it is possible to use a known object and determine properties of the employed photon pairs, and to obtain information about one photon by detecting the other.

A second branch of applications of the concept of path identity exploits the possibility of measuring correlations between two photons by detecting only one of them. Correlation measurements of photons are used ubiquitously in today's quantum optics. Traditionally, such measurements are performed using the method of coincidence detection, which is a powerful experimental tool in both fundamental science and technology (Burnham and Weinberg, 1970; Pan *et al.*, 2012).

The adaptation of these techniques to interference by path identity extends the reach of optical experiments to regimes in which only one of the photons can actually be detected (such as if one of two correlated photons is at a wavelength for which no suitable efficient detector currently exists).

From a fundamental perspective, the experiments show that information stored in the correlation of a photon pair can be accessed by measurements on only one of its constituents. In other words, a second order property of light can be transferred to a first order property and can be determined using a single detector.

A. Quantifying the momentum correlation between two photons by detecting one

Traditionally, the transverse momentum correlation between two photons is measured by the coincident detection of both photons. One way to implement such a measurement is depicted in Figs. 22(a) and 22(b). The two photons are detected with individual detectors that resolve the transverse momentum of the respective photon. The transverse momenta are proportional to the transverse component of a wave vector of signal and idler photon (denoted by $\mathbf{q}_S$ and $\mathbf{q}_I$). By scanning the relative positions of the detectors, it is possible to determine the conditional probability distribution $P(\mathbf{q}_I|\mathbf{q}_S)$ of detecting one photon with a particular momentum, given that the momentum of the other photon is known. The variance $\sigma^2(\mathbf{q}_I|\mathbf{q}_S)$ of this conditional probability distribution serves as a quantitative measure for the strength of the momentum correlation. Such measurements have been implemented in a variety of different ways (Howell *et al.*, 2004; Edgar *et al.*, 2012). However, all of these traditional methods require the joint detection of both correlated photons. Using the concept of path identity, it is possible to determine the correlation strength without this requirement.

A quantitative measurement of the momentum correlation between two photons by detecting only one of them has been demonstrated experimentally (Hochrainer *et al.*, 2017b); see

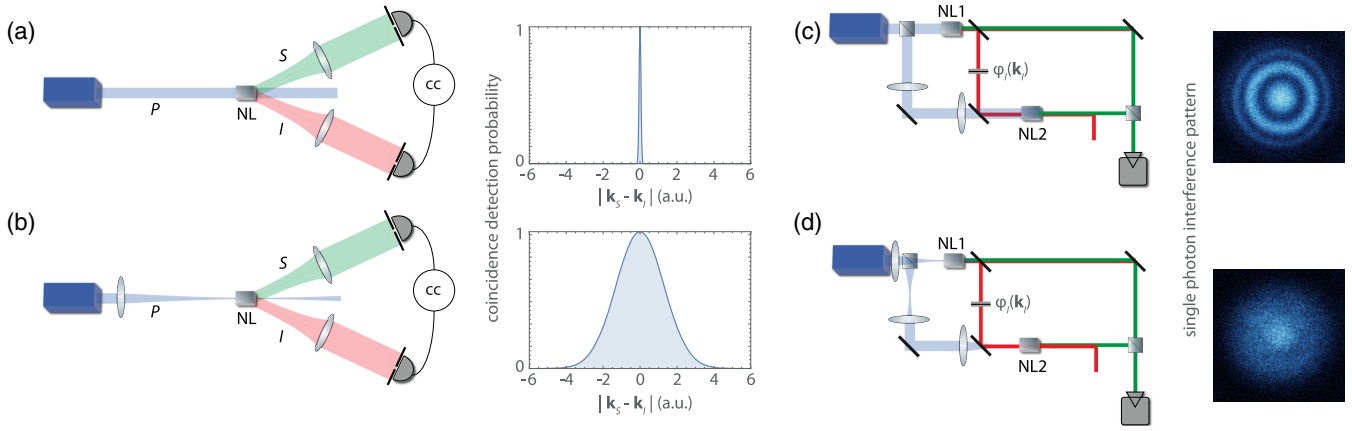

FIG. 22. Measuring the transverse momentum correlation of a photon pair with and without coincidence detection. (a),(b) In the traditional method, each of the two photons is registered by a detector in a way such that its individual momentum can be inferred. By comparing the coincidence detection events at different pairs of momenta, the correlation is quantified. (a) A sharp correlation (implemented by a large pump focus) leads to a narrow coincidence peak at a particular relative momentum, whereas (b) weakly correlated photons (small pump waist) lead to a similar amount of coincidence counts in a wider range of momenta (Monken, Ribeiro, and Pádua, 1998). Using the concept of path identity, two copies of the photon-pair source are arranged in a ZWM configuration. By introducing a spatially dependent phase shift on the undetected idler beam between the two sources, a single-photon interference pattern is observed in the superposed signal beam. The visibility of the pattern depends on how strongly signal and idler photons are correlated. (c) In the case of a loosely focused pump beam, the photons are highly correlated in momentum, and spatial features of an interference pattern are visible. (d) The opposite is true of weakly correlated photons. The visibility is determined from measurements on only one of the photons and can be used to quantitatively reconstruct the correlation between the two photons. Adapted from Hochrainer, 2019.

Lahiri *et al.* (2017b) for a theoretical description. In this experiment, a correlated photon pair is produced in a superposition of two sources NL1 and NL2. One of the photon beams from each source is aligned to be indistinguishable [Figs. 22(c) and 22(d)]. The other beams from each source are superposed on a beam splitter and subsequently detected on a camera. The detection is performed in such a way that the momentum of a detected photon can be inferred, although it is unknown which source it was initially emitted from. A momentum-dependent phase shift $\varphi_I(\mathbf{q}_I)$ is introduced on the undetected idler beam between the sources. The phase shift was experimentally implemented by defocusing the lens system between the two sources. As in Sec. IV.E, this results in the formation of a circular interference pattern on the camera.

When the momentum correlation between the signal and idler photons is varied, the appearance of the pattern changes [Figs. 22(c) and 22(d)]. This fact allows one to reconstruct how strongly the momenta of the two photons of a pair are correlated, although the measurement is performed by observing only one of them. In the experiment, the spatially dependent visibility of the resulting interference patterns was used to numerically evaluate the strength of the momentum correlation $\sigma^2(\mathbf{q}_I|\mathbf{q}_S)$ (Hochrainer *et al.*, 2017b); see Fig. 23.

The reason for the dependence of a single-photon interference pattern on the correlation between two photons becomes apparent when one considers how the pattern is formed; compare to Sec. IV.A. The camera is located behind a lens system that maps one transverse momentum of the superposed signal beam $\mathbf{q}_S$ to one point on the camera. The interference fringe at a selected point on the camera is observed by detecting signal photons and is influenced by the phase shift introduced on the corresponding partner idler photons. In the case of perfect momentum correlation between the detected signal photon and the undetected idler photon, this phase is controlled by phase shifts of a particular momentum of the

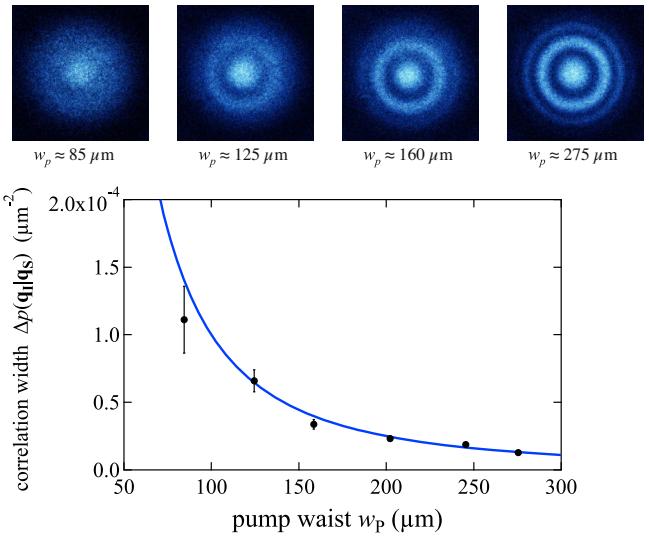

FIG. 23. Experimental results of the correlation measurement between two photons when only one of them is detected. The correlation between the signal and idler photons was tuned by changing the waist (w_P) of the pump beam in both crystals simultaneously. The fringe pattern observed in the interference of the two signal beams gradually exhibits a higher visibility as the correlation between the signal and idler photons is increased. This allows one to numerically reconstruct the variance of the conditional probability distribution of the momentum of an idler photon, given the momentum of a signal photon, without relying on coincidence detection. The results are shown compared to the theoretical prediction. Adapted from Hochrainer *et al.*, 2017b.

undetected beam. On the other hand, if the momentum correlation between the two photons is imperfect, the detection of a signal photon at a particular point on the camera does not allow one to precisely infer the momentum of its partner idler photon. Therefore, the phase shift $\varphi_I(\mathbf{q}_I)$ that determines the interference at that point on the camera can vary within a range that is determined by the momentum correlation. The observed phase in this case is not uniquely determined, but rather is given by a weighted average over the possible phase shifts corresponding to the possible $\mathbf{q}_I$. As a result, the visibility of the observed interference pattern is reduced for a weak momentum correlation.

The experiment shows that it is possible to access properties of a photon pair by measuring only a part of it. A measurement that traditionally requires coincidence detection of both photons can be performed with only one detector. In that sense, the "path identification" of the undetected beams plays the role of coincidence detection and can be used to access higher order properties of the photon pair with a single detector.

B. Quantifying quantum entanglement without coincidences

The following question arises: To what extent can the presented technique be generalized in order to perform measurements of other properties that usually require coincidence detection? It would be interesting to adapt the method to determine not only the momentum correlation but also the position correlation of a photon pair (or in general correlations in any conjugate or mutually unbiased measurement bases). This would allow an experimental test of quantum entanglement that relies solely on measurements of one photon.

A series of theoretical (Lahiri *et al.*, 2021; Zhan, 2021) and experimental (Lemos *et al.*, 2020) studies have explored how true quantum correction in the form of entanglement can be obtained in a related way. Rather than measuring the two entangled pairs, the main idea is to have two identical sources of entangled pairs. Now in the spirit of the ZWM experiment, the idler path from the first crystal is overlapped with the idler from the second crystal. In that way, a set of single-photon interference patterns can be generated. The entanglement of the two-photon quantum state can then be directly quantified by the visibility of the interference patterns. This field is still in its infancy, and we expect that the coming years will show the impact of this tool in the toolbox of quantum information experimentalists.

VI. ENTANGLED PHOTON SOURCES USING PATH IDENTITY

In this section, we explore the connection between the path-identity principle and photonic quantum information experiments. Photonic experiments that exploit quantum mechanical effects, such as Bell violations or BosonSampling, require either single-photon sources or entangled photon-pair sources. We start by explaining how to create single-photon sources using path identity. Furthermore, we describe how to generate entangled photons in higher dimensions using path identity. Finally, we present general schemes based on path identity to create genuine multiphoton and high-dimensional entangled quantum states.

Since addressing entanglement in detail is beyond the scope of this review, we refer the interested reader to Bruß (2002), Horodecki *et al.* (2009), and Plenio and Virmani (2014) for more information. Thorough reviews on how to experimentally create and detect genuine two-photon and multiphoton entanglement in two or more dimensions were given by Pan *et al.* (2012), Friis *et al.* (2019), Slussarenko and Pryde (2019), and Erhard, Krenn, and Zeilinger (2020).

A. Generation of multiphoton states with tailored parameters

The idea of frustrated or enhanced two-photon generation (see Sec. II.B) has been generalized to the case of multiple passes through the same nonlinear crystal in a resonant cavity for the SPDC photons. Among other interference effects, it has been shown that the time difference between the signal and idler photons can be controlled by filtering the emission spectrum by the cavity. This technique enables control over the correlation time (inverse bandwidth) between the signal and idler photons, which is analogous to greatly enhancing the crystal length for a particular wavelength band (Ou and Lu, 1999).

Further development of this idea led to the possibility of controlling multiple aspects of quantum states by exploiting nonlinear interference between multiple sources. Among other benefits, this approach enabled the generation of high-quality multiphoton states where the joint spectral amplitude or temporal mode structure can be tailored for specific applications (Su *et al.*, 2019; Cui *et al.*, 2020).

With the development of nanophotonic nonlinear optics, the cavity enhanced generation of photon pairs has since become an expansive field with numerous practical implications (Kues *et al.*, 2019; Feng, Guo, and Ren, 2020).

B. High-dimensional entanglement by path identity

We saw in Sec. II.C that Hardy proposed a source of polarization-entangled photons by overlapping the output of two crystals and modifying the polarization between the crystals. While this two-photon polarization-entangled source is a standard workhorse in quantum optics, it took 25 years until it was understood that the concept is much more generally applicable (Krenn *et al.*, 2017). The generalization was found only with the help of a computer program for designing quantum experiments (Krenn *et al.*, 2016; Krenn, Erhard, and Zeilinger, 2020).

To encode high-dimensional quantum information, we employ a multilevel physical degree of freedom. For photons there are several degrees of freedom capable of encoding quantum information beyond qubits. For example, the frequency bin (Olislager *et al.*, 2010; Bernhard *et al.*, 2013; Reimer *et al.*, 2016), time bin (Franson, 1989; Tittel *et al.*, 1998), path (Reck *et al.*, 1994; Schaeff *et al.*, 2012; J. Wang *et al.*, 2018), and the spatial modes (Allen *et al.*, 1992; Mair *et al.*, 2001) form such multilevel encoding degrees of freedom. In the following, we introduce the spatial degree of freedom, in particular, the orbital angular momentum (OAM) of photons (Yao and Padgett, 2011; Erhard, Fickler *et al.*, 2018).

The OAM of photons spans in principle an unbounded state space and is thus ideally suited to encode high-dimensional quantum states. Physically, the OAM essentially stems from a spatially varying phase distribution that helically wraps around the axis of propagation according to $\exp(i\ell\phi)$, with ϕ describing the azimuthal angle and the integer ℓ defining the amount of OAM in units of $\hbar$. A photon with nonzero OAM exploits one or more phase singularities[2] where the amplitude is zero. These phase singularities lead to the typical doughnut-shaped intensity distributions for light beams carrying OAM. The OAM forms an ideal test bed for proof-of-principle quantum experiments since many techniques to create, manipulate, and measure OAM on a single-photon level exist in the laboratory (Heckenberg *et al.*, 1992; Leach *et al.*, 2002; Marrucci, Manzo, and Paparo, 2006; Berkhout *et al.*, 2010; Morizur *et al.*, 2010; Babazadeh *et al.*, 2017; Fontaine *et al.*, 2019; Brandt *et al.*, 2020).

Historically, creating high-dimensional entanglement has relied on conservation laws of the utilized photon creation process (Mair *et al.*, 2001; Vaziri, Weihs, and Zeilinger, 2002; Krenn *et al.*, 2014). For example, in SPDC the OAM is conserved. Therefore, the OAM of the down-converted photons sums up to the OAM of the pump photon $\ell_p = \ell_s + \ell_i$. Using a pump beam with zero OAM ($\ell_p = 0$) yields a perfect anticorrelation $\ell_s = -\ell_i$ within the entangled quantum state. The desired coherent overlap is guaranteed since in principle no information is available on which combination of OAM modes is realized. However, the probability that a certain OAM correlation occurs is different for all OAM combinations. It is more likely that the two down-converted photons are found in a lower order OAM mode than at higher orders (Miatto *et al.*, 2012). This in turn results in inherently nonmaximal, though high-dimensional, entangled quantum states. There are methods to precompensate for (Kovlakov, Straupe, and Kulik, 2018; Liu *et al.*, 2018) or postcompensate for (Vaziri *et al.*, 2003; Dada *et al.*, 2011) this naturally occurring unbalance, which results in lower creation efficiencies or limitations in terms of versatility.

Creating high-dimensional entangled photon pairs using path identity represents a paradigm shift from previous schemes. Conceptionally, creating high-dimensional entangled photon pairs using path identity relies on indistinguishable, probabilistic, and coherently emitting photon-pair sources. As shown in Fig. 24, each nonlinear crystal probabilistically emits identical[3] photon pairs in the lowest order Gaussian spatial mode, which is denoted as $|0,0\rangle$. Inserting a mode-shifting element between two successive nonlinear crystals that is capable of performing a $+1$ operation on the quantum state $|0,0\rangle \rightarrow |1,1\rangle$ yields a d-dimensional entangled quantum state of the following form:

$$|\psi\rangle = (1/\sqrt{d})(|0,0\rangle + e^{i\phi_1}|1,1\rangle + \cdots + e^{i\phi_d}|d-1,d-1\rangle). \tag{21}$$

Adding additional control on the emission rate of each nonlinear crystal results in the ability to create arbitrary high-dimensional entangled quantum states $\sum_{i=0}^{d-1} \alpha_i |i,i\rangle$, with $\alpha \in \mathbb{C}$ and $\sum_i |\alpha_i|^2 = 1$.

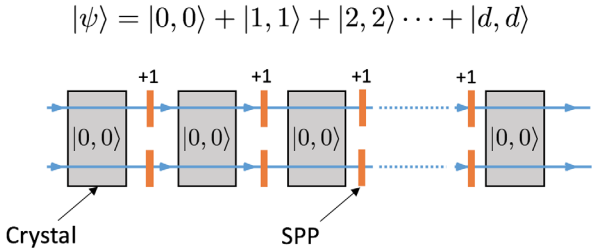

FIG. 24. New scheme to create two-photon high-dimensional entangled photon pairs using path identity, which is denoted as *entanglement by path identity* (Krenn *et al.*, 2017). Consecutively stacked indistinguishable photon-pair sources [nonlinear crystals (NLs)] coherently emit photon pairs. Identifying their paths leads to a coherent superposition of possible origins of a photon pair. Placing spiral phase plates between two NLs that add one quantum of orbital angular momentum to the incoming photons results in a d-dimensional entangled quantum state $|\psi\rangle$.

To realize this scheme experimentally (Kysela *et al.*, 2020), one needs indistinguishable photon-pair sources for all degrees of freedom. This means that their joint spectral amplitude, polarization, and paths are identical. Furthermore, to ensure coherent emission of two crystals or nonlinear crystals poses two main constraints (Zou, Wang, and Mandel, 1991; Herzog *et al.*, 1994; Jha *et al.*, 2008; Kulkarni, Kumar, and Jha, 2017).

The first condition, which is analogous to Eq. (6), is that the optical path-length difference of the pump beam and the two down-converted photons must be smaller than the coherence length of the pump laser, e.g.,

$$|L_P - L_{\mathrm{DC}}^a - L_{\mathrm{DC}}^b| \leq L_P^{\mathrm{coh}}, \tag{22}$$

with L_P denoting the optical path length of the pump beam, L_{DC} representing the optical path length of the respective down-conversion photon, and L_P^{coh} denoting the coherence length of the pump laser.

The second condition is given by the following optical path-length difference of the down-conversion photons and their coherence length:

$$|L_{\mathrm{DC}}^a - L_{\mathrm{DC}}^b| \leq L_{\mathrm{DC}}^{\mathrm{coh}}, \tag{23}$$

with $L_{\mathrm{DC}}^{\mathrm{coh}}$ describing the coherence length of the down-conversion photons.

The first condition is given by Eq. (22) and can be fulfilled by choosing a narrow band pump laser with a coherence length of several centimeters. The second condition is more difficult to satisfy. Typically, photons created via SPDC have a spectral bandwidth of the order of nanometers. In turn, this yields a coherence length of approximately tens of micrometers. Matching the optical path length of the two down-conversion photons can be difficult. For example, birefringence in the nonlinear crystals can lead to a substantial mismatch of the temporal overlap and thus to indistinguishability. These effects can be avoided altogether using a type-0 or type-I phase-matched SPDC source,[4] at the cost of the possibility of

[2]At phase singularities, the phase is undefined.

[3]In all degrees of freedom.

[4]The two create down-conversion photons with identical polarizations.

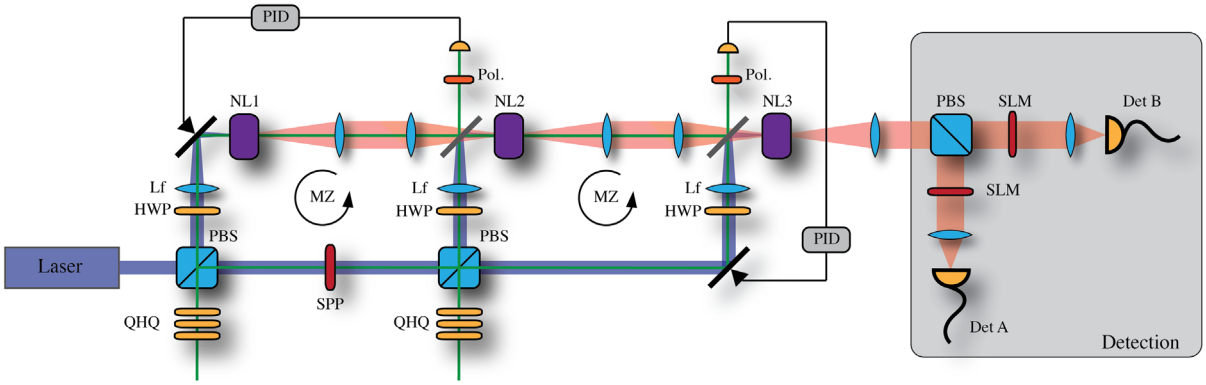

FIG. 25. Detailed experimental setup for creating three-dimensional entangled photon pairs using path identity. A continuous-wave laser centered at 405 nm is split with polarizing beam splitters (PBSs) and is guided to three NLs made from periodically poled potassium titanyl phosphate, which is better known as KTP. For experimental simplicity, the spiral phase plate (SPP) is placed within the pump beam instead of the down-converted photons (as depicted in Fig. 24). A lens (Lf) is used to focus the pump beam onto the NL. Using a $4f$ optical imaging system between two consecutive NLs ensures the spatial indistinguishability of the down-converted photon pairs. Utilization of an actively stabilized Mach-Zehnder interferometer using a proportional-integral-derivative (PID) controller ensures the interferometric stability between two NLs. The phase between two NLs can be set using the quarter-half-quarter (QHQ) wave plates of the stabilization laser depicted in green. The photon pairs are deterministically separated using a PBS in the detection part. Arbitrary superposition projections can be measured with a spatial light modulator (SLM) in combination with a single-mode fiber. From Kysela *et al.*, 2020.

deterministically splitting the photon pairs in a collinear arrangement using polarization (as for type-II sources).

A quantitative measure for the achieved indistinguishability is given by the interference visibility between the two crystals. Experimentally, the phase is adjusted by splitting the pump from the down-conversion photons and shifting the optical path length between the two, as depicted in Fig. 25. Using an additional single-mode fiber and detecting simultaneous twofold photon counts, a visibility of $97.1 \pm 0.5\%$ was demonstrated; see Fig. 26. The indistinguishability of the two photon-pair sources is an important measure because it directly determines the coherence of the entangled quantum state.

Given this basic ingredient, the next step is to introduce a mode-shifting element that is capable of shifting the spatial mode. In this first proof-of-principle experiment, the pump and down-conversion photons are split up to access both wavelengths separately. This avoids chromatic aberrations[5] and allows the simultaneous manipulation of both pump and down-conversion photons. Here the pump beam is split into three parts that coherently pump all three ppKTP crystals (where the acronym stands for periodically poled potassium titanyl phosphate). The pump beam for the second and third crystals is modified with a spiral phase plate that adds (subtracts) four quanta of OAM to (from) the pump beam. According to the conservation of OAM in the SPDC process, the second crystal thus emits photon pairs with two quanta of OAM $|2,2\rangle$ and the third crystal has the opposite $|-2,-2\rangle$ correlated photon pair. The resulting quantum state reads

$$|\psi\rangle = \alpha \underbrace{|0,0\rangle}_{\text{crystal 1}} + \beta \underbrace{|2,2\rangle}_{\text{crystal 2}} + \gamma \underbrace{|-2,-2\rangle}_{\text{crystal 3}}, \tag{24}$$

where the magnitudes of α, β, and γ are adjusted by controlling the relative pump power and the phases by adjusting the relative phase within the Mach-Zehnder interferometers. To guarantee phase stability, the two Mach-Zehnder interferometers are actively stabilized with an additional phase-locking laser.

Performing full state tomography yields reported fidelities ranging from 85% to 90% for two- and three-dimensional entangled quantum states. Different maximally and nonmaximally entangled photon pairs are thereby created in two and three dimensions to demonstrate the versatility in terms of state creation using entanglement by path identity.

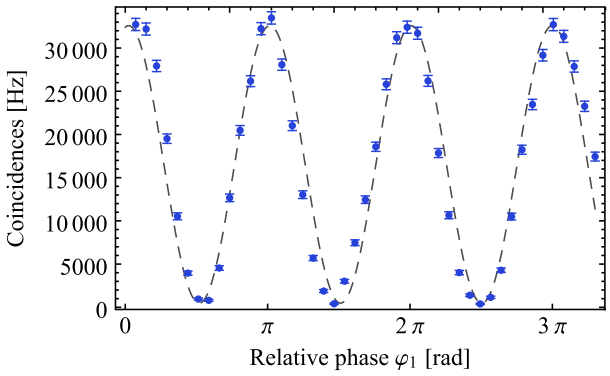

FIG. 26. Coincidence interference fringes of two consecutive nonlinear crystals. The relative phase φ_1 between NL1 and NL2 has been altered. The coincidences are measured without a SPP; thus, the interference is occurring between the fundamental Gaussian modes (denoted as 0) and the corresponding quantum state reads $|0,0\rangle_{\text{NL1}} + e^{i\varphi 1}|0,0\rangle_{\text{NL2}}$. If the observed visibility reaches 1, then the two photon-pair sources are identical, meaning that NL1 = NL2. In this experiment, a visibility of 0.971 ± 0.005 is observed. From Kysela *et al.*, 2020.

[5]Without using specially designed optical elements.

The principle of generating entanglement by path identity is suited to scale up the dimensionality of the entangled state. One possible way to scale up the dimensionality is to miniaturize the unit-dimensional cell consisting of a nonlinear crystal and a phase-shifting element. Smaller distances in combination with integrated fabrication technologies, as demonstrated by X.-L. Wang *et al.* (2018), could substantially increase the stability and cross-talk quality. Complementarily, a purely linear arrangement without an interferometer could be implemented as in the original proposal. This would require an element that performs a $+1$ operation on the down-conversion photons but not on the pump beam. The q plate (Marrucci, Manzo, and Paparo, 2006) would be a possible realization.

C. Multiphoton entanglement by path identity

Multiphotonic interference phenomena have lain at the heart of many key experiments (Pan *et al.*, 2012). These phenomena range from technological demonstrations such as quantum teleportation (Bouwmeester *et al.*, 1997; Wang *et al.*, 2015; Ren *et al.*, 2017; Luo *et al.*, 2019), entanglement swapping (Pan *et al.*, 1998), and fault-tolerant (Shor, 1996) and blind quantum computation (Barz *et al.*, 2012) to fundamentally and philosophically appealing experimental demonstrations that reject local-realistic theories using genuine multiphoton entanglement (Greenberger *et al.*, 1990; Bouwmeester *et al.*, 1999; Pan *et al.*, 2000; Zhong *et al.*, 2018).

In general, multiparticle entanglement is still an active research area due to the vast complexity that it involves. Even for small systems consisting of only four qubits, there are nine different ways to be entangled (Verstraete *et al.*, 2002); for five there are infinitely many. For further information, see Bruß (2002), Horodecki *et al.* (2009), and Plenio and Virmani (2014).

An important class of maximally entangled multiphoton states are the Greenberger-Horne-Zeilinger (GHZ) states (Greenberger, Horne, and Zeilinger, 1989). These states were investigated in the fundamentally interesting context of local-realistic theories. In contrast to Bell's theorem (Bell, 1964), the GHZ theorem allows for a qualitatively different way of refuting local-hidden-variable theories (Greenberger *et al.*, 1990; Mermin, 1990). But these maximally entangled multiparticle states are not only of fundamental interest. Error-correcting schemes in quantum computers (Shor, 1996) based on GHZ states or quantum-secret-sharing protocols (Hillery, Bužek, and Berthiaume, 1999) use these strong correlations to exceed classical limitations. These prospects have started technological developments on various physical platforms including trapped ions (Monz *et al.*, 2011), Rydberg atoms (Omran *et al.*, 2019), superconducting qubits (Kelly *et al.*, 2015; Song *et al.*, 2017), and photons (X.-L. Wang *et al.*, 2018; Zhong *et al.*, 2018).

Since this review is focused on photonic systems, we now discuss the experimental principles behind the GHZ state and introduce the concept of entanglement by path identity to the multiphotonic regime. Furthermore, we also discuss the generalization to higher-dimensional and multiphotonic systems that have recently been developed and realized (Malik *et al.*, 2016; Erhard, Malik *et al.*, 2018).

1. GHZ entanglement for qubits

For photons there is a particularly simple scheme to create an arbitrary number of entangled photons in principle. As shown in Fig. 27, we use two two-dimensional entangled photon-pair sources $|\psi\rangle = (|H,H\rangle + |V,V\rangle)/\sqrt{2}$ entangled in their polarization degree of freedom while combining one photon of one source with another photon of the other source at a polarizing beam splitter. A polarizing beam splitter reflects vertically and transmits horizontally polarized photons. Thus, the resulting quantum state reads

$$(|H,H,H,H\rangle_{ABCD} + |H,H,V,V\rangle_{ABBD} + |V,V,H,H\rangle_{ACCD} + |V,V,V,V\rangle_{ABCD})/2, \quad (25)$$

where H and V describe the polarization states (horizontal and vertical) and the indices $d1, d2, d3$, and $d4$ label the detectors.

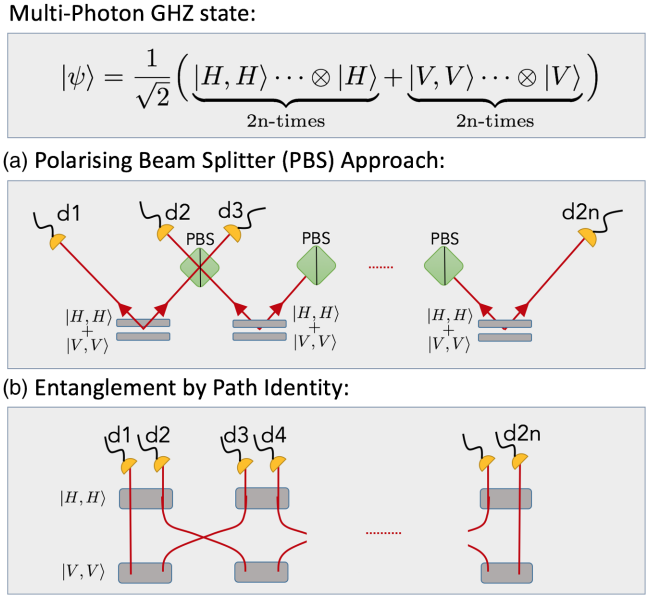

FIG. 27. Multiphoton Greenberger-Horne-Zeilinger (GHZ) state creation. (a) The commonly used technique (Pan *et al.*, 2012) to create GHZ states is to overlap two maximally entangled two photons in the state $|\phi^+\rangle = (|H,H\rangle + |V,V\rangle)/\sqrt{2}$, with H and V denoting the polarization state of the photon. Since the PBS transmits only horizontally (H) polarized photons and reflects only vertically (V) polarized photons, simultaneous $2n$-fold detection of photons at detectors $\{d1,\ldots,d2n\}$ results in a maximally and genuine multiphoton ($2n$) GHZ state. (b) Creation of multiphoton GHZ states using path identity. Displayed are two rows of n crystals, where all $2n$ crystals can coherently emit n photon pairs. The lower row creates vertically polarized photons, while the upper row solely creates horizontally polarized photon pairs. Identifying the paths of the photons in the lower row with the ones in the upper row (as previously indicated) and conditioning upon $2n$-fold photon detection result in a GHZ state. Because of the path identification, a $2n$-fold photon detection event can occur only if all crystals of the upper row emit photon pairs or if all crystals in the lower row emit photon pairs.

Postselecting on simultaneous four-photon detection events on all four detectors $d1$, $d2$, $d3$, and $d4$ results in the following desired GHZ type entangled four-photon state:

$$(|H,H,H,H\rangle_{ABCD} + |V,V,V,V\rangle_{ABCD})/\sqrt{2}. \quad (26)$$

Equation (26) can now be generalized to any photon number by adding more two-dimensional entangled photon-pair sources and combining them at polarizing beam splitters, as depicted in Fig. 27.

In contrast, using path identity one can create GHZ type entangled quantum states without using PBSs as previously described. Two rows of $2n$ NLs are coherently pumped such that they can simultaneously emit n photon pairs; see Fig. 27(b). The upper row of NLs solely emits the horizontally polarized photon pairs $|H,H\rangle$, while the lower row creates only the vertically polarized photon pairs $|V,V\rangle$. Using the path-identity principle, we now cross the path of the photons between next neighboring NLs, as depicted in Fig. 27(b). Conditioning on $2n$-fold photon events, meaning conditioning on events where all $2n$ photodetectors simultaneously detect a photon, results in a genuinely multiphoton entangled GHZ state. The reason for this is that only two possibilities for such an $2n$-fold photon detection exist. First, either all crystals from the upper row simultaneously emit one photon pair or all crystals from the lower row simultaneously emit one photon pair. Whenever only a single crystal of the lower (upper) row emits a photon pair instead of the upper (lower) row, then no $2n$-fold detection can occur because at least one detector will be empty (not detecting a photon). Since all crystals are pumped coherently and the upper and lower rows have different polarizations, we can write these two creation possibilities in a coherent superposition, as indicated by $|\psi\rangle$ in Fig. 27.

The creation efficiency of the protocol can be calculated from Eqs. (25) and (26). For n photon pairs there exist in general 2^n terms after the PBS; see Eq. (25). However, we are interested only in a maximally entangled GHZ state, which always consists of only two terms. Hence, the efficiency of the generation protocol using entangled photon pairs in combination with PBSs is given by the ratio between the two expected terms and all possible terms, which one evaluates as 2^{-n+1}.

Despite this simple principle scheme, the largest number of photons entangled in a GHZ manner is 12 (Zhong *et al.*, 2018). For one to go beyond this number, several challenges of inherently probabilistic photon-pair sources need to be overcome. For example, if the probability that one photon pair is created is p, then the probability that six photon pairs are emitted simultaneously is p^6. The probability of creating one photon pair in a single laser pulse is usually $p \approx 10^{-6} - 10^{-2}$, which leads to a 12-photon detection rate of approximately one event in 10 h. In addition, SPDC sources produce with probability p one pair and with probability p^n n photon pairs. Multipair emissions reduce the fidelity of the entangled quantum state if no number resolving detectors are utilized. Among other areas, faster triggering rates of detectors, higher photon detection efficiencies, and photon-number-resolving detectors are currently being investigated and optimized (Rudolph, 2017; Slussarenko and Pryde, 2019). While a large number of applications and fundamental tests of quantum physics allow for quantum states generated by conditioning on simultaneous n-fold detections, specifically in quantum computing, heralded quantum states are necessary. Examples are quantum gates (Knill, 2003) or GHZ states as cluster resource states in linear-optical quantum computing schemes (Gimeno-Segovia *et al.*, 2015; Bartolucci *et al.*, 2021). For that reason, much research focuses on heralded photonic entanglement (Gubarev *et al.*, 2020; Bartolucci, Birchall *et al.*, 2021), and also entanglement by path identity (Krenn *et al.*, 2021).

2. GHZ entanglement beyond qubits

Generalizing the GHZ theorem to higher-dimensional qudits only recently succeeded (Ryu *et al.*, 2013,2014; Lawrence, 2014; Tang, Yu, and Oh, 2017). In addition, the first experimental implementation of a genuinely higher-dimensional GHZ state (three dimensional) was performed shortly thereafter (Erhard, Malik *et al.*, 2018). In contrast to the two-dimensional entangled GHZ state, the experimental implementation is less simple and has been found only using computational algorithms (Krenn *et al.*, 2016; Krenn, Erhard, and Zeilinger, 2020). However, despite the unintuitive experimental creation of the three-dimensional entangled GHZ state

$$|\psi\rangle = \frac{1}{\sqrt{3}}\Big(|0,0,0,0\rangle + |1,1,1,1\rangle + |2,2,2,2\rangle\Big)$$

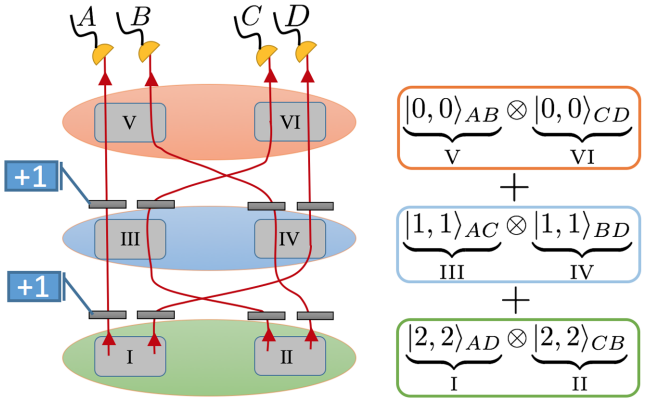

FIG. 28. Genuine multiphoton and high-dimensional quantum entanglement using path identity. Six NLs labeled with roman numbers where each NL can emit photon pairs in the transverse spatial Gaussian mode (denoted by $|0,0\rangle$) are utilized. Each photon pair emitted by one of the six crystals is connected to a pair of detectors $\{A,B,C,D\}$ as indicated on the right in such a way that overlapping paths of different crystals are identified. Simultaneous four-photon events where each detector registers a photon can occur in three possible ways: The lower, middle, or top row emits two pairs simultaneously. None of the other combinations can occur because of the specific path identification and routing of the photon paths. Inserting spiral phase plates between the different layers of crystals adds one quantum $(+1\hbar)$ of orbital angular momentum (OAM) to the incoming photons. Since all photon-pair emissions occur coherently, the three possibilities can be written in a coherent superposition yielding a genuinely four-photon and three-dimensional entangled GHZ state $|\psi\rangle$.

using linear optics, there is an intuitive way of creating such states using entanglement by path identity.

In Fig. 28, the principle of generating a four-photon three-dimensional entangled GHZ state is shown. As in the two-photon high-dimensional case, we employ the OAM of photons to illustrate entanglement by path identity for multiple photons. All six crystals (I–VI) are pumped coherently and emit with the same probability amplitude one photon pair in the fundamental Gaussian mode that is denoted as $|0,0\rangle$. Furthermore, we postselect onto events where four photons are detected simultaneously in all detectors A, B, C, and D. We can now identify the photon-pair paths such that there are exactly three possible ways in which such a four-photon detection event can appear: The two crystals in the first, second, or third row in Fig. 28 emit simultaneously. If the two photon pairs have been produced in the first row, they propagate twice through a spiral phase plate that adds one quantum of OAM to the photons. Thus, at the detector these two photon pairs are described by the probability amplitude $|2,2\rangle_{AD} \otimes |2,2\rangle_{CB}$. A similar approach is followed for the second and third rows, as depicted in Fig. 28. Since the photon-pair emission events occur such that there is in principle no information about their origin, we have to write all three possibilities in a coherent superposition

$$|\psi\rangle = \frac{1}{\sqrt{3}}(|0,0,0,0\rangle + |1,1,1,1\rangle + |2,2,2,2\rangle), \qquad (27)$$

which is exactly the desired three-dimensional entangled four-photon GHZ state.

For the two-dimensional GHZ-state creation with entanglement by path identity, no quantitative difference in terms of efficiency or achievable fidelity was found. However, for the three-dimensional GHZ state there is indeed an advantage in terms of creating efficiency. The linear-optical approach realized by Erhard, Malik *et al.* (2018) succeeds in only ≈5% of all four-photon emission events. In the entanglement using the path-identity approach, every detectable four-photon event succeeds. Thus using this new method results in a noteworthy 20-fold improvement, and hence reduces the estimated measurement time from roughly two weeks to less than a day.

From an experimental point of view, such an experiment puts stringent constraints in terms of coherent and indistinguishable photon-pair emission. As discussed in Sec. VI.B, the path length of the down-converted photons is restricted to the pump and down-conversion coherence length. While in the two-photon case a continuous-wave laser with a long coherence length can be employed, the multiphoton scenario usually requires pulsed pump lasers to identify simultaneous two-pair events. Femtosecond pulsed lasers are routinely used in such experiments and have a Fourier-limited coherence length of the order of a micrometer. In addition, the joint spectral amplitude of the down-converted photon pairs needs to be not only identical but also separable (Pan *et al.*, 2012).

Lastly, the scheme of creating genuinely three-dimensional entangled GHZ states seems to be generalizable to any d-dimensional GHZ state. It would require one to identify different paths in a nonlinear crystal network such that exactly d possible ways exist to create a four-photon detection event. This question can be answered using graph theory and has a surprising answer, which is analyzed in detail in Sec. VII.

D. Manipulating entangled states without direct interaction

After showing how to generate entangled states using path identity, we reported how the concept could be generalized to multiphoton emitters. These generalizations allow for manipulations of quantum states without ever interacting with the involved photons. The method also emphasizes the deep connection between entanglement and interference, a connection that has fascinated scientists for a long time (Horne and Zeilinger, 1986; Żukowski and Pykacz, 1988; Greenberger, Horne, and Zeilinger, 1989; Horne, Shimony, and Zeilinger, 1989; Greenberger *et al.*, 1990; Rarity and Tapster, 1990; Pan *et al.*, 2012).

In this section, the two photon sources are substituted with generalized N-photon sources, as illustrated in Fig. 29. The scheme consists of two identical sources Q and Q', each of which can coherently emit N particles simultaneously and with equal probability. As shown by Lahiri (2018), the general state produced after the beam splitters is determined by the difference of the sum of all phases Θ_m and ϕ_j and is composed of equal superpositions of Dicke states (Dicke, 1954; Tóth, 2007; Lahiri, 2018). The interesting part now is that, by changing the phases Θ_m accordingly, various entangled quantum states can be created. Hence, it opens the possibility of manipulating the state of the maximally entangled photons without ever interacting with them.

For example, in the case of a source emitting four photons and $N - M = 2$, adjusting the phases Θ_m to $2m\pi$ or

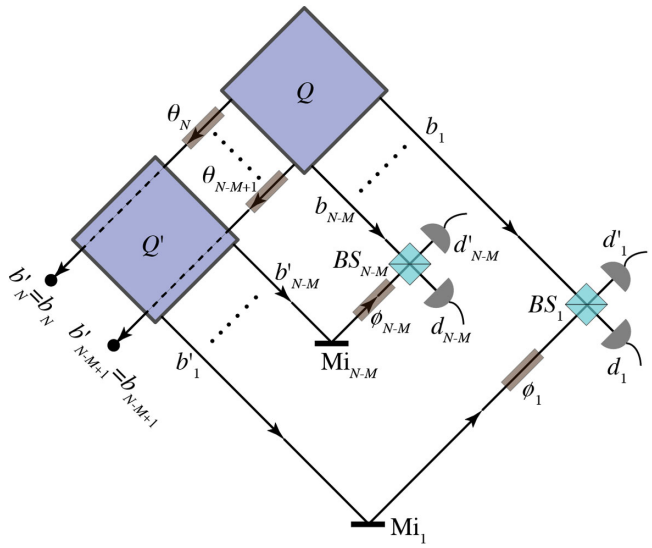

FIG. 29. Scheme of generating and controlling many-particle entangled states. Two identical N-particle sources emit particles $(1,2,\ldots,N)$ into paths $(b_1,b_2,\ldots,b_N)$ and $(b'_1,b'_2,\ldots,b'_N)$, respectively. Path identity is applied for M particles $(N-M+1,\ldots,N)$. The rest of the particles $(1,2,\ldots,N-M)$ produce many-particle interference patterns and many-particle entangled states when their paths are superposed by beam splitters. Adapted from Lahiri, 2018.

$(2m+1)\pi$ results in the $|\Psi^+\rangle$ or the $|\Phi^-\rangle$ Bell state, respectively. Increasing the number of photons coherently emitted by the two sources to six, identifying the paths of three of them, and adjusting the phases Θ_m to $(2m+1/2)\pi$ result in the creation of a three-photon GHZ state.

As mentioned in Sec. III.B, path identity can be controlled by inserting an attenuator in one or several paths of photons between the two sources. In this case the visibility of the interference patterns is decreased. This reduced interference visibility also directly alters the amount of entanglement in the detected quantum state. It thus allows one to control the amount of entanglement without interacting with the entangled photons.

VII. QUANTUM EXPERIMENTS DESCRIBED BY GRAPH THEORY

Multiphotonic quantum entanglement experiments based on path identity, such as those in Sec. VI, can ideally be described using graph theory (Krenn, Gu, and Zeilinger, 2017). This different point of view allows for more systematic manual (Gu, Chen *et al.*, 2019; Krenn, Gu, and Soltész, 2019) and algorithmic (Krenn *et al.*, 2021) design methods for quantum experiments, insights into new quantum interference effects, and connections to quantum computation (Gu, Erhard *et al.*, 2019).

We describe the connection with an example: Fig. 30(a) depicts the setup of a three-dimensional GHZ state that was already discussed in Fig. 28. The corresponding graph is shown in Fig. 30(b). Every vertex of the graph corresponds to a photon path, and every edge between two vertices corresponds to a nonlinear SPDC crystal that can produce two photons in two photonic paths. Photons produced in different layers of the crystal lead to different mode numbers. This is represented by the color of the crystals and their corresponding edges. Conditioning the outcome of the experiment on a fourfold coincidence count leads to a three-dimensional GHZ state. A fourfold coincidence count happens when every detector fires exactly once. In the corresponding graph, a fourfold coincidence count can be identified for a subset of edges, which contain every vertex exactly once. This property is denoted as *perfect matching* in graph theory. The results of a quantum optical experiment can therefore be interpreted as coherent superpositions of perfect matchings of a graph. A detailed link between quantum experiments and graphs can be seen in Table I.

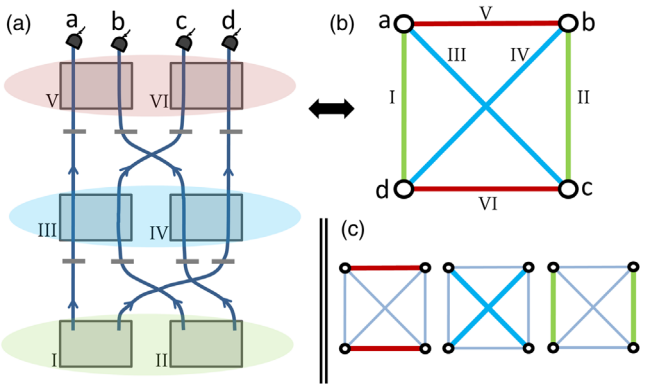

FIG. 30. Three-dimensional GHZ state via entanglement by path identity. (a) A quantum optical experiment for the generation of a three-dimensional GHZ state. (b) Its correspondence to a graph. Every vertex is a photon path, and every edge corresponds to a nonlinear crystal. Colors represent the mode numbers. (c) A resulting state, which arises conditioned on fourfold coincidence clicks, corresponds to perfect matchings of the graph.

TABLE I. Analogies between quantum experiments involving multiple crystals and graph theory. Adapted from Krenn, Gu, and Zeilinger, 2017.

Quantum experiment	Graph theory
Optical setup with crystals	Undirected graph $G(V,E)$
Crystals	Edges E
Optical paths	Vertices V
n-fold coincidence	Perfect matching
Layers of crystals	Disjoint perfect matchings
No. terms in quantum state	No. perfect matchings
Maximal dimension of photon	Degree of vertex

A. Application to designing experiments for quantum states

Designing quantum experiments is challenging because universal rules for multiphotonic systems do not exist, and multiparty quantum effects and interference are difficult to intuitively grasp. The connection between quantum experiments and graphs allows for a good descriptive tool where structures of the quantum states are encoded in the structures of the graph, and subsequently the resulting graph directly corresponds to an experimental setup.

In Sec. VI, the two-dimensional GHZ state was introduced as an important class of multiparticle entangled states. It was discovered in 2000 that three qubits could be entangled in two inequivalent ways (Dür, Vidal, and Cirac, 2000). This means that there are two classes of three-qubit states that cannot be transformed into each other using only local operations and classical communications. One of them is the GHZ state, and the other one is the so-called W state (Zeilinger, Horne, and Greenberger, 1992; Bourennane *et al.*, 2004).

An intuitive understanding is that GHZ states are the strongest entangled states, while W states encode the most robust entanglement. A three-particle W state is defined as

$$|W_3\rangle = \frac{1}{\sqrt{3}}(|1,0,0\rangle + |0,1,0\rangle + |0,0,1\rangle). \tag{28}$$

Equation (28) is a coherent superposition of one excitation (indicated as $|1\rangle$) that is delocalized over all three particles. In the n-particle generalization, it is a delocalization of one excitation over all n photons.

An experimental configuration for a four-particle W state using entanglement by path identity was shown by Krenn *et al.* (2017). Its n-party generalization was discovered by Gu, Chen *et al.* (2019), who exploited the descriptive nature of the corresponding graphs; see Fig. 31. They utilized similar techniques to generate setups using path identity for much more general high-dimensional and multipartite quantum states. Examples involve Dicke states (which generalize W states to multiexcitations) (Dicke, 1954), Schmidt-rank vector

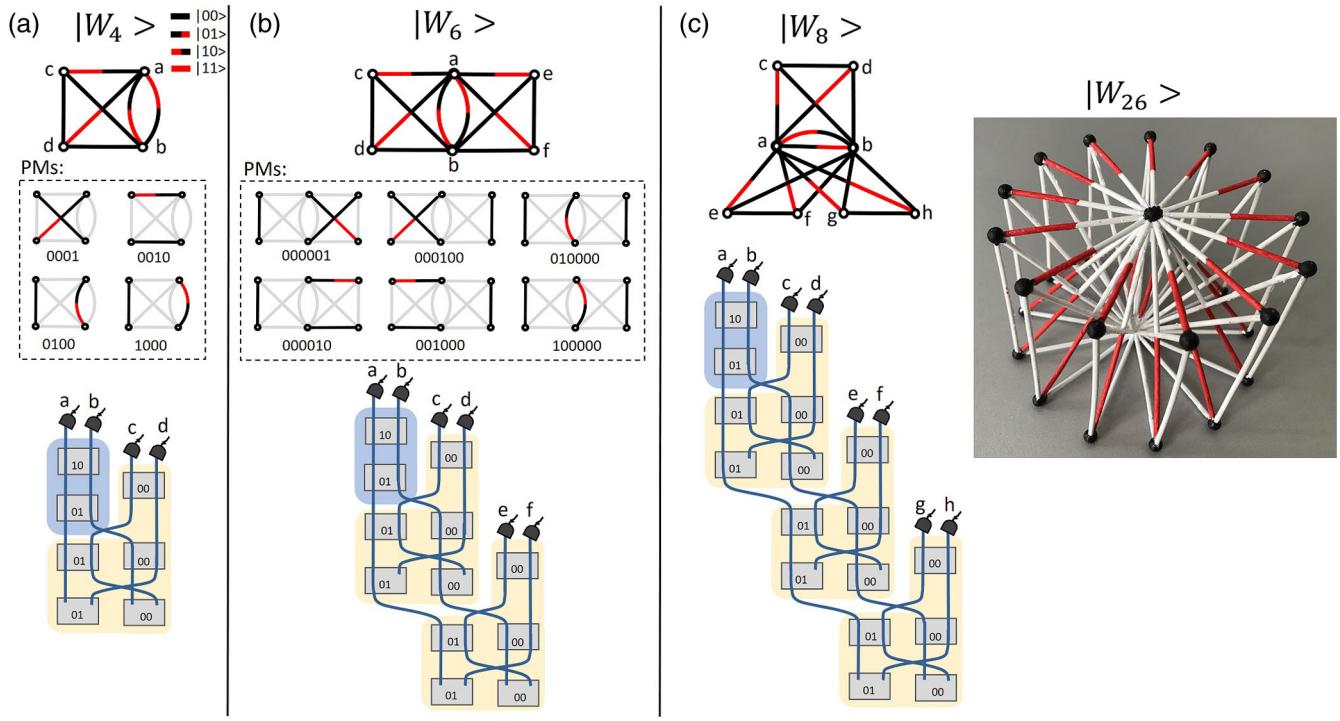

FIG. 31. Design of quantum experiments using graph theory. The connection to graph theory is an ideal descriptive tool of quantum experiments and can be used to design experiments in order to design specific quantum states. In this example, a general recipe for the generation of W states is given. From Gu, Chen *et al.*, 2019.

states (which classify quantum entanglement in a high-dimensional multipartite scenario) (Huber and de Vicente, 2013; Huber, Perarnau-Llobet, and de Vicente, 2013), and absolutely maximally entangled states (Goyeneche *et al.*, 2015; Huber *et al.*, 2018; Cervera-Lierta, Latorre, and Goyeneche, 2019). The design principle using entanglement by path identity was recently generalized to multiphoton emitters, which involve hypergraphs as an descriptive tool (Gu, Chen, and Krenn, 2020).

The bridge between graph theory and quantum experiments can also be used to show which quantum state cannot be produced with probabilistic photon-pair sources. The key idea is to translate a question in quantum physics into an equivalent question in graph theory, solve the question with the tools of graph theory, and translate it back (Krenn, Gu, and Zeilinger, 2017; Gu, Chen *et al.*, 2019). A specific example is the following: The question "Which d-dimensional n-photon GHZ state can be created with probabilistic photon-pair sources?" can be translated as "Which existing graph with n vertices has d perfect matchings that are all disjoint?" One can show that the only graphs that can fulfill this requirement are $n > 2$, $d = 2$ and $n = 4$, $d = 3$ (Bogdanov, 2017; Krenn, Gu, and Zeilinger, 2017), which restrict the generations of GHZ states (without the employment of additional tools such as ancillary states). Many similar quantum physics questions are translated into the language of graph theory and can be solved (Gu, Chen *et al.*, 2019) or still have to be solved (Krenn, Gu, and Soltész, 2019).

B. Application in quantum random networks

Classical random networks were introduced by Erdős and Rényi in 1959 to describe many real-world features of networks, such as the small-world problem (Erdős and Rényi, 1959, 1960). These graphs are described by $G = (V, E)$, where V are the vertices and E are the edges between the nodes and another parameter p that describes the probability that an edge will form between two nodes.

A notable result is that in classical networks a computational phase transition occurs. For example, as N goes to infinity, the probability that a certain subgraph exists in the network is 0 for $p < p_c(N)$ and 1 for $p > p_c(N)$, where $p_c(N)$ is a critical probability. The critical probability scales as N^z, with the critical exponent $z \in (\infty, 0]$. A concrete example is the emergence of a fully connected graph of four vertices, denoted as K_4, which happens when $z = -2/3$.

Quantum random networks (Perseguers *et al.*, 2010) were invented as generalizations of random networks in the quantum regime. The graph is built as a coherent superposition of all edges inserted (with probability p) and not inserted (with probability $\sqrt{1-p^2}$). Perseguers *et al.* (2010) showed, exploiting projective measurements and local operations and classical communications (better known as LOCC), that arbitrary quantum states of finite subgraphs can be obtained with a critical exponent of $z = -2$, which is much smaller than that of classical random networks.

Entanglement by path identity can be used to generate an arbitrary undirected graph, which creates quantum networks in the form introduced by Perseguers *et al.* (2010), as shown in Fig. 32. A single SPDC crystal produces a quantum state that can be approximated as

$$|\psi_{a,b}\rangle = \left(1 + p(\hat{a}_a^\dagger \hat{a}_b^\dagger - \hat{a}_a \hat{a}_b) + \frac{p^2}{2}(\hat{a}_a^\dagger \hat{a}_b^\dagger - \hat{a}_a \hat{a}_b)^2 + \cdots\right)|0\rangle, \tag{29}$$

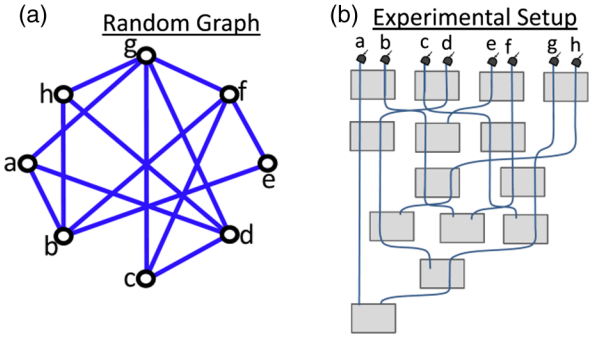

FIG. 32. Quantum random networks (Perseguers *et al.*, 2010) have interesting critical properties, such as the emergence of certain quantum states when the edge probability $p_c(N) > N^{-2}$, where N are the vertices. (a) A specific random graph with 14 edges connecting eight vertices is a quantum random network. (b) The corresponding setup consists of 14 crystals that are coherently pumped and output into $N = 8$ paths. The SPDC probability p corresponds to the edge probability. From Krenn, Gu, and Zeilinger, 2017.

where p is the SPDC amplitude. The complete quantum random network is a combination of all crystals being pumped coherently, which is a tensor product over all existing edges in the form of

$$|\psi_{\text{network}}\rangle = \bigotimes_{e(i,j)\in E} |\psi_{i,j}\rangle, \tag{30}$$

where i and j are the vertices that are connected by the edge $e \in E$. These setups can be used to simulate phenomena of quantum random networks, such as critical exponents, in a natural and inexpensive way.

C. Generalization to general linear-optical experiments

The graph-theoretical description was generalized to arbitrary linear-optical systems upon the realization that every linear transformation is related to a certain graph transformation. Thus, linear-optical elements cannot go beyond the graph-theoretical picture (Gu, Erhard *et al.*, 2019). As a consequence, all conclusions about the construction of multiphotonic quantum states hold for linear-optical setups. It allows for the explanation of a multiphotonic protocol such as quantum teleportation (Bennett *et al.*, 1993; Bouwmeester *et al.*, 1997) or entanglement swapping (Żukowski *et al.*, 1993; Pan *et al.*, 1998) using simple pictorial diagrams.

A different approach to investigating photonic experiments has been shown by Ataman (2015, 2018). The main idea is to translate creation operator rules, which define linear operators, into rules for photon paths. With that, various quantum experiments (at least for photon pairs) can be described. An example is the ZWM experiment shown in Fig. 33. Extending Ataman's description to multiphotonic experiments could be achieved by extending the graph-theoretical background, in particular, by introducing the concept in perfect matchings of graphs.

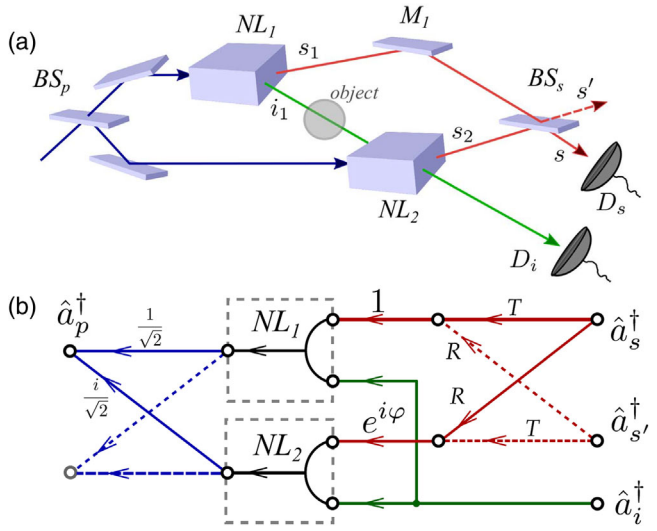

FIG. 33. Graphical approach to linear-optical quantum experiments developed by Ataman (2015, 2018). (a) Depiction of the ZWM experiment including the pump beam. (b) The translation to a graphical model. The idea is to represent photons as creation operators. The transformation of every linear-optical element as well as nonlinear crystals for the creation of photon pairs can be understood in photon transformations of the photon's paths. From Ataman, 2018.

VIII. QUANTUM INTERFERENCE IN GENERAL PHOTON CREATION PROCESSES

Here we describe some extensions of Herzog's experiment (Herzog *et al.*, 1994); see Chapter II.B. In the original experiment, two SPDC processes were organized in such a way that the resulting photon pairs were destructively or constructively interfered. We discuss three extensions of this concept. The first one shows that the photon pairs, which interfere, do not necessarily come from the same kind of source. The second extension shows a generalization to multiphotonic systems and a link to quantum computing. The third one demonstrates nonlinear interference in a four-wave mixing process in integrated photonics.

A. Weak coherent laser and SPDC

Quantum interference is agnostic to the source of the photon pairs: it is essential only that the two possibilities are fundamentally indistinguishable and share a well-defined phase relation. A notable experiment that has shown an analog to the frustrated down-conversion interference, but from two different types of sources, was presented by Resch, Lundeen, and Steinberg (2001). The sketch of their idea is shown in Fig. 34. The idea is to use weak laser beams and overlap them with the output of a SPDC process. They indeed saw high-quality interference fringes.

The experiment of Resch, Lundeen, and Steinberg (2001) indicates that any generation process that can be performed in a coherent way allows for quantum interference. It again shows the significance of information: as long as there is no information anywhere in the Universe that could help to

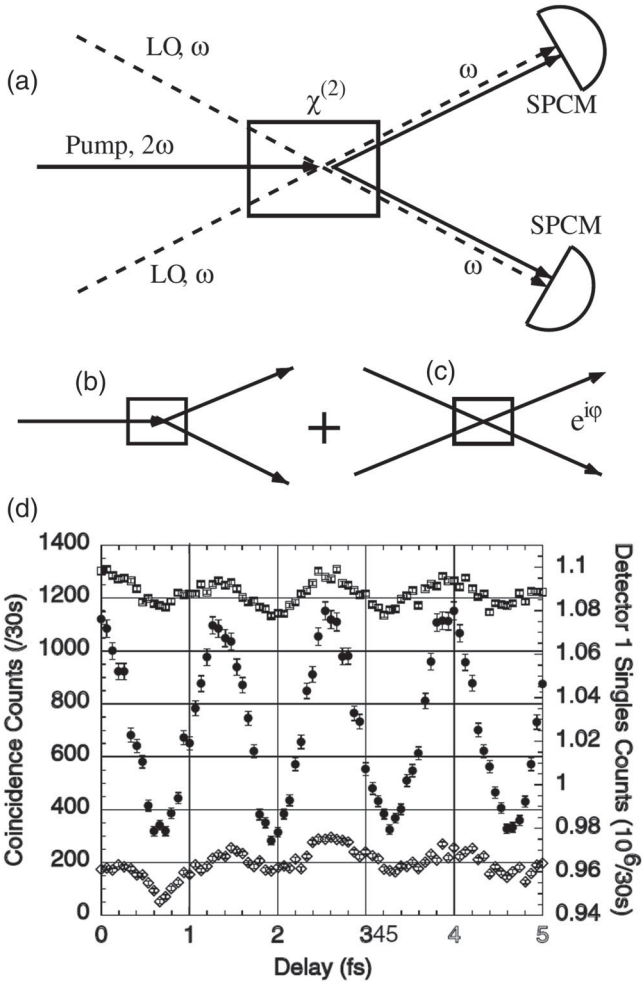

FIG. 34. Interference of photons from different sources. (a) A beam of a local oscillator (a laser beam with a defined coherence relation to the pump beam of the SPDC) overlaps with the output of a SPDC crystal. There are two different possibilities how a pair of photons could be generated: either (b) via SPDC or (c) from the weak local oscillator. Resch, Lundeen, and Steinberg were able to make these two possibilities indistinguishable, and therefore observed interference between them. In (d), the solid circles represent coincidence counts, with a fringe visibility of more than 50%. The open squares stand for the single counts, in which one can also see statistically significant modulation, as the phase between the two possibilities varies. Adapted from Resch, Lundeen, and Steinberg, 2001.

distinguish which of those processes the pair is created from, quantum interference may occur.

B. Multiphotonic quantum interference

The objective of the multiphotonic setups in Sec. VI was the production of complex novel entangled quantum states, in a way generalizing Hardy's entanglement source (Hardy, 1992) to higher dimensions and a larger number of particles. Hardy's entanglement source also has a close relation to Herzog's interference experiment (Herzog *et al.*, 1994). While in Hardy's experiment the interference can be observed by measuring entanglement, in Herzog's experiment interference can be observed by measuring direct photon count rates.

With the Hardy-Herzog analogy in mind and with the possibility of generalizing the Hardy entanglement source to multiple particles, one can ask whether Herzog's experiment can also be generalized to multiple particles. Indeed, Gu, Erhard *et al.* (2019) showed that experimental setups that can generate entanglement by path identity can be modified to show interference. In contrast to entanglement, this interference can be observed directly in the rate of emitted multiphoton states. The concept is shown in Fig. 35, in which mode shifters are replaced by phase shifters. The fourfold coincidence that arises from crystals I and II therefore has a relative phase between the four-photon term from crystals III and IV.

The down-conversion process can be approximated as a series expansion in the form of

$$\hat{U}_{a,b} = 1 + g(\hat{a}_a^\dagger \hat{a}_b^\dagger - \hat{a}_a \hat{a}_b) + \frac{g^2}{2}(\hat{a}_a^\dagger \hat{a}_b^\dagger - \hat{a}_a \hat{a}_b)^2 + \mathcal{O}(g^3), \tag{31}$$

where $\hat{a}_a^\dagger$ and $\hat{a}_a$ are creation and annihilation operators for a photon in the mode a, respectively, and g is proportional to the SPDC rate and the pump power. For simplicity, we restrict ourselves to a single-mode analysis. In the four-photon interference setup, four crystals are used. Therefore, the state can be expressed (taking only cases with one photon in each detector into account) as

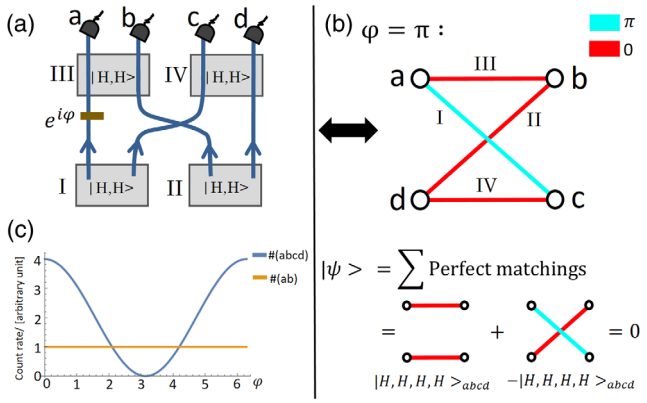

FIG. 35. Constructive and destructive quantum interference based on path identity (Gu, Erhard *et al.*, 2019). (a) Four crystals aligned such that the emission of fourfold coincidence clicks in all four detectors a, b, c, and d can happen only when crystals I and II emit a pair of photons or crystals III and IV emit a pair of photons each. Here all photons are indistinguishable. These two possibilities lead to two terms in the quantum state, which are coherently superposed. A phase shifter in one of the arms changes the relative phase between these terms, thus leading to either an increased or a decreased rate of fourfold counts. (b) An interpretation of using graph theory where weighted edges lead to phases between the perfect matchings, which can cancel each other. This interpretation will help one to find and understand follow-up applications. (c) Depiction of the rate of twofold counts in detectors a and b and fourfold counts in all four detectors when the phase ϕ is rotated. While the pair counts do not change, the fourfold counts can vanish.

$$|\psi\rangle = \hat{U}_{c,d}\hat{U}_{a,b}\hat{P}_a\hat{U}_{b,d}\hat{U}_{a,c}|0,0,0,0\rangle$$
$$= g^2(1+e^{i\varphi})|1,1,1,1\rangle + O(g^3), \quad (32)$$

where $\hat{P}_a$ introduces a phase ϕ in path a and $|1,1,1,1\rangle$ stands for a state with one photon in each path. The complete state up to second order SPDC contains exactly one term (depicted in red in Fig. 35), which stands for interference (i.e., its amplitude changes when the phase ϕ changes). No other terms, in particular, no other two-photon terms, show that behavior. Thus, this phenomenon is a genuine multiphotonic interference effect.

This interference effect has an interesting interpretation: If the phase is set to $\phi = \pi$, one will never observe fourfold coincidences in the four detectors. In this case, when one sees a photon pair in detectors a and b, one can be sure not to observe a photon pair in detectors c and d. This is surprising because all crystals produce photons pairs spontaneously (i.e., not deterministically). Furthermore, crystal IV, which would produce photon pairs in c and d, can be far from crystal III and the phase shifter. Thus, the setting information of the phase shifter needs to travel to crystal IV. This reasoning indicates that one could construct interesting experiments investigating time delays of the interference effects (Ma, Kofler, and Zeilinger, 2016).

C. On-chip quantum interference by path identity

The experiments in Sec. VII require many photon sources that are phase stable with each other. One way to guarantee stability is the integration of the entire setup into a photonic chip. Integrated sources of photon pairs have recently been demonstrated in multiple experiments (Jin *et al.*, 2014; Silverstone *et al.*, 2014, 2015; Krapick *et al.*, 2016; Santagati *et al.*, 2018; Adcock *et al.*, 2019; Feng *et al.*, 2019; Lu *et al.*, 2020).

However, it was only in 2019 that the first nonlinear interference experiment was demonstrated by Ono *et al.* (2019). They used two sources of spontaneous four-wave mixing and overlap their outputs, as shown in Fig. 36, and observed high interference visibility of 96.8%. Recently the first multiphoton quantum interference based on path identity was observed on a photonic chip (Feng *et al.*, 2021).

These experimental demonstrations could open the door to using path-identity-based interference effects as an additional powerful building block in integrated photonics. Furthermore, they pave the way to observing new interference phenomena described in Sec. VIII.B.

D. Application in quantum computation

1. Special-purpose quantum computations via sampling

The setup in Fig. 35(a) can be generalized to a random network similar to that in Sec. VII.B, with random phases between all paths. We consider the situation where the experimental setup has m output modes and N crystals, and $n/2 < m$ photon pairs (n photons) are generated. To calculate the distribution of the possible output results, one has to find all combinations of crystals that could lead to this result and sum their amplitudes in a coherent way. As m and n increase, this cannot be done efficiently anymore on a classical computer.

To understand this better, it is useful to translate the experimental setup into its corresponding graph, as shown in Sec. VII. The probability for a given combination of n detectors clicking is provided by the sum of the weights of all perfect matchings of a particular subgraph.

The problem is as follows: It is easy to verify that a given set of edges form a perfect matching (as a reminder, it is a set of edges where every vertex is contained exactly once) in a graph. However, there is no known algorithm that can find a perfect matching for arbitrary graphs in polynomial time. In the words of complexity theory, the question of finding a perfect matching is in the complexity class NP complete (where the acronym stands for nondeterministic polynomial time).

Calculating the measurement results for a given combination of detectors requires one to find all perfect matching in the graph, and each of them has a complex amplitude associated with it. Therefore, this problem is even more difficult and lays in the complexity class #P (Valiant, 1979; Aaronson, 2011).

For bipartite graphs (graphs with two sets of vertices, where an edge contains only vertices from the two sets), calculating the number of perfect matchings corresponds to calculating the matrix function *permanent* of the adjacency matrix of the graph. For general graph, the generalized matrix function referred to as *Hafnian* (Caianiello, 1953) can be used.

The scenario just described is experimentally entirely different, but mathematically closely related to an idea

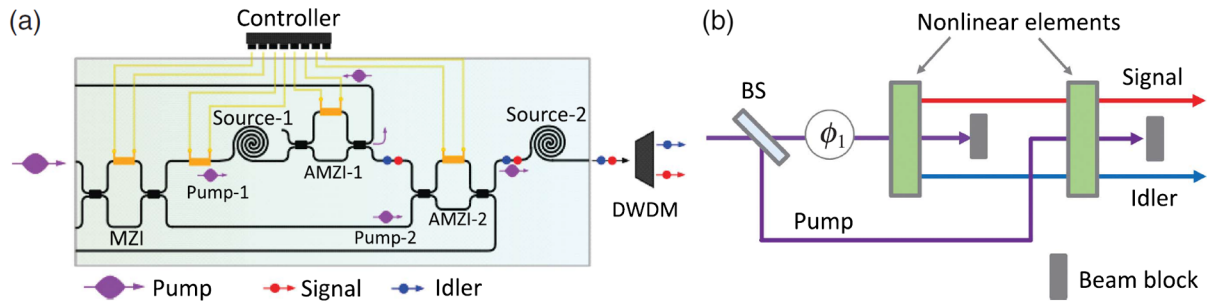

FIG. 36. Frustrated pair creation was observed on an integrated silicon photonic chip by Ono *et al.* (2019) in the Rarity group. The source of photon pairs is a spontaneous four-wave mixing process of a χ^3 nonlinearity. Two sources can each create a pair of photons. As the origin of the pair is undefined, it is in a coherent superposition of being created in either. Thus, Ono *et al.* observed constructive and destructive interference of the resulting photon pair.

proposed in 2011 denoted as *boson sampling* (Aaronson and Arkhipov, 2011). There n single photons propagate through a random network of beam splitters and phase shifters and are detected in a combination of m output detectors. The situation can be described as a bipartite graph (a set of n input modes connect to a set of m output modes). This idea was further generalized to general graphs using Gaussian boson sampling (Lund *et al.*, 2014; Hamilton *et al.*, 2017; Brádler *et al.*, 2018).

The situation has sparked a lot of interest because it would allow one (for a large enough number of photons and modes) to directly observe experimental measurement results that cannot be efficiently calculated on a classical computer. On the one hand, it is considered a method to demonstrate the first *quantum supremacy*, a calculation that is faster on a quantum device than on any available classical computer (Harrow and Montanaro, 2017). The fastest quantum boson sampling device can outperform the first electronic universal computer ENIAC (1942) and the first transistor-based electronic computer TRADIC (1954) (Wang *et al.*, 2017).

Estimating the previously described output distribution of systems also has essential implications in science and technology and could lead to real-world use of quantum hardware as special-purpose computers. One example is the spectra of vibronic (interactions between electronic and vibrational modes) modes in molecules (Huh *et al.*, 2015), which are essential in chemistry. Other algorithms involve graph theory applications such as the dense subgraph problem (Arrazola and Bromley, 2018) and the graph isomorphism problem (Brádler *et al.*, 2021).

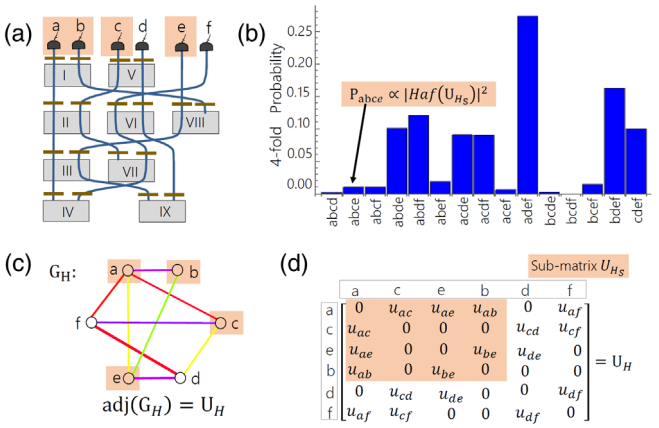

FIG. 37. Multiphotonic interference can be exploited for special-purpose quantum computation (Gu, Erhard *et al.*, 2019). (a) Path identified photons produced in a random network of crystals. The network has six output modes and is pumped in such a way that events of more than four photons can be ignored. (b) Four-photon count rates. Every experimental setup corresponds to a weighted undirected graph G_H. A fourfold coincidence count (for example, in outputs a, b, c, and e) corresponds to a subgraph G_{H_S} of those vertices in **C**. The count rate in these output modes can be calculated as the coherent sum of all weighted perfect matchings of G_{H_S}. This is equivalent to calculating the matrix function Hafnian applied on the adjacency matrix of the graph G_{H_S} seen in **D** (a problem known to be extremely difficult to calculate).

Setups built from multicrystal path-identity networks are an appealing alternative to beam-splitter-based boson sampling setups; see Fig. 37. Many important questions remain open. Specifically, concrete comparisons of efficiency, error tolerance, or experimental feasibility between the traditional methods of boson sampling and the sampling using path identity are necessary for understanding the mutual advantages and disadvantages. Since the first multiphoton path-identity interference effects were experimentally observed recently (Feng *et al.*, 2021; Qian *et al.*, 2021), the answers to these theoretical questions are pressing. This demonstrates that this alternative boson sampling approach is indeed experimentally feasible.

2. Application in gate-based quantum computation

Universal quantum computers in the gate-based model have the following scheme: An array of N qubits are initialized in a state $|0\rangle$, followed by a sequence of single- and two-qubit quantum gates that execute the quantum algorithm and subsequent measurements. These models assume that the qubits already exist at the initialization, and that they always exist during the execution. However, using a frustrated generation of qubit pairs (Herzog *et al.*, 1994), one has the additional potential of exploiting the existence or nonexistence of the qubit itself. This potential has been largely unexplored thus far in the realm of quantum algorithms.

An initial attempt to describe such interference effects in the language of quantum gates was made by Alipour, Krenn, and Zeilinger (2017). They extended the qubits to qutrits (three-level systems) to carry the additional information of whether the mode is occupied by a photon or not. An example of frustrated SPDC is shown in Fig. 38. This would allow for a natural way of encoding quantum information for ternary quantum computers (where instead of qubits, quantum systems with three levels are used) (Bocharov *et al.*, 2016; Bocharov, Roetteler, and Svore, 2017). It is an open question how all of the generalized approaches presented here can be translated to the language of quantum gates and quantum

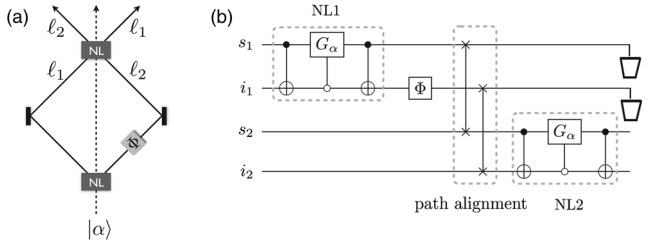

FIG. 38. (a) Quantum circuit describing a frustrated SPDC (Herzog *et al.*, 1994). (b) Each mode is interpreted as a three-level state. The first level is the state of a nonexistent photon, while states 2 and 3 encode the usual computational qubit. The pair creation of NL1 and NL2 (nonlinear crystals 1 and 2) are described by two CNOT gates and one controlled-unitary gate. If no qubit exists in the mode, it creates one in the computational state $|1\rangle$. If a qubit with state $|1\rangle$ exists, it will annihilate the qubit. Formally, the mode can be considered as a qutrit (three-level system). The path alignment between the crystals is governed by two SWAP gates. From Alipour, Krenn, and Zeilinger, 2017.

circuits, and whether they can inspire new ideas in the design of quantum algorithms.

IX. CONCLUSIONS AND OUTLOOK

We have discussed the concept of path identity and its applications to fundamental and applied physics. Although the concept lay hidden in the literature since the early 1990s, it is only the recent developments that show its significance for future directions of research. In addition to its implications for fundamental problems, the concept of path identity has pushed frontiers of imaging, spectroscopy, and quantum information science. In the fields of imaging and spectroscopy, the concept has indicated that it is possible to retrieve object information without detecting the radiation that illuminates the object. Therefore, the concept of path identity allows us to study the properties of an object at a wavelength for which good detectors are not available, and thereby to extend our experimental reach. As for quantum information science, the concept has led to distinct avenues of creating, controlling, and measuring entanglement. Furthermore, this concept of path identity has also inspired graph-theoretical descriptions of quantum experiments, thus promoting a much more systematic and efficient way to design future experiments.

Although all of the experiments discussed here are performed in the optical domain (i.e., by detecting photons), the concept of path identity is also applicable to other quantum entities. In this context, an important fact is that none of the experiments discussed in this review require stimulated emission. Therefore, the ideas pertaining to such experiments can also be applied to design experiments with fermionic systems. We expect that future experiments with nonphotonic quantum systems based on the concept of path identity will not only extend our knowledge of fundamental physics but also result in numerous applications.

In a similar spirit, path identity could also be applied in atoms. In 2004, Paul Lett argued that an atomic variation of the ZWM experiment could be performed with pairs of atoms emitted from two Bose-Einstein condensates (Lett, 2004). Experimentally controlled Bose-Einstein condensates in conjunction with single-atom detection [such as metastable helium (Dos Santos *et al.*, 2001; Robert *et al.*, 2001; Vassen *et al.*, 2012; Keller *et al.*, 2014)] have improved significantly, allowing for quantum optics experiments [such as Hong-Ou-Mandel analogs (Lopes *et al.*, 2015)]. This progress could ultimately also lead to atomic variations of path-identity experiments.

Many other vital questions (both theoretical and experimental) raised over the last five years remain open. How can we experimentally increase the wavelength difference of signal and idler photons in order to build highly efficient imaging, spectroscopy, and microscopy (Kviatkovsky *et al.*, 2020; Paterova *et al.*, 2020) techniques for the deep-UV or terahertz regime (Sec. IV)? Can the effective wavelength, which controls the interference properties, be applied in superresolution schemes (Sec. IV.E)? Is it possible to detect quantum entanglement by measuring only one of the photons? Can this idea be generalized to multiphotonic entanglement to perform a GHZ-like paradox (Sec. V)? Can one experimentally build a scalable high-dimensional source based on path identity (Sec. VI.B)? Are high-dimensional multiphotonic sources based on path identity experimentally more efficient (Sec. VI.C)? Can the multiphotonic interference, which generalizes the idea of frustrated down-conversion to many photons, be observed in the laboratory (Sec. VIII)? Can path identity be observed in other systems, such as with electrons or atoms?

Recently, path identity, a sleeping beauty, was awakened and since then she shows her applicability and inspires new ideas and connections in diverse fields of quantum optics. We are looking forward to the progress in the coming years.

ACKNOWLEDGMENTS

A. Z. thanks the late Mike Horne and Danny Greenberger for many discussions of the fundamental questions of the topics, and their consequences over many years. The authors thank Sven Ramelow and Daniel Molter for feedback on the manuscript. This work was supported by the Austrian Academy of Sciences (ÖAW), the University of Vienna via the project QUESS, and the Austrian Science Fund (FWF) with Project No. SFB F40 (FOQUS). M. E. and A. H. acknowledge support from FWF Project No. W 1210-N25 (CoQuS). M. K. acknowledges support from the FWF via the Erwin Schrödinger Fellowship No. J4309.

REFERENCES

Aaronson, S., 2011, "A linear-optical proof that the permanent is #P-hard," Proc. R. Soc. A **467**, 3393–3405.

Aaronson, S., and A. Arkhipov, 2011, "The computational complexity of linear optics," in *Proceedings of the Forty-Third Annual ACM Symposium on Theory of Computing, New York, 2011* (ACM, New York), pp. 333–342.

Adcock, J. C., C. Vigliar, R. Santagati, J. W. Silverstone, and M. G. Thompson, 2019, "Programmable four-photon graph states on a silicon chip," Nat. Commun. **10**, 3528.

Alipour, S., M. Krenn, and A. Zeilinger, 2017, "Quantum gate description for induced coherence without induced emission and its applications," Phys. Rev. A **96**, 042317.

Allen, L., M. W. Beijersbergen, R. Spreeuw, and J. Woerdman, 1992, "Orbital angular momentum of light and the transformation of Laguerre-Gaussian laser modes," Phys. Rev. A **45**, 8185.

Arrazola, J. M., and T. R. Bromley, 2018, "Using Gaussian Boson Sampling to Find Dense Subgraphs," Phys. Rev. Lett. **121**, 030503.

Ataman, S., 2015, "The quantum optical description of three experiments involving non-linear optics using a graphical method," Eur. Phys. J. D **69**, 44.

Ataman, S., 2018, "A graphical method in quantum optics," J. Phys. Commun. **2**, 035032.

Babazadeh, A., M. Erhard, F. Wang, M. Malik, R. Nouroozi, M. Krenn, and A. Zeilinger, 2017, "High-Dimensional Single-Photon Quantum Gates: Concepts and Experiments," Phys. Rev. Lett. **119**, 180510.

Barbosa, G., 1994, "Forced indistinguishability in 'induced coherence without stimulated emission,'" Phys. Rev. A **50**, 3379.

Bartolucci, S., P. M. Birchall, M. Gimeno-Segovia, E. Johnston, K. Kieling, M. Pant, T. Rudolph, J. Smith, C. Sparrow, and M. D. Vidrighin, 2021, "Creation of entangled photonic states using linear optics," arXiv:2106.13825.

Bartolucci, S., *et al.*, "Fusion-based quantum computation," 2021, arXiv:2101.09310.
Barz, S., E. Kashefi, A. Broadbent, J. F. Fitzsimons, A. Zeilinger, and P. Walther, 2012, "Demonstration of blind quantum computing," Science **335**, 303–308.
Belinsky, A., and D. Klyshko, 1992, "Interference of classical and non-classical light," Phys. Lett. A **166**, 303–307.
Bell, J. S., 1964, "On the Einstein Podolsky Rosen paradox," Phys. Phys. Fiz. **1**, 195.
Bennett, C. H., G. Brassard, C. Crépeau, R. Jozsa, A. Peres, and W. K. Wootters, 1993, "Teleporting an Unknown Quantum State via Dual Classical and Einstein-Podolsky-Rosen Channels," Phys. Rev. Lett. **70**, 1895.
Bennink, R. S., S. J. Bentley, R. W. Boyd, and J. C. Howell, 2004, "Quantum and Classical Coincidence Imaging," Phys. Rev. Lett. **92**, 033601.
Berkhout, G. C., M. P. Lavery, J. Courtial, M. W. Beijersbergen, and M. J. Padgett, 2010, "Efficient Sorting of Orbital Angular Momentum States of Light," Phys. Rev. Lett. **105**, 153601.
Bernhard, C., B. Bessire, T. Feurer, and A. Stefanov, 2013, "Shaping frequency-entangled qudits," Phys. Rev. A **88**, 032322.
Bocharov, A., S. X. Cui, M. Roetteler, and K. M. Svore, 2016, "Improved quantum ternary arithmetic," Quantum Inf. Comput. **16**, 862–884.
Bocharov, A., M. Roetteler, and K. M. Svore, 2017, "Factoring with qutrits: Shor's algorithm on ternary and metaplectic quantum architectures," Phys. Rev. A **96**, 012306.
Bogdanov, I., 2017, https://mathoverflow.net/q/267013.
Bohr, N., 1928, "The quantum postulate and the recent development of atomistics," Naturwissenschaften **16**, 245.
Born, M., and E. Wolf, 1999, *Principles of Optics: Electromagnetic Theory of Propagation, Interference and Diffraction of Light*, 7th ed. (Cambridge University Press, Cambridge, England).
Bourennane, M., M. Eibl, C. Kurtsiefer, S. Gaertner, H. Weinfurter, O. Gühne, P. Hyllus, D. Bruß, M. Lewenstein, and A. Sanpera, 2004, "Experimental Detection of Multipartite Entanglement Using Witness Operators," Phys. Rev. Lett. **92**, 087902.
Bouwmeester, D., J.-W. Pan, M. Daniell, H. Weinfurter, and A. Zeilinger, 1999, "Observation of Three-Photon Greenberger-Horne-Zeilinger Entanglement," Phys. Rev. Lett. **82**, 1345.
Bouwmeester, D., J.-W. Pan, K. Mattle, M. Eibl, H. Weinfurter, and A. Zeilinger, 1997, "Experimental quantum teleportation," Nature (London) **390**, 575.
Brádler, K., P.-L. Dallaire-Demers, P. Rebentrost, D. Su, and C. Weedbrook, 2018, "Gaussian boson sampling for perfect matchings of arbitrary graphs," Phys. Rev. A **98**, 032310.
Brádler, K., S. Friedland, J. Izaac, N. Killoran, and D. Su, 2021, "Graph isomorphism and Gaussian boson sampling," Spec. Matrices **9**, 166–196.
Brandt, F., M. Hiekkamäki, F. Bouchard, M. Huber, and R. Fickler, 2020, "High-dimensional quantum gates using full-field spatial modes of photons," Optica **7**, 98–107.
Bruß, D., 2002, "Characterizing entanglement," J. Math. Phys. (N.Y.) **43**, 4237.
Burnham, D. C., and D. L. Weinberg, 1970, "Observation of Simultaneity in Parametric Production of Optical Photon Pairs," Phys. Rev. Lett. **25**, 84.
Caianiello, E. R., 1953, "On quantum field theory—I: Explicit solution of Dyson's equation in electrodynamics without use of Feynman graphs," Nuovo Cimento **10**, 1634–1652.
Casado, A., T. W. Marshall, and E. Santos, 1997, "Parametric downconversion experiments in the Wigner representation," J. Opt. Soc. Am. B **14**, 494–502.
Cervera-Lierta, A., J. I. Latorre, and D. Goyeneche, 2019, "Quantum circuits for maximally entangled states," Phys. Rev. A **100**, 022342.
Chekhova, M., and Z. Ou, 2016, "Nonlinear interferometers in quantum optics," Adv. Opt. Photonics **8**, 104–155.
Clauser, J. F., 1974, "Experimental distinction between the quantum and classical field-theoretic predictions for the photoelectric effect," Phys. Rev. D **9**, 853.
Cui, L., J. Su, J. Li, Y. Liu, X. Li, and Z. Ou, 2020, "Quantum state engineering by nonlinear quantum interference," Phys. Rev. A **102**, 033718.
Dada, A. C., J. Leach, G. S. Buller, M. J. Padgett, and E. Andersson, 2011, "Experimental high-dimensional two-photon entanglement and violations of generalized Bell inequalities," Nat. Phys. **7**, 677–680.
Dicke, R. H., 1954, "Coherence in spontaneous radiation processes," Phys. Rev. **93**, 99.
Dos Santos, F. P., J. Léonard, J. Wang, C. Barrelet, F. Perales, E. Rasel, C. Unnikrishnan, M. Leduc, and C. Cohen-Tannoudji, 2001, "Bose-Einstein Condensation of Metastable Helium," Phys. Rev. Lett. **86**, 3459.
Dür, W., G. Vidal, and J. I. Cirac, 2000, "Three qubits can be entangled in two inequivalent ways," Phys. Rev. A **62**, 062314.
Edgar, M. P., D. S. Tasca, F. Izdebski, R. E. Warburton, J. Leach, M. Agnew, G. S. Buller, R. W. Boyd, and M. J. Padgett, 2012, "Imaging high-dimensional spatial entanglement with a camera," Nat. Commun. **3**, 984.
Englert, B.-G., 1996, "Fringe Visibility and Which-Way Information: An Inequality," Phys. Rev. Lett. **77**, 2154.
Erdős, P., and A. Rényi, 1959, "On random graphs I," Publ. Math. Debrecen **6**, 290.
Erdős, P., and A. Rényi, 1960, "On the evolution of random graphs," Publ. Math. Inst. Hung. Acad. Sci. **5**, 17.
Erhard, M., R. Fickler, M. Krenn, and A. Zeilinger, "Twisted photons: New quantum perspectives in high dimensions," 2018, Light Sci. Appl. **7**, 17146.
Erhard, M., M. Krenn, and A. Zeilinger, 2020, "Advances in high-dimensional quantum entanglement," Nat. Rev. Phys. **2**, 365–381.
Erhard, M., M. Malik, M. Krenn, and A. Zeilinger, 2018, "Experimental Greenberger-Horne-Zeilinger entanglement beyond qubits," Nat. Photonics **12**, 759–764.
Fein, Y. Y., P. Geyer, P. Zwick, F. Kiałka, S. Pedalino, M. Mayor, S. Gerlich, and M. Arndt, 2019, "Quantum superposition of molecules beyond 25 kDa," Nat. Phys. **15**, 1242–1245.
Feng, L.-T., G.-C. Guo, and X.-F. Ren, 2020, "Progress on integrated quantum photonic sources with silicon," Adv. Quantum Technol. **3**, 1900058.
Feng, L.-T., M. Zhang, D. Liu, Y.-J. Cheng, G.-P. Guo, D.-X. Dai, G.-C. Guo, M. Krenn, and X.-F. Ren, 2021, "Observation of nonlocal quantum interference between the origins of a four-photon state in a silicon chip," arXiv:2103.14277.
Feng, L.-T., M. Zhang, X. Xiong, Y. Chen, H. Wu, M. Li, G.-P. Guo, G.-C. Guo, D.-X. Dai, and X.-F. Ren, 2019, "On-chip transverse-mode entangled photon pair source," npj Quantum Inf. **5**, 2.
Fercher, A. F., W. Drexler, C. K. Hitzenberger, and T. Lasser, 2003, "Optical coherence tomography—Principles and applications," Rep. Prog. Phys. **66**, 239.
Feynman, R. P., R. B. Leighton, and M. Sands, 1965, *Quantum Mechanics: The Feynman Lectures on Physics*, Vol. 3 (Addison-Wesley, Reading, MA).
Fontaine, N. K., R. Ryf, H. Chen, D. T. Neilson, K. Kim, and J. Carpenter, 2019, "Laguerre-Gaussian mode sorter," Nat. Commun. **10**, 1865.

Fortunato, S., *et al.*, 2018, "Science of science," Science **359**, aao0185.
Franson, J. D., 1989, "Bell inequality for position and time," Phys. Rev. Lett. **62**, 2205.
Friis, N., G. Vitagliano, M. Malik, and M. Huber, 2019, "Entanglement certification from theory to experiment," Nat. Rev. Phys. **1**, 72–87.
Fuenzalida, J., A. Hochrainer, G. B. Lemos, E. Ortega, R. Lapkiewicz, M. Lahiri, and A. Zeilinger, 2022, "Resolution of quantum imaging with undetected photons," Quantum **6**, 646.
Fujimoto, J. G., M. E. Brezinski, G. J. Tearney, S. A. Boppart, B. Bouma, M. R. Hee, J. F. Southern, and E. A. Swanson, 1995, "Optical biopsy and imaging using optical coherence tomography," Nat. Med. **1**, 970–972.
Gatti, A., E. Brambilla, M. Bache, and L. A. Lugiato, 2004, "Ghost Imaging with Thermal Light: Comparing Entanglement and Classical Correlation," Phys. Rev. Lett. **93**, 093602.
Ghosh, R., and L. Mandel, 1987, "Observation of Nonclassical Effects in the Interference of Two Photons," Phys. Rev. Lett. **59**, 1903.
Gilaberte Basset, M., A. Hochrainer, S. Töpfer, F. Riexinger, P. Bickert, J. R. León-Torres, F. Steinlechner, and M. Gräfe, 2021, "Video-rate imaging with undetected photons," Laser Photonics Rev. **15**, 2000327.
Gimeno-Segovia, M., P. Shadbolt, D. E. Browne, and T. Rudolph, 2015, "From Three-Photon Greenberger-Horne-Zeilinger States to Ballistic Universal Quantum Computation," Phys. Rev. Lett. **115**, 020502.
Goyeneche, D., D. Alsina, J. I. Latorre, A. Riera, and K. Życzkowski, 2015, "Absolutely maximally entangled states, combinatorial designs, and multiunitary matrices," Phys. Rev. A **92**, 032316.
Grayson, T., and G. Barbosa, 1994, "Spatial properties of spontaneous parametric down-conversion and their effect on induced coherence without induced emission," Phys. Rev. A **49**, 2948.
Grayson, T., X. Zou, D. Branning, J. Torgerson, and L. Mandel, 1993, "Interference and indistinguishability governed by time delays in a low-Q cavity," Phys. Rev. A **48**, 4793.
Greenberger, D. M., M. A. Horne, A. Shimony, and A. Zeilinger, 1990, "Bell's theorem without inequalities," Am. J. Phys. **58**, 1131.
Greenberger, D. M., M. A. Horne, and A. Zeilinger, 1989, in *Bell's Theorem, Quantum Theory and Conceptions of the Universe*, edited by M. Kafatos (Springer, New York), pp. 69–72.
Greenberger, D. M., M. A. Horne, and A. Zeilinger, 1993, "Multiparticle interferometry and the superposition principle," Phys. Today **46**, No. 8, 22.
Greenberger, D. M., and A. Yasin, 1988, "Simultaneous wave and particle knowledge in a neutron interferometer," Phys. Lett. A **128**, 391–394.
Gu, X., L. Chen, and M. Krenn, 2020, "Quantum experiments and hypergraphs: Multiphoton sources for quantum interference, quantum computation, and quantum entanglement," Phys. Rev. A **101**, 033816.
Gu, X., L. Chen, A. Zeilinger, and M. Krenn, 2019, "Quantum experiments and graphs. III. High-dimensional and multiparticle entanglement," Phys. Rev. A **99**, 032338.
Gu, X., M. Erhard, A. Zeilinger, and M. Krenn, 2019, "Quantum experiments and graphs II: Quantum interference, computation, and state generation," Proc. Natl. Acad. Sci. U.S.A. **116**, 4147–4155.
Gubarev, F., I. Dyakonov, M. Y. Saygin, G. Struchalin, S. Straupe, and S. Kulik, 2020, "Improved heralded schemes to generate entangled states from single photons," Phys. Rev. A **102**, 012604.
Haase, B., M. Kutas, F. Riexinger, P. Bickert, A. Keil, D. Molter, M. Bortz, and G. Von Freymann, 2019, "Spontaneous parametric down-conversion of photons at 660 nm to the terahertz and subterahertz frequency range," Opt. Express **27**, 7458–7468.
Hamilton, C. S., R. Kruse, L. Sansoni, S. Barkhofen, C. Silberhorn, and I. Jex, 2017, "Gaussian Boson Sampling," Phys. Rev. Lett. **119**, 170501.
Hardy, L., 1992, "Source of photons with correlated polarisations and correlated directions," Phys. Lett. A **161**, 326–328.
Harrow, A. W., and A. Montanaro, 2017, "Quantum computational supremacy," Nature (London) **549**, 203–209.
Heckenberg, N., R. McDuff, C. Smith, and A. White, 1992, "Generation of optical phase singularities by computer-generated holograms," Opt. Lett. **17**, 221–223.
Herzog, T., J. Rarity, H. Weinfurter, and A. Zeilinger, 1994, "Frustrated Two-Photon Creation via Interference," Phys. Rev. Lett. **72**, 629.
Heuer, A., R. Menzel, and P. Milonni, 2015a, "Complementarity in biphoton generation with stimulated or induced coherence," Phys. Rev. A **92**, 033834.
Heuer, A., R. Menzel, and P. Milonni, 2015b, "Induced Coherence, Vacuum Fields, and Complementarity in Biphoton Generation," Phys. Rev. Lett. **114**, 053601.
Heuer, A., G. Pieplow, and R. Menzel, 2015, "Phase-selective quantum eraser," Phys. Rev. A **92**, 013803.
Hillery, M., V. Bužek, and A. Berthiaume, 1999, "Quantum secret sharing," Phys. Rev. A **59**, 1829.
Hochrainer, A., 2019, "Path indistinguishability in photon pair emission," Ph.D. thesis (University of Vienna).
Hochrainer, A., M. Lahiri, R. Lapkiewicz, G. B. Lemos, and A. Zeilinger, 2017a, "Interference fringes controlled by noninterfering photons," Optica **4**, 341–344.
Hochrainer, A., M. Lahiri, R. Lapkiewicz, G. B. Lemos, and A. Zeilinger, 2017b, "Quantifying the momentum correlation between two light beams by detecting one," Proc. Natl. Acad. Sci. U.S.A. **114**, 1508–1511.
Hong, C.-K., Z.-Y. Ou, and L. Mandel, 1987, "Measurement of Subpicosecond Time Intervals between Two Photons by Interference," Phys. Rev. Lett. **59**, 2044.
Horne, M. A., A. Shimony, and A. Zeilinger, 1989, "Two-Particle Interferometry," Phys. Rev. Lett. **62**, 2209.
Horne, M. A., and A. Zeilinger, 1986, "Einstein-Podolsky-Rosen interferometry," Ann. N.Y. Acad. Sci. **480**, 469–474.
Horodecki, R., P. Horodecki, M. Horodecki, and K. Horodecki, 2009, "Quantum entanglement," Rev. Mod. Phys. **81**, 865.
Howell, J. C., R. S. Bennink, S. J. Bentley, and R. Boyd, 2004, "Realization of the Einstein-Podolsky-Rosen Paradox Using Momentum- and Position-Entangled Photons from Spontaneous Parametric Down Conversion," Phys. Rev. Lett. **92**, 210403.
Huang, D., *et al.*, 1991, "Optical coherence tomography," Science **254**, 1178–1181.
Huber, F., C. Eltschka, J. Siewert, and O. Gühne, 2018, "Bounds on absolutely maximally entangled states from shadow inequalities, and the quantum MacWilliams identity," J. Phys. A **51**, 175301.
Huber, M., and J. I. de Vicente, 2013, "Structure of Multidimensional Entanglement in Multipartite Systems," Phys. Rev. Lett. **110**, 030501.
Huber, M., M. Perarnau-Llobet, and J. I. de Vicente, 2013, "Entropy vector formalism and the structure of multidimensional entanglement in multipartite systems," Phys. Rev. A **88**, 042328.
Huh, J., G. G. Guerreschi, B. Peropadre, J. R. McClean, and A. Aspuru-Guzik, 2015, "Boson sampling for molecular vibronic spectra," Nat. Photonics **9**, 615–620.

Jaeger, G., M. A. Horne, and A. Shimony, 1993, "Complementarity of one-particle and two-particle interference," Phys. Rev. A **48**, 1023.

Jha, A. K., M. N. O'Sullivan, K. W. C. Chan, and R. W. Boyd, 2008, "Temporal coherence and indistinguishability in two-photon interference effects," Phys. Rev. A **77**, 021801(R).

Jin, H., F. Liu, P. Xu, J. Xia, M. Zhong, Y. Yuan, J. Zhou, Y. Gong, W. Wang, and S. Zhu, 2014, "On-Chip Generation and Manipulation of Entangled Photons Based on Reconfigurable Lithium-Niobate Waveguide Circuits," Phys. Rev. Lett. **113**, 103601.

Kalashnikov, D. A., A. V. Paterova, S. P. Kulik, and L. A. Krivitsky, 2016, "Infrared spectroscopy with visible light," Nat. Photonics **10**, 98–101.

Ke, Q., E. Ferrara, F. Radicchi, and A. Flammini, 2015, "Defining and identifying sleeping beauties in science," Proc. Natl. Acad. Sci. U.S.A. **112**, 7426–7431.

Keller, M., M. Kotyrba, F. Leupold, M. Singh, M. Ebner, and A. Zeilinger, 2014, "Bose-Einstein condensate of metastable helium for quantum correlation experiments," Phys. Rev. A **90**, 063607.

Kelly, J., *et al.*, 2015, "State preservation by repetitive error detection in a superconducting quantum circuit," Nature (London) **519**, 66–69.

Kimble, H. J., M. Dagenais, and L. Mandel, 1977, "Photon Antibunching in Resonance Fluorescence," Phys. Rev. Lett. **39**, 691.

Klyshko, D., 1993, "Ramsey interference in two-photon parametric scattering," Zh. Eksp. Teor. Fiz. **104**, 2676–2684, http://jetp.ras.ru/cgi-bin/dn/e_077_02_0222.pdf.

Knill, E., 2003, "Bounds on the probability of success of postselected nonlinear sign shifts implemented with linear optics," Phys. Rev. A **68**, 064303.

Kolobov, M. I., E. Giese, S. Lemieux, R. Fickler, and R. W. Boyd, 2017, "Controlling induced coherence for quantum imaging," J. Opt. **19**, 054003.

Kovlakov, E., S. Straupe, and S. Kulik, 2018, "Quantum state engineering with twisted photons via adaptive shaping of the pump beam," Phys. Rev. A **98**, 060301.

Krapick, S., B. Brecht, H. Herrmann, V. Quiring, and C. Silberhorn, 2016, "On-chip generation of photon-triplet states," Opt. Express **24**, 2836–2849.

Krenn, M., M. Erhard, and A. Zeilinger, 2020, "Computer-inspired quantum experiments," Nat. Rev. Phys. **2**, 649–661.

Krenn, M., X. Gu, and D. Soltész, 2019, "Questions on the structure of perfect matchings inspired by quantum physics," arXiv:1902.06023.

Krenn, M., X. Gu, and A. Zeilinger, 2017, "Quantum Experiments and Graphs: Multiparty States as Coherent Superpositions of Perfect Matchings," Phys. Rev. Lett. **119**, 240403.

Krenn, M., A. Hochrainer, M. Lahiri, and A. Zeilinger, 2017, "Entanglement by Path Identity," Phys. Rev. Lett. **118**, 080401.

Krenn, M., M. Huber, R. Fickler, R. Lapkiewicz, S. Ramelow, and A. Zeilinger, 2014, "Generation and confirmation of a (100×100)-dimensional entangled quantum system," Proc. Natl. Acad. Sci. U.S.A. **111**, 6243–6247.

Krenn, M., J. Kottmann, N. Tischler, and A. Aspuru-Guzik, 2021, "Conceptual Understanding through Efficient Automated Design of Quantum Optical Experiments," Phys. Rev. X **11**, 031044.

Krenn, M., M. Malik, R. Fickler, R. Lapkiewicz, and A. Zeilinger, 2016, "Automated Search for new Quantum Experiments," Phys. Rev. Lett. **116**, 090405.

Kues, M., C. Reimer, J. M. Lukens, W. J. Munro, A. M. Weiner, D. J. Moss, and R. Morandotti, 2019, "Quantum optical microcombs," Nat. Photonics **13**, 170–179.

Kulkarni, G., P. Kumar, and A. K. Jha, 2017, "Transfer of temporal coherence in parametric down-conversion," J. Opt. Soc. Am. B **34**, 1637–1643.

Kutas, M., B. Haase, P. Bickert, F. Riexinger, D. Molter, and G. von Freymann, 2020, "Terahertz quantum sensing," Sci. Adv. **6**, eaaz8065.

Kutas, M., B. Haase, J. Klier, D. Molter, and G. von Freymann, 2021, "Quantum-inspired terahertz spectroscopy with visible photons," Optica **8**, 438–441.

Kviatkovsky, I., H. M. Chrzanowski, E. G. Avery, H. Bartolomaeus, and S. Ramelow, 2020, "Microscopy with undetected photons in the mid-infrared," Sci. Adv. **6**, eabd0264.

Kviatkovsky, I., H. M. Chrzanowski, and S. Ramelow, 2022, "Mid-infrared microscopy via position correlations of undetected photons," Opt. Express **30**, 5916–5925.

Kwiat, P. G., A. M. Steinberg, and R. Y. Chiao, 1994, "Three proposed 'quantum erasers,' " Phys. Rev. A **49**, 61.

Kwiat, P. G., E. Waks, A. G. White, I. Appelbaum, and P. H. Eberhard, 1999, "Ultrabright source of polarization-entangled photons," Phys. Rev. A **60**, R773(R).

Kysela, J., M. Erhard, A. Hochrainer, M. Krenn, and A. Zeilinger, 2020, "Path identity as a source of high-dimensional entanglement," Proc. Natl. Acad. Sci. U.S.A. **117**, 26118–26122.

Lahiri, M., 2011, "Wave-particle duality and polarization properties of light in single-photon interference experiments," Phys. Rev. A **83**, 045803.

Lahiri, M., 2018, "Many-particle interferometry and entanglement by path identity," Phys. Rev. A **98**, 033822.

Lahiri, M., A. Hochrainer, R. Lapkiewicz, G. B. Lemos, and A. Zeilinger, 2017a, "Partial polarization by quantum distinguishability," Phys. Rev. A **95**, 033816.

Lahiri, M., A. Hochrainer, R. Lapkiewicz, G. B. Lemos, and A. Zeilinger, 2017b, "Twin-photon correlations in single-photon interference," Phys. Rev. A **96**, 013822.

Lahiri, M., A. Hochrainer, R. Lapkiewicz, G. B. Lemos, and A. Zeilinger, 2019, "Nonclassicality of induced coherence without induced emission," Phys. Rev. A **100**, 053839.

Lahiri, M., R. Lapkiewicz, A. Hochrainer, G. B. Lemos, and A. Zeilinger, 2021, "Characterizing mixed-state entanglement through single-photon interference," Phys. Rev. A **104**, 013704.

Lahiri, M., R. Lapkiewicz, G. B. Lemos, and A. Zeilinger, 2015, "Theory of quantum imaging with undetected photons," Phys. Rev. A **92**, 013832.

Lawrence, J., 2014, "Rotational covariance and Greenberger-Horne-Zeilinger theorems for three or more particles of any dimension," Phys. Rev. A **89**, 012105.

Leach, J., M. J. Padgett, S. M. Barnett, S. Franke-Arnold, and J. Courtial, 2002, "Measuring the Orbital Angular Momentum of a Single Photon," Phys. Rev. Lett. **88**, 257901.

Lee, S. K., T. H. Yoon, and M. Cho, 2017, "Quantum optical measurements with undetected photons through vacuum field indistinguishability," Sci. Rep. **7**, 6558.

Lemos, G. B., V. Borish, G. D. Cole, S. Ramelow, R. Lapkiewicz, and A. Zeilinger, 2014, "Quantum imaging with undetected photons," Nature (London) **512**, 409–412.

Lemos, G. B., R. Lapkiewicz, A. Hochrainer, M. Lahiri, and A. Zeilinger, 2020, "Measuring mixed state entanglement through single-photon interference," arXiv:2009.02851.

Lett, P. D., 2004, "Correlated photons for correlated atoms," J. Mod. Opt. **51**, 1817–1827.

Lindner, C., J. Kunz, S. J. Herr, S. Wolf, J. Kießling, and F. Kühnemann, 2021, "Nonlinear interferometer for

Fourier-transform mid-infrared gas spectroscopy using near-infrared detection," Opt. Express **29**, 4035–4047.
Lindner, C., S. Wolf, J. Kiessling, and F. Kühnemann, 2020, "Fourier transform infrared spectroscopy with visible light," Opt. Express **28**, 4426–4432.
Liu, S., Z. Zhou, S. Liu, Y. Li, Y. Li, C. Yang, Z. Xu, Z. Liu, G. Guo, and B. Shi, 2018, "Coherent manipulation of a three-dimensional maximally entangled state," Phys. Rev. A **98**, 062316.
Lopes, R., A. Imanaliev, A. Aspect, M. Cheneau, D. Boiron, and C. I. Westbrook, 2015, "Atomic Hong-Ou-Mandel experiment," Nature (London) **520**, 66–68.
Lu, L., *et al.*, 2020, "Three-dimensional entanglement on a silicon chip," npj Quantum Inf. **6**, 30.
Luis, A., and J. Peřina, 1996, "SU(2) coherent states in parametric down-conversion," Phys. Rev. A **53**, 1886.
Lund, A., A. Laing, S. Rahimi-Keshari, T. Rudolph, J. L. O'Brien, and T. Ralph, 2014, "Boson Sampling from a Gaussian State," Phys. Rev. Lett. **113**, 100502.
Luo, Y.-H., *et al.*, 2019, "Quantum Teleportation in High Dimensions," Phys. Rev. Lett. **123**, 070505.
Ma, X.-s., J. Kofler, and A. Zeilinger, 2016, "Delayed-choice gedanken experiments and their realizations," Rev. Mod. Phys. **88**, 015005.
Mair, A., A. Vaziri, G. Weihs, and A. Zeilinger, 2001, "Entanglement of the orbital angular momentum states of photons," Nature (London) **412**, 313–316.
Malgieri, M., P. Onorato, and A. De Ambrosis, 2017, "Test on the effectiveness of the sum over paths approach in favoring the construction of an integrated knowledge of quantum physics in high school," Phys. Rev. Phys. Educ. Res. **13**, 010101.
Malik, M., M. Erhard, M. Huber, M. Krenn, R. Fickler, and A. Zeilinger, 2016, "Multi-photon entanglement in high dimensions," Nat. Photonics **10**, 248–252.
Mandel, L., 1991, "Coherence and indistinguishability," Opt. Lett. **16**, 1882–1883.
Mandel, L., E. G. Sudarshan, and E. Wolf, 1964, "Theory of photoelectric detection of light fluctuations," Proc. Phys. Soc. London **84**, 435.
Mandel, L., and E. Wolf, 1995, *Optical Coherence and Quantum Optics* (Cambridge University Press, Cambridge, England).
Marrucci, L., C. Manzo, and D. Paparo, 2006, "Optical Spin-to-Orbital Angular Momentum Conversion in Inhomogeneous Anisotropic Media," Phys. Rev. Lett. **96**, 163905.
Mermin, N. D., 1990, "Extreme Quantum Entanglement in a Superposition of Macroscopically Distinct States," Phys. Rev. Lett. **65**, 1838.
Miatto, F., D. Giovannini, J. Romero, S. Franke-Arnold, S. Barnett, and M. Padgett, 2012, "Bounds and optimisation of orbital angular momentum bandwidths within parametric down-conversion systems," Eur. Phys. J. D **66**, 178.
Mista, Jr., L., J. Herec, V. Jelínek, J. Rehácek, and J. Perina, 2000, "Quantum and semiclassical optics quantum dynamics and statistics of two coupled down-conversion processes," J. Opt. B **2**, 726.
Monken, C. H., P. S. Ribeiro, and S. Pádua, 1998, "Transfer of angular spectrum and image formation in spontaneous parametric down-conversion," Phys. Rev. A **57**, 3123.
Monz, T., P. Schindler, J. T. Barreiro, M. Chwalla, D. Nigg, W. A. Coish, M. Harlander, W. Hänsel, M. Hennrich, and R. Blatt, 2011, "14-Qubit Entanglement: Creation and Coherence," Phys. Rev. Lett. **106**, 130506.
Morizur, J.-F., L. Nicholls, P. Jian, S. Armstrong, N. Treps, B. Hage, M. Hsu, W. Bowen, J. Janousek, and H.-A. Bachor, 2010, "Programmable unitary spatial mode manipulation," J. Opt. Soc. Am. A **27**, 2524–2531.
Olislager, L., J. Cussey, A. T. Nguyen, P. Emplit, S. Massar, J.-M. Merolla, and K. P. Huy, 2010, "Frequency-bin entangled photons," Phys. Rev. A **82**, 013804.
Omran, A., *et al.*, 2019, "Generation and manipulation of Schrödinger cat states in Rydberg atom arrays," Science **365**, 570–574.
Ono, T., G. F. Sinclair, D. Bonneau, M. G. Thompson, J. C. Matthews, and J. G. Rarity, 2019, "Observation of nonlinear interference on a silicon photonic chip," Opt. Lett. **44**, 1277–1280.
Ou, Z., 1997, "Nonlocal correlation in the realization of a quantum eraser," Phys. Lett. A **226**, 323–326.
Ou, Z., and X. Li, 2020, "Quantum SU(1, 1) interferometers: Basic principles and applications," APL Photonics **5**, 080902.
Ou, Z., and Y. Lu, 1999, "Cavity Enhanced Spontaneous Parametric Down-Conversion for the Prolongation of Correlation Time between Conjugate Photons," Phys. Rev. Lett. **83**, 2556.
Pan, J.-W., D. Bouwmeester, M. Daniell, H. Weinfurter, and A. Zeilinger, 2000, "Experimental test of quantum nonlocality in three-photon Greenberger-Horne-Zeilinger entanglement," Nature (London) **403**, 515–519.
Pan, J.-W., D. Bouwmeester, H. Weinfurter, and A. Zeilinger, 1998, "Experimental Entanglement Swapping: Entangling Photons That Never Interacted," Phys. Rev. Lett. **80**, 3891.
Pan, J.-W., Z.-B. Chen, C.-Y. Lu, H. Weinfurter, A. Zeilinger, and M. Żukowski, 2012, "Multiphoton entanglement and interferometry," Rev. Mod. Phys. **84**, 777.
Pancharatnam, S., 1956, "Generalized theory of interference and its applications," Proc. Indian Acad. Sci. **44**, 398–417.
Paterova, A., S. Lung, D. A. Kalashnikov, and L. A. Krivitsky, 2017, "Nonlinear infrared spectroscopy free from spectral selection," Sci. Rep. **7**, 42608.
Paterova, A., H. Yang, C. An, D. Kalashnikov, and L. Krivitsky, 2018a, "Measurement of infrared optical constants with visible photons," New J. Phys. **20**, 043015.
Paterova, A., H. Yang, C. An, D. Kalashnikov, and L. Krivitsky, 2018b, "Tunable optical coherence tomography in the infrared range using visible photons," Quantum Sci. Technol. **3**, 025008.
Paterova, A. V., and L. A. Krivitsky, 2020, "Nonlinear interference in crystal superlattices," Light Sci. Appl. **9**, 82.
Paterova, A. V., S. M. Maniam, H. Yang, G. Grenci, and L. A. Krivitsky, 2020, "Hyperspectral infrared microscopy with visible light," Sci. Adv. **6**, eabd0460.
Perseguers, S., M. Lewenstein, A. Acín, and J. I. Cirac, 2010, "Quantum random networks," Nat. Phys. **6**, 539–543.
Pittman, T., Y. Shih, D. Strekalov, and A. V. Sergienko, 1995, "Optical imaging by means of two-photon quantum entanglement, Phys. Rev. A **52**, R3429(R).
Plenio, M. B., and S. S. Virmani, 2014, in *Quantum Information and Coherence*, edited by E. Andersson and P. Öhberg (Springer, New York), pp. 173–209.
Puliafito, C. A., M. R. Hee, C. P. Lin, E. Reichel, J. S. Schuman, J. S. Duker, J. A. Izatt, E. A. Swanson, and J. G. Fujimoto, 1995, "Imaging of macular diseases with optical coherence tomography," Ophthalmology **102**, 217–229.
Qian, K., K. Wang, L. Chen, Z. Hou, M. Krenn, S. Zhu, and X.-S. Ma, 2021, "Multiphoton non-local quantum interference controlled by an undetected photon," arXiv:2112.11658.
Ragy, S., and G. Adesso, 2012, "Nature of light correlations in ghost imaging," Sci. Rep. **2**, 651.
Rarity, J., and P. Tapster, 1990, "Experimental Violation of Bell's Inequality Based on Phase and Momentum," Phys. Rev. Lett. **64**, 2495.

Rauch, H., and S. A. Werner, 2015, *Neutron Interferometry: Lessons in Experimental Quantum Mechanics* (Oxford University Press, New York).

Reck, M., A. Zeilinger, H. J. Bernstein, and P. Bertani, 1994, "Experimental Realization of Any Discrete Unitary Operator," Phys. Rev. Lett. **73**, 58.

Reimer, C., *et al.*, 2016, "Generation of multiphoton entangled quantum states by means of integrated frequency combs," Science **351**, 1176–1180.

Ren, J.-G., *et al.*, 2017, "Ground-to-satellite quantum teleportation," Nature (London) **549**, 70–73.

Resch, K., J. Lundeen, and A. Steinberg, 2001, "Nonlinear Optics with Less Than One Photon," Phys. Rev. Lett. **87**, 123603.

Robert, A., O. Sirjean, A. Browaeys, J. Poupard, S. Nowak, D. Boiron, C. I. Westbrook, and A. Aspect, 2001, "A Bose-Einstein condensate of metastable atoms," Science **292**, 461–464.

Rojas-Santana, A., G. J. Machado, D. Lopez-Mago, and J. P. Torres, 2020, "Frequency-correlation requirements on the biphoton wave function in an induced-coherence experiment between separate sources," Phys. Rev. A **102**, 053711.

Rudolph, T., 2017, "Why I am optimistic about the silicon-photonic route to quantum computing," APL Photonics **2**, 030901.

Ryff, L., 1995a, "Changing the relative amplitudes of wave packets to induce nonlocal effects," Phys. Rev. A **51**, 79.

Ryff, L. C., 1995b, "Interference, distinguishability, and apparent contradiction in an experiment on induced coherence," Phys. Rev. A **52**, 2591.

Ryff, L. C., 2015, "Comment on 'On phase selective quantum eraser,' " arXiv:1509.04673.

Ryu, J., C. Lee, Z. Yin, R. Rahaman, D. G. Angelakis, J. Lee, and M. Żukowski, 2014, "Multisetting Greenberger-Horne-Zeilinger theorem," Phys. Rev. A **89**, 024103.

Ryu, J., C. Lee, M. Żukowski, and J. Lee, 2013, "Greenberger-Horne-Zeilinger theorem for N qudits," Phys. Rev. A **88**, 042101.

Santagati, R., *et al.*, 2018, "Witnessing eigenstates for quantum simulation of Hamiltonian spectra," Sci. Adv. **4**, eaap9646.

Schaeff, C., R. Polster, R. Lapkiewicz, R. Fickler, S. Ramelow, and A. Zeilinger, 2012, "Scalable fiber integrated source for higher-dimensional path-entangled photonic quNits," Opt. Express **20**, 16145–16153.

Shor, P. W., 1996, "Fault-tolerant quantum computation," in *Proceedings of the 37th Conference on Foundations of Computer Science, Burlington, VT, 1996* (IEEE, New York), pp. 56–65.

Silverstone, J. W., R. Santagati, D. Bonneau, M. J. Strain, M. Sorel, J. L. O'Brien, and M. G. Thompson, 2015, "Qubit entanglement between ring-resonator photon-pair sources on a silicon chip," Nat. Commun. **6**, 7948.

Silverstone, J. W., *et al.*, 2014, "On-chip quantum interference between silicon photon-pair sources," Nat. Photonics **8**, 104–108.

Slussarenko, S., and G. J. Pryde, 2019, "Photonic quantum information processing: A concise review," Appl. Phys. Rev. **6**, 041303.

Song, C., *et al.*, 2017, "10-Qubit Entanglement and Parallel Logic Operations with a Superconducting Circuit," Phys. Rev. Lett. **119**, 180511.

Spaide, R. F., J. G. Fujimoto, N. K. Waheed, S. R. Sadda, and G. Staurenghi, 2018, "Optical coherence tomography angiography," Prog. Retinal Eye Res. **64**, 1–55.

Stewart, B., 2004, *Infrared Spectroscopy: Fundamentals and Applications* (Wiley, New York).

Su, J., L. Cui, J. Li, Y. Liu, X. Li, and Z. Ou, 2019, "Versatile and precise quantum state engineering by using nonlinear interferometers," Opt. Express **27**, 20479–20492.

Tang, W., S. Yu, and C. Oh, 2017, "Multisetting Greenberger-Horne-Zeilinger paradoxes," Phys. Rev. A **95**, 012131.

Tittel, W., J. Brendel, H. Zbinden, and N. Gisin, 1998, "Violation of Bell Inequalities by Photons More Than 10 km Apart," Phys. Rev. Lett. **81**, 3563.

Tonouchi, M., 2007, "Cutting-edge terahertz technology," Nat. Photonics **1**, 97–105.

Tóth, G., 2007, "Detection of multipartite entanglement in the vicinity of symmetric Dicke states," J. Opt. Soc. Am. B **24**, 275–282.

Valiant, L. G., 1979, "The complexity of computing the permanent," Theor. Comput. Sci. **8**, 189–201.

Vallés, A., G. Jiménez, L. J. Salazar-Serrano, and J. P. Torres, 2018, "Optical sectioning in induced coherence tomography with frequency-entangled photons," Phys. Rev. A **97**, 023824.

Vanselow, A., P. Kaufmann, I. Zorin, B. Heise, H. M. Chrzanowski, and S. Ramelow, 2020, "Frequency-domain optical coherence tomography with undetected mid-infrared photons," Optica **7**, 1729–1736.

Vassen, W., C. Cohen-Tannoudji, M. Leduc, D. Boiron, C. I. Westbrook, A. Truscott, K. Baldwin, G. Birkl, P. Cancio, and M. Trippenbach, 2012, "Cold and trapped metastable noble gases," Rev. Mod. Phys. **84**, 175.

Vaziri, A., J.-W. Pan, T. Jennewein, G. Weihs, and A. Zeilinger, 2003, "Concentration of Higher Dimensional Entanglement: Qutrits of Photon Orbital Angular Momentum," Phys. Rev. Lett. **91**, 227902.

Vaziri, A., G. Weihs, and A. Zeilinger, 2002, "Experimental Two-Photon, Three-Dimensional Entanglement for Quantum Communication," Phys. Rev. Lett. **89**, 240401.

Verstraete, F., J. Dehaene, B. De Moor, and H. Verschelde, 2002, "Four qubits can be entangled in nine different ways," Phys. Rev. A **65**, 052112.

Viswanathan, B., G. B. Lemos, and M. Lahiri, 2021a, "Position correlation enabled quantum imaging with undetected photons," Opt. Lett. **46**, 3496–3499.

Viswanathan, B., G. B. Lemos, and M. Lahiri, 2021b, "Resolution limit in quantum imaging with undetected photons using position correlations," Opt. Express **29**, 38185–38198.

Wang, J., *et al.*, 2018, "Multidimensional quantum entanglement with large-scale integrated optics," Science **360**, 285–291.

Wang, L., and J.-K. Rhee, 1999, "Propagation of transient quantum coherence," Phys. Rev. A **59**, 1654.

Wang, L., X. Zou, and L. Mandel, 1991, "Induced coherence without induced emission," Phys. Rev. A **44**, 4614.

Wang, L., X. Zou, and L. Mandel, 1992, "Time-varying induced coherence," J. Opt. Soc. Am. B **9**, 605–609.

Wang, X.-L., X.-D. Cai, Z.-E. Su, M.-C. Chen, D. Wu, L. Li, N.-L. Liu, C.-Y. Lu, and J.-W. Pan, 2015, "Quantum teleportation of multiple degrees of freedom of a single photon," Nature (London) **518**, 516–519.

Wang, X.-L., *et al.*, 2017, "High-efficiency multiphoton boson sampling," Nat. Photonics **11**, 361–365.

Wang, X.-L., *et al.*, 2018, "18-Qubit Entanglement with Six Photons' Three Degrees of Freedom," Phys. Rev. Lett. **120**, 260502.

Wiseman, H., and K. Mølmer, 2000, "Induced coherence with and without induced emission," Phys. Lett. A **270**, 245–248.

Wolf, E., 1959, "Coherence properties of partially polarized electromagnetic radiation," Nuovo Cimento **13**, 1165–1181.

Wolf, J.-P., and Y. Silberberg, 2016, "Spooky spectroscopy," Nat. Photonics **10**, 77–79.

Wootters, W. K., and W. H. Zurek, 1979, "Complementarity in the double-slit experiment: Quantum nonseparability and a quantitative statement of Bohr's principle," Phys. Rev. D **19**, 473.

Yao, A. M., and M. J. Padgett, 2011, "Orbital angular momentum: Origins, behavior and applications," Adv. Opt. Photonics **3**, 161–204.

Yurtsever, U., and G. Hockney, 2005, "Signalling, entanglement and quantum evolution beyond Cauchy horizons," Classical Quantum Gravity **22**, 295.

Zajonc, A., L. Wang, X. Zou, and L. Mandel, 1991, "Quantum eraser," Nature (London) **353**, 507–508.

Zeilinger, A., 1986, "Complementarity in neutron interferometry," Physica (Amsterdam) **137B+C**, 235–244.

Zeilinger, A., M. A. Horne, and D. M. Greenberger, 1992, in *Proceedings of Squeezed States and Quantum Uncertainty*, edited by D. Han, Y. S. Kim, and W. W. Zachary, NASA Publication No. 3135 (NASA, Washington, DC).

Zhan, X., 2021, "Determining the mixed high-dimensional Bell state of a photon pair through the measurement of a single photon," Phys. Rev. A **103**, 032437.

Zhong, H.-S., *et al.*, 2018, "12-Photon Entanglement and Scalable Scattershot Boson Sampling with Optimal Entangled-Photon Pairs from Parametric Down-Conversion," Phys. Rev. Lett. **121**, 250505.

Zou, X., T. Grayson, G. Barbosa, and L. Mandel, 1993, "Control of visibility in the interference of signal photons by delays imposed on the idler photons," Phys. Rev. A **47**, 2293.

Zou, X., T. Grayson, and L. Mandel, 1992, "Observation of Quantum Interference Effects in the Frequency Domain," Phys. Rev. Lett. **69**, 3041.

Zou, X., T. Grayson, L. Wang, and L. Mandel, 1992, "Can an 'Empty' de Broglie Pilot Wave Induce Coherence?," Phys. Rev. Lett. **68**, 3667.

Zou, X., L. Wang, T. Grayson, and L. Mandel, 1992, "New technique for controlling the degree of coherence of two light beams," Opt. Laser Technol. **24**, 289–291.

Zou, X., L. J. Wang, and L. Mandel, 1991, "Induced Coherence and Indistinguishability in Optical Interference," Phys. Rev. Lett. **67**, 318.

Żukowski, M., and J. Pykacz, 1988, "Bell's theorem: Proposition of realizable experiment using linear momenta," Phys. Lett. A **127**, 1–4.

Żukowski, M., A. Zeilinger, M. A. Horne, and A. K. Ekert, 1993, " 'Event-Ready-Detectors' Bell Experiment via Entanglement Swapping," Phys. Rev. Lett. **71**, 4287.